Toward Distributed Control for Autonomous Electrical Energy Systems

by

Xia Miao

B.S., Huazhong University of Science & Technology (2012)
M.S., Carnegie Mellon University (2014)

Submitted to the Department of Electrical Engineering and Computer Science
in partial fulfillment of the requirements for the degree of

Doctor of Philosophy

at the

MASSACHUSETTS INSTITUTE OF TECHNOLOGY

February 2020

Author .... Signature redacted ....
Department of Electrical Engineering and Computer Science
September 18, 2019

Certified by.... Signature redacted ....
Marija D. Ilić
Senior Research Scientist, LIDS
Senior Research Staff, MIT Lincoln Laboratory
Thesis Supervisor

Accepted by .... Signature redacted ....
Leslie A. Kolodziejski
Professor of Electrical Engineering and Computer Science
Chair, Department Committee on Graduate Students

Toward Distributed Control for Autonomous Electrical Energy Systems

by

Xia Miao

Submitted to the Department of Electrical Engineering and Computer Science
on September 18, 2019, in partial fulfillment of the
requirements for the degree of
Doctor of Philosophy

Abstract

In this thesis we study the problem of enabling autonomous electrical energy systems (AEESs) by means of distributed control. We first propose a modular modeling approach that represents a general electrical energy system (EES) as a negative feedback configuration comprising a planar electrical network subsystem and a subsystem of single-port components. The input-output specifications of all components are in terms of power and voltage. This mathematical modeling supports the basic physical functionality of balancing power supply and demand at the acceptable Quality of Service (QoS). These input-output specifications are met by the controllable components equipped with the newly proposed distributed control. We show that these controllers enable stable and feasible system-level closed-loop dynamics. Moreover, an interactive algorithm for autonomous adjustments of their controller set points based on the information exchange with neighboring components is introduced. This serves as a proof-of-concept illustration of how components adjust their power and voltage toward a system-level equilibrium. Such process is the basis for autonomous reconfigurable operation of small microgrids. As the first step toward scaling up the proposed concepts, we consider the problem of enhanced automatic generation control (E-AGC) for systems with highly dynamic load variations, including effects of intermittent renewable generation. Further work is needed to fully generalize this approach for control design of large-scale EES. In addition to theoretical results, we also report the results of several numerical and hardware tests. These show the effectiveness of the proposed approach in fairly complex scenarios, including unplanned large faults and hard-to-predict fast-varying power disturbances.

Thesis Supervisor: Marija D. Ilić
Title: Senior Research Scientist, LIDS
Senior Research Staff, MIT Lincoln Laboratory

Acknowledgments

I would like to express my sincere gratitude to my advisor, Professor Marija D. Ilić for her constant support and guidance. Working with Professor Ilić for the past 6 years has been my greatest fortune. I do not remember how many late nights we worked together on research problems; what I only remember is her enormous passion. Of course, the outcome was always exciting. It is her guidance and patience that have been directing me from a ME student to an EE researcher; it is her insightful vision that has been enlightening me to find a suitable and interesting research topic; it is her enthusiasm and inspiration that have been shaping my life-time career path.

I also would like to express my deepest gratitude to my committee members, Professor Alexandre Megretski and Professor James Kirtley. They have asked many intriguing questions and have provided many constructive comments, which helped me a lot in sharpening this thesis. I also want to thank my colleagues from Siemens, Dr. Ulrich Muenz and Dr. Xiaofan Wu, for motivating me to work on autonomous electrical energy systems.

I transferred from CMU to MIT in the middle of my Ph.D. study. My time at MIT would not be so enjoyable without many friends and colleagues at LIDS and MIT. This includes Professor Jeffery Lang, Professor Le Xie, Dr. Audun Botterud, Chris Smith, Ryan Wiechens, Erik Limpaecher, Dr. Chengtao Li, Wenhan Dai, Zhenyu Liu, Tianheng Wang, Dr. Omer Tanovic, Yue Guan, Tianyi Peng, Zehao Yu, Xinzhe Fu, Bai Liu, Jianan Zhang, Tianli Zhou, Dr. Ye Ding, Xin Zhao, weijia Wu, Zhequn Xiong, Dr. Bolun Xu, Yibao Jiang, Yuxiao Liu, Jingwei Yang, Tong Huang, Dr. Xinbo Geng, Dr. Xueying Lu, Dr. Qing Yu and others too numerous to name. They brought me lots of support, comfort, and fun along the stressful Ph.D. journey.

I would like to thank my Pokemon Go Team, Xuenan Ni, Xiaoyan Shen, and Dr. Hongzhou Lin, for all the legendary pokemon that we caught, the exercise that we did together and the joy that we shared. I also would like to thank my "party group", Dr. Jun Li, Dr. Yang Wu, Zhen Yang, Dr. Haizheng Zhang, Weichen Liu, and Jia Fang, for the delicious homemade dinner, BBQ, and hiking. They made me feel never left home. I want to specifically thank my officemates, Dr. Kevin Bachovchin, Rupamathi, Jaddivada, Ana Jevtic, Dr. Hongyi Zhang, Jingzhao Zhang, and Dr. Quan Li, for the deep discussions about the life, research and many tough moments that we shared. I remember that Kevin and I enjoyed ice cream in Dave & Andy's after heavy-loaded project meetings. I also could not forget 2018 New Year's Eve. While working in the office, Hongyi and I came up with a startup plan to solve the loneliness. This mission is still active. Jingzhao, Hongyi and I will make it come true. By the way, the food court in our office is the best.

I could not forget to thank my colleagues and friends at Carnegie Mellon University. I am grateful to have a large group of excellent colleagues and friends. I want to thank Dr. Qixing Liu, Dr. Dinghuan Zhu, Dr. Rui Yang, Dr. Xiaoqi Yin, Dr. Xiao Zhang, Dr. Tao Cui, Professor Yang Weng, Dr. Guofan Wu, Dr. Liangyan Gui, Dr. Yuxiong Wang, Dr. Milos Cvetkovic, Dr. Jhi-Young Joo, Dr. Stefanos Baros, Xuan Tang, Lingchen Li, Haotian Shi and others too numerous to name, for giving me so many unforgettable moments. They were always there for me, offering me advice about my future career path, and being a constant source of help.

Back to the people in my home country, I am sincerely thankful to my classmates, including Xiao Yao, Yufei Ruan, Hui Liu, Ting Li, Wei Zhu, Yinxue Wang, Shini Feng and others, for giving me endless support to move on. Our friendship has been invaluable to me.

Last but not least, I offer my enormous gratitude to my family and dedicate my thesis to them. To pursue my dream, I left my home for 7 years. Every Friday night is our skype time. Although they did not say, I know waiting for my call is the only thing on their schedule. I owe them too much. To my wonderful parents, Aichen Miao and Fengcai Liu, for providing me everything they have, and never left me feeling alone. Finally, to Xinhui, for filling my struggling Ph.D. journey with happiness.

This dissertation was supported in part by the National Institute of Standards and Technology (NIST), and in part by the ONR (Office of Naval Research). I gratefully appreciate the financial support.

DISTRIBUTION STATEMENT A.

Approved for public release. Distribution is unlimited. This material is based upon work supported by the Department of the Navy under Air Force Contract No. FA8702-15-D-0001. Any opinions, findings, conclusions or recommendations expressed in this material are those the author and do not necessarily reflect the views of the Department of the Navy. I gratefully appreciate the financial support.

Contents

List of Figures

List of Tables

Chapter 1

Introduction

1.1 Thesis motivation and problem formulation

Over the past decades, researchers and engineers have been actively looking for the way to achieve self-healing and autonomous functionalities of the electrical energy systems (EESs) [2–5]. Self-healing and autonomous functionalities indicate that the system can continue to function during the large changes and recover on its own. As an example, let us consider a self-healing smart city. If an attack occurred at the airport, nearby residential buildings should detect the change and automatically reconnect to provide help to the airport. Each building self-adjusts its roof-top PVs and available storage so that the airport has an uninterrupted electricity service.

It is appealing to have such highly resilient and flexible EESs. However, there exist many challenges to implementing such functions. To start with, implementing an AEES requires well-defined notion of such system, and this has not been formalized yet.

Second, the EES is currently into a system with large intermittent disturbances but smaller system inertia. This is because old power plants are being replaced with power electronically components smaller solar PVs, wind power plants, storage, and responsive loads. Figure 1-1(a) shows a typical solar radiation. It can be seen that the PV panels inject both fast varying and large generation changes to the system, unlike conventional coal power plants whose generation output is smooth, shown in

Figure 1-1(b). With small system inertia, an EES is sensitive to these hard-to-predict disturbances.

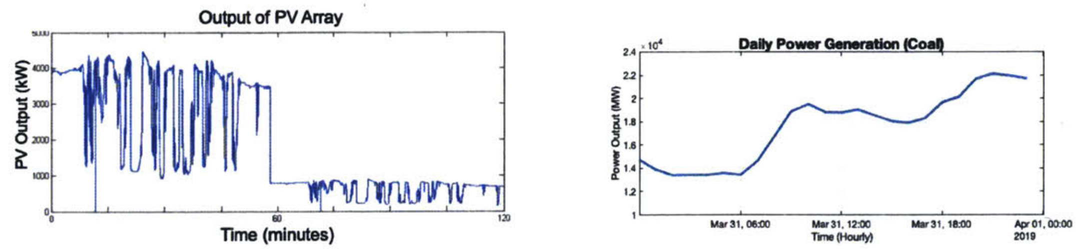

(a) Typical Solar Radiation [1]

(b) Typical Coal Generation March, 2019 (PJM)

Figure 1-1: Power Generation

Third, Today's control design of large power plants does not solve the challenges of power electronically distributed energy sources(DERs). The interaction with the grid becomes stronger and it is not clear whether the time-scale separation assumption of existing hierarchical control approaches is valid or not. Besides, since most of the existing controllers are tuned for predefined operating conditions, any unexpected faults may lead to cascading failures or power outages [6]. The New York substation explosion (December 27, 2018) [7], for example, was triggered by a sudden electric spike. Although the fault was detected, the programmed controller failed to make correct action causing the voltage to collapse and then the substation to explode.

Last but not the least, challenges also arise from the economic side. It is ideal to have coordination of energy resources so that the capacity of existing equipments can be fully utilized. This will greatly improve the efficiency, and reduce the investment cost by avoiding installing new devices or upgrading the existing ones.

1.1.1 Problem statement

In this thesis, we study the problem of enabling autonomous electrical energy systems. We first propose a working definition of an AEES. Conceptually, each subsystem of an AEES must supply its local loads when connected to the grid and when in standalon ("islanded"). Furthermore, the transition between different operating conditions should be seamless.

Definition 1.1.1 (Autonomous Electrical Energy System (AEES)). *A component (or a group of components) of an AEES should be able to self-adjust in a bounded input bounded output (BIBO) and stable manner. Through minimal information exchange with directly connected components, the component adjusts its power generation so that the power with the neighboring components is balanced. Consequently, system frequency and voltages are feasible and stable.*

To overcome above challenges, we seek an implementable approach in support of AEES. In particular, we focus on the following three problems:

- Problem 1: Establish modular and system-level specifications for which the EES is feasible and stable.
- Problem 2: Design distributed nonlinear control so that components meet their specifications for the well-defined ranges of disturbances.
- Problem 3: Achieve system-level feasibility and stability by further specifying the ranges of operating conditions

1.2 Brief literature review of relevant system theoretic concepts

We can categorize existing system theory into two groups, namely the centralized-type approach and the modular-type approach.

The centralized-type approaches include Nyquist criterion [8], Routh-Hurwitz criterion [9, 10], Direct and indirect Lyapunov methods [11], Lasalle's invariance principle [11] and other extensions [12–14]. They have been used to establish the stability conditions and to guide the control design. However, these approaches are of less interest to us. Because they are generally not suitable for large-scale EESs, due to the nonlinearity and complexity. The centralized-type approaches require the information of the overall system that is usually hard to get. Besides, checking the stability conditions in a centralized manner often requires huge computational resources. For a complex EES, this is still true even with tools [15–17] developed for speeding up the numerical computation.

Unlike above mentioned centralized-type approaches, almost all the modular-type methods turn an interconnected system into a feedback configuration with two subsystems H_N and H_S. The structure is shown in Figure 1-2. Then, the problem becomes to analyze the subsystems' properties and their interconnection. Notably, we are not covering all the literature. What we listed below are several milestones which inspire us on developing the proposed approach.

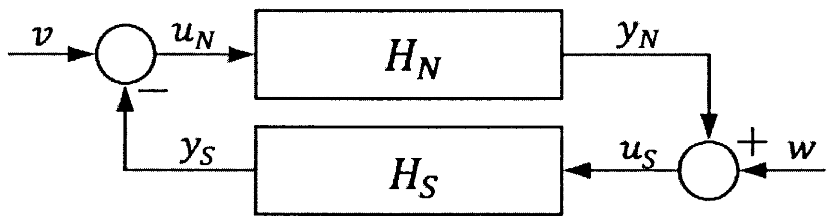

Figure 1-2: A feedback configuration

1.2.1 Lyapunov theory-based approach

The first milestone utilizes the theory of Lyapunov functions. One approach is to design competitive control so that couplings between stable subsystems are weaker than the couplings which are internal to each subsystem [18–20].

Another approach is to analyze input-output properties of subsystems in time domain [21–23], or in frequency domain (circle criterion and Popov criterion) [24–28]. In particular, Lur'e proposed a special form for a group of nonlinear uncertain dynamical systems [29]. Hereafter, there is sizable literature dealing with the stability of Lur'e system [30–32].

Notably, one common challenge of the Lyapunov theory-based approach is how to find proper candidate Lyapunov functions. [33–35] focus on constructing Lyapunov functions under specific assumptions. But there is no systematic method for deriving the least-conservative Lyapunov function for a general nonlinear system.

1.2.2 Small-gain theorem-based approach

Small-gain theorem has been instrumental for the stability analysis and control design of interconnected systems since early 1960 [36]. Explanation and examples of the classical small-gain theorem can be found in the textbook [11]. As a nonlinear generalization and powerful tool, the concept and examples of input-to-state stability (ISS) small-gain theorem can be found in the textbook [37]. The survey paper [38] provides a good road map if readers are interested in the theory evolution. [38] has many references on hybrid systems, delayed systems, discrete switched systems, etc.

1.2.3 Passivity/Dissipativity theory-based approach

The notion of passivity/dissipativity has its root in the fundamental property of any physical system, as the phenomenon of loss of energy can be observed everywhere. The innovative two part papers [39, 40] formally introduce the dissipativity to the field of control theory. It opens a new energy perspective for stability analysis and control synthesis, i,e., to look into the physics. The dissipativity/passivity becomes an active research topic ever since [41–44].

We emphasize below two functions associated with the dissipativity/passivity, as they will be frequently used in this thesis.

- *Storage function* $V(x)$: the amount of energy stored in the system
- *Supply rate* $w(u, y)$: the rate of energy flow (into the system)

For a dissipative system, the increase in $V(x)$ is not greater than the $w(u, y)$. In addition, the system cannot store more energy than the total supply from the outside. The relation between $V(x)$ and $w(u, y)$ is called dissipation inequality. It should be noted that the passive system is a special case of the dissipative system with supply rate defined as $w(u, y) = u^T y$.

As pointed out by [44–46], dissipativity is *invariant* under parallel and negative feedback interconnection. Thus, it is naturally to extend the passivity and dissipativity results from standalone components to interconnected systems. In addition, the storage function $V(x)$ is closely related to stability. A dissipative or passive system with a positive definite storage function V(x), under mild conditions, can be proved to be stable in the sense of Lyapunov. The storage function $V(x)$ can be viewed as a candidate Lyapunov function.

Motivated by KYP lemma [47, 48], [45, 46] and the references therein provide a way to numerically check the dissipativity of both components and interconnected systems with quadratic supply rate function $w(u, y)$. It has been shown that finite gain stability, small gain theorem and passivity theorem are special cases with supply rate functions written in particular forms. Recently, along the same line, some extensions have been made for incremental case and equilibrium independent case [44, 49–51]. In this thesis, we are going to utilize the passivity concept, and think the problem in terms of energy and power.

1.2.4 Integral quadratic constraints (IQC)-based approach

[52] introduces a unified approach, integral quadtratic constraints (IQCs), to robust analysis by characterizing input-output properties of systems. It was first introduced to analyze the stability of an interconnection of a linear system in feedback with another causal but maybe nonlinear or even uncertain system. Figure 1-2 is the main structure considered in the IQC framework.

Notably, IQC greatly simplifies the analysis and transforms the stability problem into a numerical tractable optimization. A family of IQC functions as well S-procedure are proposed by [52] which forms the basis for stability analysis and control design for interconnected systems. However, the original IQC is formulated in the frequency domain. The link between the time domain and the frequency domain notions is established in [53] using the KYP LMI. In addition, reconciling the IQC and dissipativity theory is still an active area, some partial results can be found in [54, 55].

1.3 Brief literature review of relevant electrical energy system concepts

The purpose of this section is to review the existing control methods for EESs. We organize the section into two parts: the first part reviews the relevant control design for DERs, and the second part reviews the control design for large-scale EESs. Generally speaking, most of control methods focus on generation units, synchronous machines (SM) in particular. The stability of interconnected systems is determined using off-line small signal analysis.

1.3.1 Control design for DERs

The commonly-used primary controllers of DERs are constant-gain control tuned for predefined operating conditions, such as the PID control.

Thanks to the advancements and maturity of power electronic-controlled hardware, recent research efforts have aimed at utilizing these fast controllers. Droop-based control by imposing virtual impedance is widely used inside the controllers of DERs [2,56]. It is simple in implementation, but the performance heavily depends on the accuracy of line parameters. Voltage deviations and current sharing errors still exist in practice. Also, there is no guarantee for stability as the negative incremental resistance occurs [57].

To improve the robustness and flexibility, nonlinear control designs have been also proposed [58–61]. However, most of them require a high gain which may lead to control saturation when large disturbances occur. As a result, these techniques generally do not ensure that voltage remains within the acceptable bounds. To overcome this problem, model predictive control (MPC) is proposed in [62, 63]. But MPC generally requires significant computational effort, which may not be implementable for a large-scale EES.

Another promising approach is to utilize energy related concepts, such as energy-based control [64, 65], passivity-based control [66]. In this thesis, we follows this approach. Building on the existing work, we propose a novel distributed control for components.

1.3.2 Control design for large-scale electrical energy systems

In order to ensure the stability of a large scale EES, one approach is to conduct the stability analysis on the quasi-static or steady state model derived for a particular operating point. Tools like PV curves, critical clearance time, etc. [67, 68] are used. However, these approaches are restricted by the static or quasi-static models.

The second approach is to use singular perturbation techniques [69] so that a fast and a slow-reduced order model can be derived and used. For example, [70, 71] introduces a coherency-based method for the analysis of an electrical energy system. Machines are aggregated into several groups based on the strength of the coupling. Each group is represented by an equivalent machine, since the machines comprising a group are with close electrical connections; [72] introduces the centers of inertia (COIs) concept to simplify the stability analysis of an electrical energy system; [73] considers the frequency dynamics with sustained high oscillations; [74] gives a centralized Lyapunov method to check the stability of an electrical energy systems.

Besides above mentioned model-based analytic methods, The third approach for the stability analysis is based on signal processing techniques [75–77]. Note that these methods are designed for the small signal model, which may not be valid if large disturbances occur.

The fourth approach is through the local decentralized competitive control design [31, 58, 78, 79]. Based on the vector lyapunov method, [80] introduces a multi-layered control design framework for the small signal frequency dynamics of an electrical energy systems. Such control design framework ensures the system-level stability by minimizing unstable interactions. However, most of existing approaches focus on slow time scale dynamics, known and fixed topologies and predefined operating modes. For general electrical energy systems, distributed control design for ensuring the expected quality of service (QoS) remains a major challenge.

The fifth approach is to utilize the previously mentioned modular-type system theory. Right now, they have had limited applications in EESs, especially when detailed dynamical models are used. This is mainly because of the inherent nonlinearity and complexity of electrical energy systems. [81] summarizes partial small-gain theorem-based and passivity-based results. However, all of these stability criteria are proposed for simple systems like DC electrical energy systems, standalone components, etc. More recently, plug and play operation is introduced based on the simplified linear model or the linearized model neglecting the network dynamics in [82–84]. However, the line inductance and load dynamics are sources of instability, thus cannot be neglected [85]. To consider general EESs, the author proposes a solution for plug and play operation with the provable performance in [86]. Such modular approach forms the basis of this thesis. We will discuss it in detail.

1.4 Thesis contributions

In this thesis we makes four contributions:

1. We propose a modular modeling approach that represents a general EES as a negative feedback configuration comprising a planar electrical network subsystem H_N and a subsystem H_S of single-port components. We propose a new input-output pair (P and $\dot{V}/V$) for each component enabling a novel incremental passivity using transformed state space (TSS) model. The TSS model is suitable for designing nonlinear controllers for EESs so that power produced/consumed and the rate of change of the terminal voltage are controlled. This thesis provides examples of such unifying controllers, including electrical machines, and inverter-based control of batteries and solar PVs.

2. We propose control specifications under which an EES is stable and feasible. On the one hand, for the stability requirements, we apply the passivity theorem known for negative feedback architecture to establish a set of input-output specifications for subsystems. On the other hand, for the feasibility requirements, we define an additional set of conditions under which we can connect different

components. Notably, these feasibility conditions are given in terms of input, output and initial condition bounds of each stand-alone component assuming disturbances and control saturations are known and bounded. A two-bus system is used as an example to show the concept.

3. We propose a multi-layered distributed control using the TSS model so that the above incremental passivity conditions and feasibility conditions (in terms of P and $\dot{V}/V$) are met. The AEES implementation for systems with all controlled modules is enabled through their interactive information exchange. Components of H_S adjust their output interactively to ensure that the output of components in H_N remain within the assumed bounds. This feature is fundamental to the autonomy of such interconnected system. We numerically show on simple system examples these interactive adjustments by the components. Then, we evaluate the effectiveness of the proposed control on microgrids. It is shown that our proposed control enables autonomous reconfigurable operations.

4. The modular modeling and control approach introduced in this thesis is scalable. While more work remains to fully develop this, we illustrate the possible way forward by considering the problem of enhanced automatic generation control (E-AGC) for systems with highly dynamic load variations. A multi-layered yet simplified extension of the negative feedback configuration modeling is proposed for each sub-system; each subsystem interacts with the neighboring subsystems. We show using simulations that potential instabilities between subsystems can be eliminated using nonlinear control introduced for small single systems. As a topic for future work, it is fundamentally possible to generalize the approach proposed for a single level system and to define conditions for provably stable multi-layered E-AGC.

1.5 Thesis outline

The remainder of this thesis is organized as follows.

In Chapter 2, we propose a negative feedback modeling approach.

In Chapter 3, we first introduce the modular (component-level) specifications. Then, we propose a distributed nonlinear control which ensures the modular specifications are met.

In Chapter 4, we introduce the system-level specifications further imposed on operating ranges of components so that the interconnected system is feasible. We introduce a handshaking method for implementing iterative interaction of components so that system-level feasibility is implemented.

In Chapter 5 and Chapter 6, we provide examples of the proposed control. Moreover, we evaluate the effectiveness of the proposed controller utilizing microgrid systems.

In Chapter 7, we provide an extension of the proposed modeling and control approach to large-scale EESs. The problem of enhanced automatic generation control (E-AGC) for systems with highly dynamic load variations is considered.

In Chapter 8, we conclude the thesis, and provide several possible future research directions.

Chapter 2

Modular modeling of electrical energy systems: A feedback configuration approach

2.1 Introduction

The primary purpose of this chapter is to introduce a novel mathematical model for EESs.

In electrical energy systems, numerous modeling approaches have been proposed for stability analysis, operation planing and control design. One main principle is that the appropriate model should be able to capture the dynamics of interest. In particular, the simple models are preferred for the sake of analytical tractability and scalability.

The model used for control design is often derived under strong assumptions, such as ignoring the electromagnetic dynamics [68]. This assumption is currently mainly satisfied through careful equipment sizing and network parameter design [87]. For example, the synchronous machine model introduced in [68, 88] neglects the stator current and voltage dynamics, on the basis that the rotor speed evolves at a much slower time scale. However, fast dynamics may no longer be negligible, especially for the changing electric power systems with lots of renewable energy integration, as they are expected to operate in qualitatively different operating modes as well as during large disturbances caused by intermittent resources. Therefore, there arises a need for new modeling methods which can reflect both the temporal and spatial complexities of electrical power systems.

To address the above modeling challenges, we propose a novel modular modeling approach. More specifically, the proposed modeling approach represents the system in a negative feedback configuration which lends itself suitable for system control theories. Recall that the major challenge of operating an EES is to control the power produced/consumed and the rate of change of the terminal voltage. We next propose a new input-output pair for each component, leading to a transformed state space (TSS) model with a novel incremental passivity.

2.1.1 Chapter outline

The chapter is organized as follows. We first introduce a few concepts and assumptions in Section 2.2, as they form the basis for the proposed modular modeling approach. Next, we present the proposed modular modeling approach in Section 2.3. Two standard state space models for EESs are derived in Section 2.3.2 and Section 2.3.3, respectively. In particular, the new input-output pair and the corresponding model are introduced in Section 2.3.3. Typical components and system examples are illustrated as examples. Then, we discuss the new incremental passivity associated with the proposed model in Section 2.4.

2.2 Component types and modeling assumptions

Components comprising electrical energy systems can be classified as either the single-port component or the two-port component. The definitions of these two component types are stated below.

Definition 2.2.1 (Single-port component [89]). *Components that have only one port are belonging to the single-port component class.*

Definition 2.2.2 (Two port component [89]). *Components that have two ports are belonging to the two-port component class.*

Fo example, synchronous machines and loads are single-port components, while electrical wires are two-port components. Visual representation of a single-port component and a two-port component is shown in Figure 2-1.

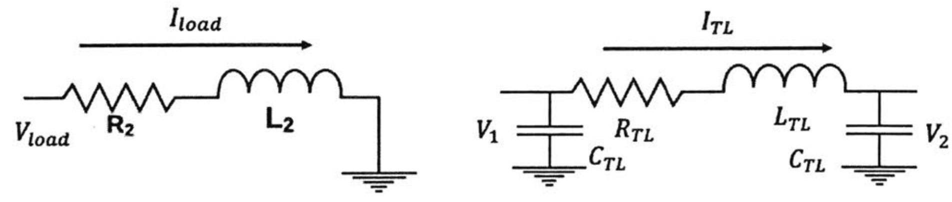

(a) RL load (b) Transmission line

Figure 2-1: Visual representation of single and two-port component

There are three modeling assumptions in this thesis:

Assumption 2.2.1 (modeling rule). *All components of electrical power systems are modeled using lumped parameter dynamic models [88].*

Assumption 2.2.1 implies that the dynamics of each component can be expressed in the following standard state space form [90]:

$$\dot{x} = f(x, c, u) \qquad y = h(x, c, u) \tag{2.1}$$

where x is the vector of state variables; y is the vector of output variables; c is the vector of controllable inputs; u is the vector of port inputs determined by its connection with the rest of the system.

Assumption 2.2.2 (connection rule). *Single-port components only connect to two-port components.*

Consider an electrical energy system consisting of a distributed energy resource (DER) and a load. Assumption 2.2.2 implies that the DER and the load are connected with each other via an electrical wire.

Assumption 2.2.3 (model structure). *Two-port components have a capacitor at their port interfaces.*

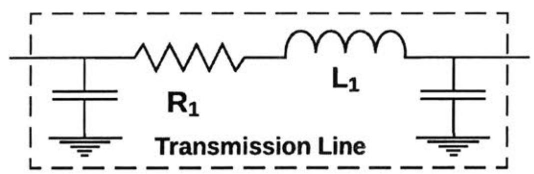

Figure 2-2: Visual representation of an electrical wire component

On the one hand, Assumption 2.2.3 implies that the topology of an electrical wire has the structure shown in Figure 2-2, so-called π model. In this thesis, we assume that all electrical wires are modeled by such lumped π model (Figure 2-2) [68]. On the other hand, as discussed in [90], Assumption 2.2.3 eliminates the inductor cut-set issue at the cost of increasing the model complexity.

2.3 Proposed modular modeling approach

In this section, we present a modular modeling approach, which leads to a model with a negative feedback configuration. The obtained model has an electrical network subsystem H_N and a subsystem H_S with all single-port components.

To simplify the notations, in what follows, we leave physical interpretations aside temporarily. Two standard state space models with different input-output pairs are derived next in Section 2.3.2 and Section 2.3.3.

2.3.1 Modular modeling procedure

To illustrate the concept, the proposed modular modeling approach is visualized in Figure 2-3 and Figure 2-4. Figure 2-3 shows the physical topology of an electrical energy system, while Figure 2-4 graphically shows the structure of the obtained model. It is clear that the obtained model (Figure 2-4) has a feedback configuration. The general procedure is explained as follows: We first define the input and output for the single-port and the two-port component group. Next, we derive the dynamic model of each component in two groups, which further provides us the dynamic model of each subsystem (2.7). As the last step, we define the interconnection between two subsystems and connect their dynamics following (2.8).

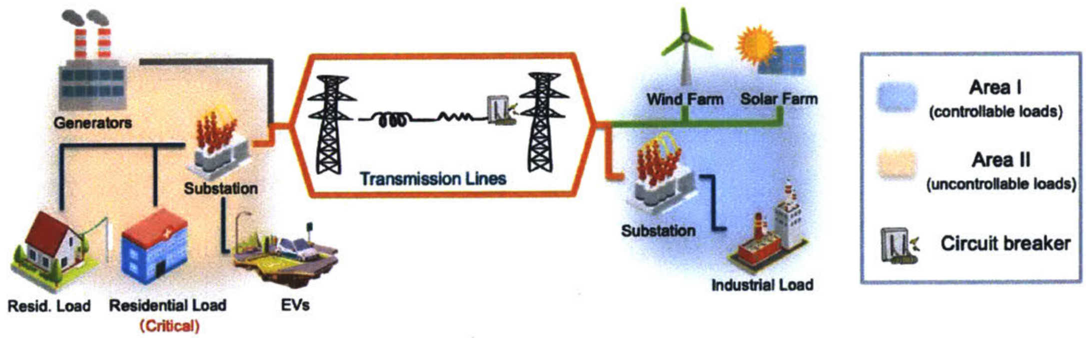

Figure 2-3: An electrical energy system: Area I and Area II are connected via the transmission network. Each area has different generation units and loads

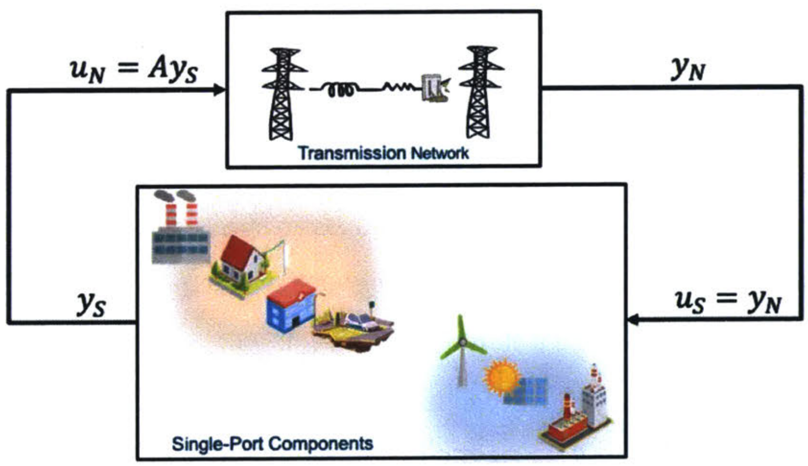

Figure 2-4: Visualization of the obtained model with feedback configuration: all transmission lines are in the upper subsystem, while all single-port components are in the lower subsystem

Next, we show how to mathematically express the above modeling procedures. As the first step, we define a few notations:

To differentiate different component type, we introduce three index sets, namely a node (bus) set $\mathcal{N} = \{1, ..., N_0\}$, a single-port component set $\mathcal{N}_{one} = \{1, ..., N_1\}$ and a two-port component set $\mathcal{N}_{two} = \{1, ..., N_2\}$.

Besides, we define the following functions that map $\mathcal{N}_{one}$ and $\mathcal{N}_{two}$ to $\mathcal{N}$:

$$\begin{aligned} M_S : N_i \in \mathcal{N}_{one} \rightarrow N_j \in \mathcal{N} \\ M_{N,L} \,\&\, M_{N,R} : N_i \in \mathcal{N}_{two} \rightarrow N_j \in \mathcal{N} \end{aligned} \tag{2.2}$$

M_S provides the node index at which a single-port component connects. $M_{N,L}$ and $M_{N,R}$ provide the node indexes to which the left and the right port of a two-port component connect, respectively.

Similarly, we also define the inverse mappings that provide the indexes of all connected component for the given node N_i:

$$\begin{aligned} M_S^{-1} : N_i \in \mathcal{N} \rightarrow \{1, ..., N_m\} \subseteq \mathcal{N}_{one} \\ M_{N,L}^{-1} : N_i \in \mathcal{N} \rightarrow \{1, ..., N_{nL}\} \subseteq \mathcal{N}_{two} \\ M_{N,R}^{-1} : N_i \in \mathcal{N} \rightarrow \{1, ..., N_{nR}\} \subseteq \mathcal{N}_{two} \end{aligned} \tag{2.3}$$

These mappings define the network topology.

In what follows, we use x_i, y_i, c_i and u_i to denote state variables, output variables, control input and external input variables, respectively. Subscript $i = \{S, N\}$ denotes the single-port or the two-port component group. In particular, for two-port component $j \in \mathcal{N}_{two}$, its input and output are $u_{N,j} = [u_{N,jL}, u_{N,jR}]^T$ and $y_{N,j} = [y_{N,jL}, y_{N,jR}]^T$.

As the second step, we derive the dynamics of single-port and two-port components, respectively. The dynamics of single-port component $j \in \mathcal{N}_{one}$ is:

$$\begin{aligned} \dot{x}_{S,j} &= f_{S,j}(x_{S,j}, c_{S,j}, u_{S,j}) = L^x_{S,j} f_S(x_S, c_S, u_S) \\ y_{S,j} &= h_{S,j}(x_{S,j}, c_{S,j}, u_{S,j}) = L^y_{S,j} h_S(x_S, c_S, u_S) \end{aligned} \tag{2.4}$$

where

$$x_{S,j} = L^x_{S,j} x_S \qquad c_{S,j} = L^c_{S,j} c_S \qquad u_{S,j} = L^u_{S,j} u_S \qquad y_{S,j} = L^y_{S,j} y_S \tag{2.5}$$

$x_{S,j}$, $c_{S,j}$, $u_{S,j}$ and $y_{S,j}$ are component's states, control input, external input and output, respectively. L^*_* is an operator. $x_{S,j} = L^x_{S,j} x_S$ implies that $x_{S,j}$ is part of x_S.

Similarly, the dynamics of two-port component $j \in \mathcal{N}_{two}$ is:

$$\begin{aligned} \dot{x}_{N,j} &= f_{N,j}(x_{N,j}, c_{N,j}, u_{N,j}) = L^x_{N,j} f_N(x_N, c_N, u_N) \\ y_{N,j} &= h_{N,j}(x_{N,j}, c_{N,j}, u_{N,j}) = L^y_{N,j} h_N(x_N, c_N, u_N) \\ where \;\; x_{N,j} &= L^x_{N,j} x_N \qquad c_{N,j} = L^c_{N,j} c_N \\ u_{N,j} = L^u_{N,j} u_N &+ \sum_{k_L} L^{x_k}_{N,j} x_{N,k_L} + \sum_{k_R} L^{x_k}_{N,j} x_{N,k_R} \quad y_{N,j} = L^y_{N,j} y_N \end{aligned} \tag{2.6}$$

k_L and k_R are two index sets defined as:

$$k_L \in \{M^{-1}_{N,L} \circ M_{N,L}(j) \cup M^{-1}_{N,R} \circ M_{N,L}(j)\} \qquad k_R \in \{M^{-1}_{N,L} \circ M_{N,R}(j) \cup M^{-1}_{N,R} \circ M_{N,R}(j)\}$$

Therefore, we can model the single-port subsystem H_S and the network subsystem H_N in the standard state space form as:

$$\begin{aligned} \dot{x}_S = f_S(x_S, c_S, u_S) \qquad y_S = h_S(x_S, c_S, u_S) \qquad u_S \in \mathbb{R}^{N_0} \; y_S \in \mathbb{R}^{N_1} \\ \dot{x}_N = f_N(x_N, c_N, u_N) \qquad y_N = h_N(x_N, c_N, u_N) \qquad u_N \in \mathbb{R}^{N_0} \; y_N \in \mathbb{R}^{N_0} \end{aligned} \tag{2.7}$$

Now, we have introduced the dynamic models of subsystem H_S and H_N. As the last step, to connect H_S and H_N, we define the interconnection between two subsystems as:

$$u_N = A y_S \qquad u_S = y_N \tag{2.8}$$

where incident matrix A is N_0-by-N_1 and its element is:

$$A_{ij} = \begin{cases} 1 & \text{single-port component } j \text{ connects to node } i = M_S(j) \\ 0 & otherwise \end{cases} \tag{2.9}$$

Notably, since the components of electrical energy systems are designed for a predefined operating region, there are additional constraints need to be modeled.

Considering component i, we have:

$$c_i(t) \in \Phi_{c,i} \qquad u_i(t) \in \Phi_{u,i} \quad i \in \{\mathcal{N}_{one} \cup \mathcal{N}_{two}\} \qquad \forall\ t \tag{2.10}$$

$\Phi_{c,i}$ is the feasible control set; $\Phi_{u,i}$ denotes the predefined operating region. In this thesis, we assume that Φ_{c_i} and Φ_{u_i} are given and bounded.

Hence, we obtain the interconnected system model:

$$(2.7),\ (2.8),\ (2.10) \tag{2.11}$$

Notably, when we consider the physical meaning of (x_i, y_i, c_i, u_i), we could have different dynamic models even though they share the same mathematical form (2.7) and (2.8). In the following sections, we provide two dynamical models derived using different input-output pairs.

2.3.2 V-I state space model

For single-port component i, we choose its input and output as:

$$u_{S,i} = V_{S,i} \qquad y_{S,i} = I_{S,i} \qquad i \in \mathcal{N}_{one} \tag{2.12}$$

where $V_{S,i}$ denotes the instantaneous voltage. $I_{S,i}$ denotes the instantaneous current.

Hence, the component dynamics has the form:

$$\dot{x}_{S,i} = f_{S,i}(x_{S,i}, c_{S,i}, u_{S,i}) \qquad y_{S,i} = C_{S,i}x_{S,i} \tag{2.13}$$

where $x_{S,i} = [x_{i,int}, I_{S,i}]^T$ and $C_{S,i} = [\mathbf{0}_{1\times m}, 1]$. $x_{i,int} \in \mathbb{R}^m$ denotes the internal states.

For two-port component j, we can choose its input and output as:

$$u_{N,j} = [I_{j,L}, I_{j,R}]^T \qquad y_{N,j} = [V_{j,L}, V_{j,R}]^T \qquad j \in \mathcal{N}_{two} \tag{2.14}$$

where subscript L and R denote the left and right port, respectively. $I_{j,L/R}$ is instantaneous current injection. $V_{j,L/R}$ is instantaneous voltage.

The component dynamics has the form:

$$\dot{x}_{N,j} = f_{N,j}(x_{N,j}, c_{N,j}, u_{N,j}) \qquad y_{N,j} = C_{N,j} x_{N,j} \tag{2.15}$$

where $x_{N,j} = [x_{j,int}, V_{j,L}, V_{j,R}]^T$ and $C_{N,j} = diag(\mathbf{0}_{2\times m}, \mathbf{I}_{\mathbf{d}2\times 2})$. $x_{j,int} \in \mathbb{R}^m$ denotes the internal states.

To better illustrate the concept, we consider a RL load and a transmission line as examples. Their topologies are shown in Figure 2-1(a) and Figure 2-1(b), respectively. The dynamic model for each component is listed below.

Example 2.3.1 (RL load [91]). *We choose instantaneous current I_{load}, terminal voltage V_{load} as the state variable and the input, respectively. I_{load} is chosen as the output. The dynamic model is:*

$$L_2 \dot{I}_{load} = -R_2 I_{load} + u_{load} \qquad u_{load} = V_{load} \quad y_{load} = I_{load} \tag{2.16}$$

Example 2.3.2 (Transmission line [91]). *We choose port voltages (V_1, V_2) and current I_{TL} as the state variables. Current injected from both ports (I_{left}, I_{right}) and port voltages (V_1, V_2) are chosen as the input and the output, respectively. The dynamic model is:*

$$\begin{gathered} L_{TL}\dot{I}_{TL} = -R_{TL}I_{TL} + V_1 - V_2 \quad C_{TL}\dot{V}_1 = -I_{TL} + I_{left} \quad C_{TL}\dot{V}_2 = I_{TL} + I_{right} \\ u_{TL} = [I_{left}, I_{right}]^T \qquad y_{TL} = [V_1, V_2]^T \end{gathered} \tag{2.17}$$

where u_{TL} and y_{TL} are input and output, respectively.

Next, based on the topology, we define the mapping functions (2.2) and (2.3). Besides, we could construct the incident matrix A required by (2.8). Therefore, the interconnected system model can be obtained by connecting two subsystems. Notably, in this case, voltage V and current I are the interface between single-port and two-port components.

2.3.3 Transformed state space (TSS) model

In this section, we propose a new set of input-output pair for single-port and two-port components, aiming to reflect the dynamics of energy conversion. Because we observe that all electrical energy systems are driven by the energy conversion taking place inside and between components. To control the electrical energy system, it is important to capture then control the interactions.

For single-port component i, $i \in \mathcal{N}_{one}$, the new input-output pair is:

$$\begin{aligned} u_{S,i} &= \dot{V}_{S,i}/V_{S,i} \quad & y_{S,i} &= P_{S,i} \qquad & when\ V_{S,i} \neq 0 \\ u_{S,i} &= \dot{V}_{S,i} \quad & y_{S,i} &= I_{S,i} \qquad & when\ V_{S,i} = 0 \end{aligned} \tag{2.18}$$

where $\dot{V}_{S,i}/V_{S,i}$ is the normalized rate of voltage. $P_{S,i}$ denotes the instantaneous power.

Since

$$\int_0^t (\dot{V}_{S,i}/V_{S,i}) d\tau = \ln \frac{V_{S,i}(t)}{V_{S,i}(0)} \tag{2.19}$$

we have:

$$V_{S,i}(t) = V_{S,i}(0) e^{\int_0^t (\dot{V}_{S,i}/V_{S,i}) d\tau} = V_{S,i}(0) e^{\int_0^t u_{S,i} d\tau} \tag{2.20}$$

It can be seen that the input of V-I state space model can be represented as function of $\dot{V}_{S,i}/V_{S,i}$. Hence, we can derive a new dynamical model by substituting (2.20) into (2.13).

An alternative way of deriving the dynamical model is via coordinate transformation. Output $y_{S,i}$ is chosen as a state variable. In addition, we add the controller dynamics. We call such an augmented model a transformed state space model of component i:

$$\dot{x}_{S,i} = f_{S,i}(x_{S,i}, \xi_{S,i}, u_{S,i}) \quad y_{S,i} = h_{S,i}(x_{S,i}, \xi_{S,i}, u_{S,i}) \qquad x_{S,i} = [x_{i,int}, c_{S,i}, y_{S,i}]^T \tag{2.21}$$

where new control input $\xi_{S,i} \in \mathbb{R}^k$ determines the rate of $c_{S,i}$.

Notably, there are two cases when we define input $u_{S,i}$. When $V_{S,i} \neq 0$, $x_{S,i}$

dynamics has the form:

$$\begin{aligned}
\dot{x}_{int,i} &= f_{S,i}(x_{int,i}, P_{S,i}) \\
\dot{P}_{S,i} &= -(k_1 - u_{S,i})P_{S,i} + g_{S,i}(P_{S,i}, u_{S,i})c_{S,i} \\
\dot{c}_{S,i} &= \xi_{S,i}
\end{aligned} \tag{2.22}$$

where k_1 represents the damping coefficient.

When $V_{S,i} = 0$, $u_{S,i} = \dot{V}_{S,i}$. $x_{S,i}$ dynamics becomes:

$$\begin{aligned}
\dot{x}_{int,i} &= f_{S,i}(x_{int,i}, P_{S,i}) \\
\dot{P}_{S,i} &= -k_1 P_{S,i} - Q_{S,i} \\
\dot{c}_{S,i} &= \xi_{S,i}
\end{aligned} \tag{2.23}$$

where $Q_{S,i} = -\dot{V}_{S,i}I_{S,i} + \dot{I}_{S,i}V_{S,i}$ denotes the instantaneous reactive power [92]. Recall that $I_{S,i}$ can be approximated from:

$$L\dot{I}_{S,i} = -RI_{S,i} + V_{S,i} - c_{S,i} \qquad V_{S,i} = V_{S,i}(0)e^{\int_0^t u_{S,i}d\tau} \tag{2.24}$$

It can be seen from (2.23) that single-port component i is uncontrollable when $V_{S,i} = 0$. Because $c_{S,i}$ cannot affect $P_{S,i}$ dynamics.

For two-port component j, we choose its input and output as:

$$\begin{aligned}
u_{N,j} = [P_{j,L}, P_{j,R}]^T \quad P_{j,L} = I_{j,L}V_{j,L} \quad P_{j,R} = I_{j,R}V_{j,R} \qquad j \in \mathcal{N}_{two} \\
y_{N,j} = [\dot{V}_{j,L}/V_{j,L}, \dot{V}_{j,R}/V_{j,R}]^T \quad when\ V_{j,R} \neq 0 \quad V_{j,L} \neq 0
\end{aligned} \tag{2.25}$$

where subscript L and R denote the left and right port, respectively. $I_{j,L/R}$ is the instantaneous current injection. $V_{j,L/R}$ is the instantaneous voltage.

Regarding the dynamical model of two-port component j, we can modify (2.15) with the new input-output pair. This new model has the following general form:

$$\dot{x}_{N,j} = f_{N,j}(x_{N,j}, c_{N,j}, u_{N,j}) \qquad y_{N,j} = h_{N,j}(x_{N,j}, c_{N,j}, u_{N,j}) \tag{2.26}$$

where $x_{N,j} = [V_{j,L}, V_{j,R}, I_{N,j}]$ is the state variable.

Remark 2.3.1. *When instantaneous voltage $V_{j,L} = 0$ or $V_{j,R} = 0$, we define the corresponding output as $\dot{V}_{j,L}$ or $\dot{V}_{j,R}$ to avoid infeasibility. In this case, the input becomes the current injection, $u_{N,j} = [I_{j,L}, I_{j,R}]^T$.*

In what follows, we revisit the RL load and the transmission line examples. The proposed model for each component is given. Their topologies and notations are shown in Figure 2-5(a) and Figure 2-5(b).

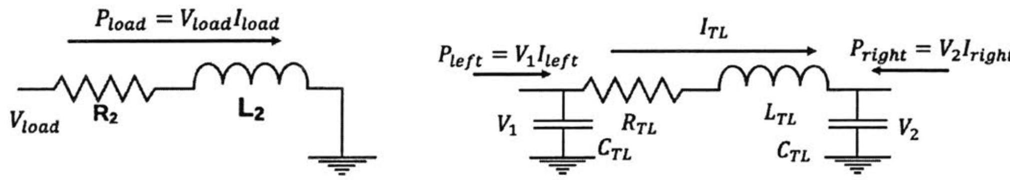

(a) RL load

(b) Transmission line

Figure 2-5: Typical single-port and two-port components

Example 2.3.3 (RL load [91]). *As shown in Figure 2-5(a), we choose instantaneous power $x_{load} = P_{load}$ as the state variable and relative terminal voltage rate $u_{load} = \dot{V}_{load}/V_{load}$ as the input.*

When $V_{load} \neq 0$, the transformed state space model of the RL load is:

$$\begin{aligned} \dot{x}_{load} &= -\frac{R_2}{L_2} x_{load} + x_{load} u_{load} - \frac{V_{load}^2}{R} u_{load} \\ y_{load} &= \frac{R_2}{L_2} x_{load} = \frac{R_2}{L_2} P_{load} \end{aligned} \tag{2.27}$$

where $V_{load} = V_{load}(0) e^{\int_0^t u_{load} d\tau}$.

When $V_{load} = 0$, the transformed state space model is:

$$\begin{aligned} \dot{x}_{load} = -\frac{R_2}{L_2} x_{load} + I_{load} u_{load} \qquad \dot{I}_{load} = -\frac{R_2}{L_2} I_{load} \\ y_{load} = I_{load} \end{aligned} \tag{2.28}$$

Example 2.3.4 (Transmission line [91]). *As shown in Figure 2-5(b), state variable is $x_{TL} = [V_1, V_2, I_{TL}]^T$. When V_1 and V_2 are not zero, input and output are $u_{TL} =$*

$[P_{left}, P_{right}]^T$ and $y_{TL} = [\dot{V}_1/V_1, \dot{V}_2/V_2]^T$.

The transformed state space model is:

$$\begin{aligned} C_{TL}\dot{V}_1 &= -I_{TL} + \frac{1}{V_1}P_{left} \\ C_{TL}\dot{V}_2 &= I_{TL} + \frac{1}{V_2}P_{right} \\ L_{TL}\dot{I}_{TL} &= -R_{TL}I_{TL} + V_1 - V_2 \\ u_{TL} = [P_{left}, P_{right}]^T &\quad y_{TL} = [\dot{V}_1/V_1, \dot{V}_2/V_2]^T \end{aligned} \tag{2.29}$$

When $V_1 = 0$, the transformed state space model becomes:

$$\begin{aligned} C_{TL}\dot{V}_1 &= -I_{TL} + I_{left} \\ C_{TL}\dot{V}_2 &= I_{TL} + \frac{1}{V_2}P_{right} \\ L_{TL}\dot{I}_{TL} &= -R_{TL}I_{TL} + V_1 - V_2 \\ u_{TL} = [I_{left}, P_{right}]^T &\quad y_{TL} = [\dot{V}_1, \dot{V}_2/V_2]^T \end{aligned} \tag{2.30}$$

Similar model can be derived for the case when $V_2 = 0$. We omit the derivation for brevity.

Now, we have introduced the TSS model for the single-port and two-port component. Next, we define the mapping functions (2.2), (2.3) and incident matrix A based on the given topology. Therefore, the interconnected system model can be obtained by connecting two subsystems. Notably, utilizing the TSS model, voltage deviation $\dot{V}/V$ and power P are the interface between single-port and two-port components.

Remark 2.3.2. *Three-phase balanced instantaneous voltage V becomes $[V_d, V_q]^T$ if it is modeled in the rotating reference frame. In the rotating reference frame, $u_{S,i}$ and $y_{N,i}$ become $[\frac{\dot{V}_i}{V_i}, \omega_i]^T$. $y_{S,i}$ and $u_{N,i}$ become $[P_i, Q_i]^T$. Here, $\frac{\dot{V}_i}{V_i}$ represents the relative voltage magnitude change. So there is no need to explicitly consider $V_i = 0$ case. ω_i represents the frequency distortion. P_i and Q_i are the real and reactive power in the rotating reference frame. We design the control using such rotating reference frame. More examples will be given in the following chapters.*

2.4 Benefits of using the TSS model

Voltage and current are widely used as the input-output pair for components of electrical enregy systems, due to many good properties. For example, it is well-known that a RLC circuit is passive with respect to voltage and current [11]. However, voltage and current (V-I) pair has its limitations.

From the control perspective, the V-I pair is not good in designing passivity-based control, due to the dissipation obstacle issue [43]. Hence, [93–95] and many other works propose different input-output pairs under different assumptions.

From the practical perspective, the V-I pair may create a gap between the control design and existing unit-testing standards of EESs. Note that existing unit-testing standards use the power change as the test input and then define the maximum voltage deviation as the specifications. MIL-STD-1332B, for example, lists the voltage and frequency limits for each generator type under the fixed power rating and the fixed power changes. Hence, the gap arises because we are designing the controller in the voltage and current (V-I) space but testing it in power and voltage (P-V).

We think the proposed input-output pair is one of such kinds to overcome above issues. We list three benefits of the proposed model.

First, the proposed input-output pair provides more practical insights in control design and unit-testing. Notice that (2.18) and (2.25) are in terms of power deviation and normalized voltage rate. Thus, it is aligned with existing power and voltage specifications of unit-testing standards.

Second, the proposed models (2.21) and (2.26) enable us to have meaningful modular specifications. We can propose modular specifications on the input and the output of each component, which are in terms of power deviations and voltage deviations. Thus, these specifications do not rely on the test system, which is more general than existing unit-testing standards.

Last but not the least, the new input-output pair preserves a novel incremental passivity which avoids the dissipation obstacle issue. We will show the incremental passivity using two examples in the following section.

2.4.1 New incremental passivity concept

In this section, we present the new incremental passivity associated with with (2.18) and (2.25). Figure 2-5(a) and Figure 2-5(b) examples are used to show the concept. The main claims are summarized in the following two lemmas.

Lemma 2.4.1. *RL load is output strictly equilibrium-independent passive.*

Lemma 2.4.2. *Under assumption 2.2.3, transmission line is output strictly equilibrium-independent passive.*

Proof for Lemma 2.4.1. The TSS model is given in Example 2.3.3. To show the EIP, we first introduce the equilibrium:

$$I_{load}^* = \frac{V_{load}}{R_2} \qquad u^* = 0 \qquad P_{load}^* = \frac{V_{load}^2}{R_{load}} \tag{2.31}$$

Then, if we choose a storage function:

$$W = \frac{1}{2}R(I_{load} - I_{load}^*)^2 \tag{2.32}$$

we have:

$$\dot{W} = -R(I_{load} - I_{load}^*)^2 - \frac{L}{R}\frac{\dot{V}_{load}}{V_{load}}(P - P^*) \leq uy$$

This completes the proof. □

Proof for Lemma 2.4.2 . As the first step, we introduce the equilibrium set:

$$I_{TL}^* = \frac{V_1 - V_2}{R_{TL}} \qquad \dot{I}_{TL}^* = \frac{\dot{V}_1 - \dot{V}_2}{R_{TL}} \qquad P_{left}^* = I^* V_1 \qquad P_{right} = I_{TL}^* V_2 \tag{2.33}$$

Then , if we choose a storage function:

$$W = \frac{1}{2}R_{TL}(I_{TL} - I_{TL}^*)^2 \tag{2.34}$$

Calculating the time derivative, we have:

$$\begin{aligned}
\dot{W} &= -\frac{R_{TL}}{L_{TL}}(I_{TL} - I^*_{TL})^2 + \dot{V}_1(I_{TL} - I^*_{TL}) - \dot{V}_2(I_{TL} - I^*_{TL}) \\
&\leq \dot{V}_1(-C_{TL}\dot{V}_1 + \frac{1}{V_1}P_{left} - I^*_{TL}) - \dot{V}_2(-C_{TL}\dot{V}_2 - \frac{1}{V_2}P_{right} - I^*_{TL}) \\
&= -C_{TL}(\dot{V}_1^2 + \dot{V}_2^2) + \frac{\dot{V}_1}{V_1}(P_{left} - P^*_{left}) + \frac{\dot{V}_2}{V_2}(P_{right} - P^*_{right}) \\
&\leq -\delta u^T u + (u - u^*)(y - 0)
\end{aligned} \tag{2.35}$$

where $\delta > 0$ is a time-varying constant. This completes the proof. □

2.5 Summary

In this chapter, we propose a novel modular modeling approach that models an EES into a negative feedback configuration. Besides, we propose a new input-output pair for each component, leading to a transformed state space (TSS) model with a novel incremental passivity. We choose a typical RL load and a transmission line component as examples to illustrate the concept. The proposed modular modeling approach and the novel TSS model form the basis for later analysis and control design.

Chapter 3

Modular specifications and distributed control for an AEES

3.1 Introduction and problem formulation

3.1.1 Introduction

Consider a representative small AEES (microgrid) comprising heterogeneous components such as small generators, solar, battery and loads, as shown in Figure 3-1. This grid is either connected to the utility (via the switch in Figure 3-1) or it is disconnected from the utility (islanded).

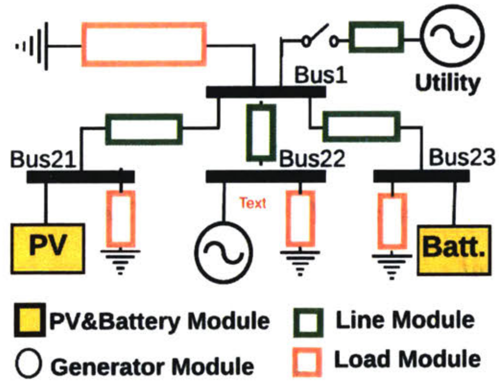

Figure 3-1: One Line Diagram of 2015 Microgrid Test System [1]

As an AEES, it is required to deliver power to loads at the acceptable quality of service (QoS), as loads and solar power vary over time, or even as topology changes in a planned or unplanned way. However, enabling AEES is challenging because the dynamics of components are highly diverse and nonlinear. Sources of disturbances include internal dynamics of DERs, power electronic switching, network dynamics, power flow interactions, etc.

While the state of the art microgrid control design focuses on stable operation around a grid operating point, regulation in response to large disturbances has not been studied much. In Chapter 2, we have proposed a novel modular modeling approach that represents a general EES as a feedback configuration comprising a subsystem H_S and a subsystem H_N. In this chapter, we study the problem of defining control design specifications for each subsystem. In particular, we focus on the following two questions in this chapter:

1. develop modular specifications for each subsystem from the feasibility and stability perspective
2. design distributed control to support the modular specifications

3.1.2 Problem formulation

To formulate the problem, we introduce the following notations: state set $\Phi_{x,i}$, initial condition set $\Phi_{x_0,i}$, control input set $\Phi_{c,i}$, output set $\Phi_{y,i}$ and external input set $\Phi_{u,i}$ for each component i.

Then, we make an assumption on the existence of feasible operating points.

Assumption 3.1.1 (existence of equilibrium). *Consider an electrical energy system modeled by* (2.11) *with subsystems H_S and H_N. There exists a set* (x_S^*, x_N^*, c_S^*, c_N^*, u_S^*, u_N^*, y_S^*, y_N^*) *such that*

$$
\begin{aligned}
0 &= f_S(x_S^*, c_S^*, u_S^*) \qquad & 0 &= f_N(x_N^*, c_N^*, u_N^*) \\
y_S^* &= h_S(x_S^*, c_S^*, u_S^*) \qquad & y_N^* &= h_N(x_N^*, c_N^*, u_N^*)
\end{aligned}
$$

Now, we are ready to formulate the problem:

Given:

1. Assumption 2.2.1 - 2.2.3 and Assumption 3.1.1

2. System topology and component dynamics (2.21) and (2.26)

3. The allowed control and external input set of Component i: Φ_{c_i} and Φ_{u_i}. $i \in \mathcal{N}_{one} \cup \mathcal{N}_{two}$

To do:

1. find modular specifications for single-port and two-port components using their input and output variable $(u_{S,i},\ y_{S,i})$ and $(u_{N,i},\ y_{N,i})$.

2. design modular control $C : \Phi_{x,i} \times \phi_{u,i} \to \Phi_{c,i}$, initial condition set $x_{i0} \in \phi_{x0,i}$ and disturbance subset $\phi_{u,i} \subseteq \Phi_{u,i}$ so that above modular specifications are satisfied.

3.1.3 Chpater outline

The remainder of this chapter is organized as follows. To solve the first problem, we propose the modular stability and feasibility specifications for subsystems H_S and H_N in Section 3.2. For the second problem, we provide two distributed nonlinear control methods for single-port and two-port components in Section 3.3. A proof-of-concept example is then illustrated in Section 3.4. Section 3.5 concludes the chapter.

3.2 Modular specifications

Recall that the components of EESs are designed for a certain operational region. Besides, the EES has to meet the quality of service (QoS) constraints. In this section, we propose two types of modular specifications. One accounts for the stability requirements, and the other accounts for the feasibility requirements.

Before stating the main results, we first briefly review the passivity theorem. Because the proposed modular stability specifications are closely related to the passivity theorem.

3.2.1 Brief review on the passivity concepts

Recall the general dynamical system shown in Figure 1-2. Two subsystems H_N and H_S are connected in a negative feedback configuration. The passivity theorem known for such configuration is stated below.

Proposition 3.2.1. *([45]) If both H_S and H_N are passive, then the feedback system is stable. Asymptotic stability follows if, in addition, any one of the following conditions is satisfied:*

1. *$H_S H_N$ is zero state detectable and H_S is output strictly passive*

Proposition 3.2.1 provides important insight concerning specifications that need to be met so that the system is stable. Next, we utilize Proposition 3.2.1 to define modular stability specifications.

3.2.2 Modular stability specifications

Notably, Proposition 3.2.1 cannot be directly applied if one interests in nonzero equilibrium. Recall the passivity definition: a component is passive if there exists a storage function W whose rate satisfies:

$$\dot{W} \leq u^T y \tag{3.1}$$

where u and y denote the input and the output, respectively.

It can be seen that u and y have to be zero when the system is in steady state ($\dot{W} = 0$). So if one interests in nonzero equilibrium (when $u \neq 0$ and $y \neq 0$), the conflict arises, so-called dissipation obstacle issue [43].

Notably, the ESS is not operating around the origin. In order to avoid the dissipation obstacle issue, we extend Proposition 3.2.1 with the notion of equilibrium-independent passivity (EIP) [96], which requires an incremental form inequality:

$$\dot{W} \leq (u - u^*)^T (y - y^*) \tag{3.2}$$

Note that no prior knowledge of u^* and y^* are required.

Under Assumption 3.1.1, we state the modular stability specifications below:

1. For single-port component i, $i \in \mathcal{N}_{one}$, there exists a positive semidefinite storage function $W_{S,i}$ and a positive constant $\delta_i > 0$ such that:

$$\dot{W}_{S,i} \leq -\delta_i \bar{y}_{S,i}^T \bar{y}_{S,i} + u_{S,i}^T \bar{y}_{S,i} \qquad \forall t \tag{3.3}$$

   where $\bar{y}_{S,i} = y_{S,i} - y_{S,i}^*$.

2. For two-port component i, $i \in \mathcal{N}_{two}$, there exists a positive semidefinite storage function $W_{N,i}$ and a positive constant $\delta_i \geq 0$ such that:

$$\dot{W}_{N,i} \leq -\delta_i y_{N,i}^T y_{N,i} + \bar{u}_{N,i}^T y_{N,i} \qquad \forall t \tag{3.4}$$

   where $\bar{u}_{N,i} = [y_{i,L} - y_{i,L}^*, y_{i,R} - y_{i,R}^*]^T$.

From the stability perspective, we require that single-port components to be output strictly EIP and two-port components to be EIP or output strictly EIP. Following from above two specifications, we can further claim the following two conclusions for subsystems H_S and H_N, respectively.

Lemma 3.2.1. *Subsystem H_S is output strictly EIP, if its comprising components are output strictly EIP.*

Proof. This is because components of H_S are in parallel connection. Candidate storage function family for the subsystem H_S could be chosen as the convex combination of individual storage functions. Discussions on dissipative systems with parallel connection can be found in [97]. □

Lemma 3.2.2. *Subsystem H_N is output strictly EIP, if its comprising components are output strictly EIP.*

Proof. We choose the storage function W_N of subsystem H_N as the sum of all $W_{N,i}$, $i \in \mathcal{N}_{two}$. It can be checked that W_N is convex and positive semi-definite. The proof is completed following from Proposition 3 (Tellegan's theroem) and Proposition 4 in [93]. □

Next, we focus on proposing modular feasibility specifications for H_S and H_N from the input-output perspective.

3.2.3 Modular feasibility specifications

The feasibility requirements are treated as constraints on the input and the output set. To characterize the set, we first introduce a measure.

Definition 3.2.1 (ϵ-bounded Set Ω_ϵ^2). *$\forall\ u(\tau) \in \Omega_\epsilon^2$, $u = [u_1, ..., u_n]^T$, we have*

$$\max_{i=1,\dots,n} \int_0^\infty (u_i(\tau))^2 d\tau \leq \epsilon^2 \tag{3.5}$$

Ω_ϵ^2 is a set of signals, the integral of whose elements has a finite bound.

Then, we state the modular feasibility specifications below.

1. For subsystem H_S: suppose there exist $\epsilon_1 > 0$ that bound the input:

$$u_S \in \Omega_{\epsilon_1}^2 \tag{3.6}$$

For the given initial condition set $\phi_{x_0,S}$, output $y_{S,i}$ of single-port component i satisfies

$$\|y_{S,i} - y_{S,i}^*\| \leq \beta_{1i}(\|x_{S,i}(0)\|) + \beta_{2i}(\epsilon_1) \leq \epsilon_S \quad x_{S,i}(0) \in \phi_{x_0,i} \quad i \in \mathcal{N}_{one} \tag{3.7}$$

where $\epsilon_S = \sup_i(\beta_{1i}(\|x_{S,i}(0)\|) + \beta_{2i}(\epsilon_1))$, is determined by ϵ_1 and $\phi_{x_0,S}$. $\beta_{1i}(*)$ and $\beta_{2i}(*)$ are $\mathcal{K}$ functions.

2. For subsystem H_N: given constant $\epsilon_N > 0$, suppose input $u_{N,j}$ is bounded:

$$\|u_{N,j}(\tau) - u_{N,j}^*\| \leq \epsilon_N \qquad \forall j \in \mathcal{N}_{two} \tag{3.8}$$

Then, there exist $\epsilon_2 > 0$ and initial condition set $\phi_{x_0,N}$ such that output $y_{N,j}$ of two-port component j satisfies:

$$y_{N,j} \in \Omega^2_{\epsilon_2} \tag{3.9}$$

where ϵ_2 depends on ϵ_N and $\phi_{x_0,N}$.

Notably, (3.7) and (3.9) imply that each subsystem is bounded input bounded output (BIBO).

Remark 3.2.1. *If we use a different measure to bound the input and the output set, we may have a different constraints.*

In support of meeting the modular stability and feasibility specifications, we propose two distributed control for controllable components next.

3.3 Distributed nonlinear control

We organize this section into two parts. In the first part, we introduce a distributed nonlinear control for the controllable single-port components. In the second part, we introduce a passivity-based control for the two-port components. Both of them provably ensure that the modular specifications are met. Moreover, the proposed control is applicable to all components, including induction machines, inverters, etc. Examples are given later in Chapter 5 and Chapter 6.

3.3.1 Single-port component

Recall the TSS model of component i:

$$\begin{aligned}
\dot{x}_{i,int} &= f_{i,1}(x_{i,int}, P_{S,i}) \\
\dot{P}_{S,i} &= -(k_1 - u_{S,i})P_{S,i} + g_{i,1}(P_{S,i}, u_{S,i})c_{S,i} \\
\dot{c}_{S,i} &= \xi_{S,i}
\end{aligned} \tag{3.10}$$

where input $u_{S,i} = \dot{V}_{S,i}/V_{S,i}$, and output $y_{S,i} = P_{S,i}$. $k_1 > 0$ is a constant, representing the natural damping. New control input $\xi_{S,i} \in \mathbb{R}^k$ determines the rate of $c_{S,i}$.

Keep in mind that our idea of meeting modular specifications is via controlling power and voltage. Therefore, we propose a two-layered control: a power layer and an energy layer. The power layer aims at controlling power $P_{S,i}$, while the energy layer is designed to keep terminal voltage $V_{S,i}$ within a feasible region around the voltage set point V^{ref}.

Power layer control design

More specifically, the power layer has two control objectives, namely, 1) ensuring that the component is output strictly equilibrium-independent passivity (EIP); 2) ensuring that the internal dynamics is stable. Since output strictly EIP implies that the component is finite-gain stable, both the modular stability and feasibility specification are satisfied.

To illustrate the control design, we neglect $c_{S,i}$ dynamics and saturation for brevity. In implementation, $\xi_{S,i}$ is designed using back-stepping techniques.

Recall $P_{S,i}$ dynamics in (3.10). We design $c_{S,i}$ as:

$$c_{S,i} = g_{i,1}(*)^{-1}(k_1 P_{S,i} - k_2(P_{S,i} - P^*_{S,i}) + v_i) \tag{3.11}$$

where v_i is the new control input. Then, we choose v_i as:

$$v_i = \phi(x_{S,i}, x^*_{S,i}) u_{S,i} \tag{3.12}$$

where $\phi(x_{S,i}, x^*_{S,i}) : \mathbb{R}^n \to \mathbb{R}$ is a feedback design.

Substituting (3.11) and (3.12) into (3.10), we obtain a nonlinear system:

$$\begin{aligned} \dot{x}_{S,i} &= \underbrace{\begin{bmatrix} f_{i,1}(x_{i,int}, P_{S,i}) \\ -k_2(P_{S,i} - P^*_{S,i}) \end{bmatrix}}_{A(x_i)} + \underbrace{\begin{bmatrix} 0 \\ P_{S,i} + \phi(x_{S,i}, x^*_{S,i}) \end{bmatrix}}_{B(x_i, v_i)} u_{S,i} \\ x_{S,i} &= [x_{i,int}, P_{S,i}]^T \in \mathbb{R}^n \qquad y_{S,i} = P_{S,i} \end{aligned} \tag{3.13}$$

where k_2 is the control gain; $P^*_{S,i}$ is the power output set point.

Therefore, the control objective becomes to design k_2, $P^*_{S,i}$ and v_i so that (3.13) is output strictly EIP. Next, we choose an incremental storage function $V_{x^*} = \frac{1}{2}(x_{S,i} - x^*_{S,i})^T M(x_{S,i} - x^*_{S,i})$ where M is a positive definite matrix. Let $Q = -\rho$ and $S = \frac{1}{2}$, $\rho > 0$. The distributed control should satisfy the following conditions. We omit subscript S for brevity.

Lemma 3.3.1. *Suppose that control input $c_{S,i}$ is within the saturation limit. Then, the closed-loop system* (3.13) *is output strictly equilibrium-independent passive with respect to the incremental storage function $V_{x^*_i}$ and the quadratic supply rate $w(u_i, y_i) := (y_i - y^*_i)^2 Q(y_i - y^*_i) + (y_i - y^*_i)^T S u_i$ if and only if there exist Q, a feedback design $\phi(x_i, x^*_i)$ and a function $L : \mathbb{R}^n \to \mathbb{R}$ such that: $L(x, x^*) = L(x) - L(x^*)$*

$$[M(x_i - x^*_i)]^T [A(x_i) - A(x^*_i)] = [y_i - y^*_i]^T Q[y_i - y^*_i] - L(x_i, x^*_i)^T L(x_i, x^*_i) \quad (3.14a)$$
$$\frac{1}{2}[M(x_i - x^*_i)]^T B(x_i, v_i) = [y_i - y^*_i]^T S \quad (3.14b)$$

Proof. Lemma 3.3.1 follows directly from Hill-Moylan Condition in [45] and Lemma 3.4 in [51] by setting $R = W = 0$. □

If conditions of Lemma 3.3.1 are satisfied, it can be shown that single-port component i is finite-gain stable. This is an application of Lemma 6.5 in [11]. We state the result below.

Lemma 3.3.2. *If conditions of Lemma 3.3.1 are satisfied, single-port component i is finite-gain stable with $\mathcal{L}_2$ gain less or equal to $\frac{1}{\rho}$. Thus, the modular feasibility specification* (3.7) *is satisfied.*

Energy layer control design

Recall the index mappings introduced in Section 2.3. We further define the following index sets to simplify the notations used in this section:

$$
\begin{aligned}
M_S(i) &: \text{index of the node that component } i \text{ connects to } (j = M_S(i)) \\
M_S^{-1} \circ M_S(i) &: \text{single-port components connecting to Node } j \\
M_{N,L}^{-1} \circ M_S(i) &: \text{two-port components whose left port connects to Node } j \\
M_{N,R}^{-1} \circ M_S(i) &: \text{two-port components whose right port connects to Node } j \\
\mathcal{N}_{S,c} &: \text{controllable single-port components connecting to Node } j \\
\mathcal{N}_{S,nc} &: \text{uncontrollable single-port components connecting to Node } j
\end{aligned}
$$

where we have:

$$\mathcal{N}_{S,c} \cup \mathcal{N}_{S,nc} = M_S^{-1} \circ M_S(i) \tag{3.15}$$

The energy layer aims at keeping terminal voltage feasible. This is achieved by providing proper set points to the power layer. In particular, we introduce a new variable $E_{S,i}$, the stored energy of the connecting node (e.g. a shunt capacitor). $E_{S,i}$ is a function of the terminal voltage, thus its dynamics reflects the terminal voltage behavior. According to the law of conservation of energy, $E_{S,i}$ dynamics is:

$$\dot{E}_{S,i} = \sum_{j \in M_S^{-1} \circ M_S(i)} P_{S,j} - P_{S,dis} - \sum_{j \in M_{N,L}^{-1} \circ M_S(i)} V_{N,jL} I_{N,j} + \sum_{j \in M_{N,R}^{-1} \circ M_S(i)} V_{N,jR} I_{N,j} \tag{3.16}$$

where $P_{S,j}$ is the output of single-component j, $j \in M_S^{-1} \circ M_S(i)$. $P_{S,dis}$ denotes the power dissipated at the interface. $V_{N,jL}$ and $V_{N,jR}$ are the left and right port voltage of two-port component j, respectively. $I_{N,j}$ denotes the inductor current of two-port component j. $V_{N,jL} I_{N,j}$ denotes the instantaneous power flows into the line; $V_{N,jR} I_{N,j}$ denotes the instantaneous power flows from the line. They are visualized in Figure 3-2.

It can be seen from (3.16) that $E_{S,i}$ is the integral of $P_{S,i}$, which implies that the time scale separation may exist if $P_{S,i}$ reacts faster than $E_{S,i}$. This is achievable by

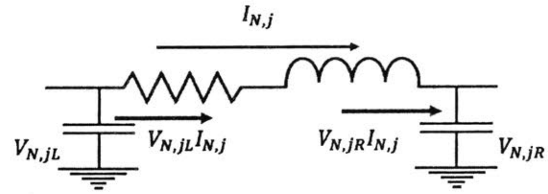

Figure 3-2: Two-port component j: positive direction is defined from the left port to the right port

designing proper k_2 in the power layer. Assuming so, we utilize singular perturbation techniques to replace $P_{S,i}$ with $P^*_{S,i}$ ($i \in \mathcal{N}_{S,c}$) in (3.16):

$$\begin{aligned} \dot{E}_{S,i} = & \sum_{j\in\mathcal{N}_{S,c}} P^*_{S,j} \\ & \underbrace{+ \sum_{j\in\mathcal{N}_{S,nc}} P_{S,j} - P_{S,dis} - \sum_{j\in M^{-1}_{N,L}\circ M_S(i)} V_{N,jL}I_{N,j} + \sum_{j\in M^{-1}_{N,R}\circ M_S(i)} V_{N,jR}I_{N,j}}_{P_{meas}} \end{aligned} \tag{3.17}$$

Let $|N_c|$ denotes the number of indexes in $\mathcal{N}_c$.

If we design $P^*_{S,i}$ as:

$$P^*_{S,i} = sat(\frac{1}{|N_c|}(-P^{ref}_{meas} - K_v(V_i^2 - (V_i^{ref})^2)) \qquad i \in \mathcal{N}_{S,c} \tag{3.18}$$

where K_v is the feedback gain. P^{ref}_{meas} denotes the real power target. A saturation function is added to ensure the $P^*_{S,i}$ is within the feasible range. For the stability purpose, we can choose $P^{ref}_{meas} = P_{meas}$, which can be obtained by exchanging information with neighboring components.

Substituting (3.18) into Eqn.(3.17) yields:

$$\dot{E}_{S,i} = -K_v(V_i^2 - (V_i^{ref})^2) + (P_{meas} - P^{ref}_{meas}) \tag{3.19}$$

If we model the interface as a shunt capacitor with capacitance C, thus $E_{S,i} = \frac{1}{2}CV_i^2$. Assuming that $P^*_{S,i}$ is within the feasible range, above close-loop dynamics becomes:

$$\dot{E}_{S,i} = -\frac{2K_v}{C}(E_{S,i} - E^{ref}_{S,i}) + (P_{meas} - P^{ref}_{meas}) \tag{3.20}$$

It can be concluded from (3.20) that closed-loop $E_{S,i}$ dynamics is finite-gain stable with respect to input $P_{meas} - P_{meas}^{ref}$ and output $E_{S,i} - E_{S,i}^{ref}$. We formally state the result below.

Lemma 3.3.3. *Let $\mathcal{N}_{S,c}$ be the index set of controllable single-port components as defined in* (3.15). *Suppose that the stored energy of the common interface is $E_{S,i} = \frac{1}{2}CV_i^2$, whose dynamics is described by* (3.16).

If k_2 in (3.11) *of each single-port component i, $i \in \mathcal{N}_{S,c}$, satisfies:*

$$k_2 \gg \frac{2K_v}{C} \tag{3.21}$$

and if (3.11) *and* (3.18) *do not reach their saturation limits, control design* (3.18) *therefore guarantees that*

$$||E_{S,i} - E_{S,i}^{ref}||_2 \leq \frac{C}{2K_v}||P_{meas} - P_{meas}^{ref}||_2 \tag{3.22}$$

Proof. Note that condition (3.21) ensures that the time-scale separation exists between $P_{S,i}$ and $E_{S,i}$ dynamics. Therefore, we can replace $P_{S,i}$ in (3.17) with the design (3.18). This results in a closed-loop linear dynamics (3.20) with $E_{S,i} - E_{S,i}^{ref}$ and $P_{meas} - P_{meas}^{ref}$ as the state variables and the input, respectively. Hence, (3.20) is finite-gain stable with $\mathcal{L}_2$ gain as $\frac{C}{2K_v}$. The proof is completed. □

Since $E_{S,i}$ is in terms of terminal voltage V_i, we can conclude the following result on the terminal voltage behavior.

Corollary 3.3.1. *If the conditions of Lemma 3.3.3 are satisfied and $P_{meas}(t) \to P_{meas}^{ref}$ as $t \to \infty$, control design* (3.18) *ensures that $V_{S,i}(t) \to V^{ref}$ as $t \to \infty$.*

Proof. If the conditions of Lemma 3.3.3 are satisfied. we know $E_{S,i}$ has the closed-loop form:

$$\dot{E}_{S,i} = -\frac{2K_v}{C}(E_{S,i} - E_{S,i}^{ref}) + (P_{meas} - P_{meas}^{ref}) \tag{3.23}$$

It can be seen that $E_{S,i}$ exponentially converges to $E_{S,i}^{ref}$, if $P_{meas} = P_{meas}^{ref}$. Therefore, if $P_{meas} \to P_{meas}^{ref}$ as $t \to \infty$, we can conclude that $E_{S,i} \to E_{S,i}^{ref}$, which is equivalent

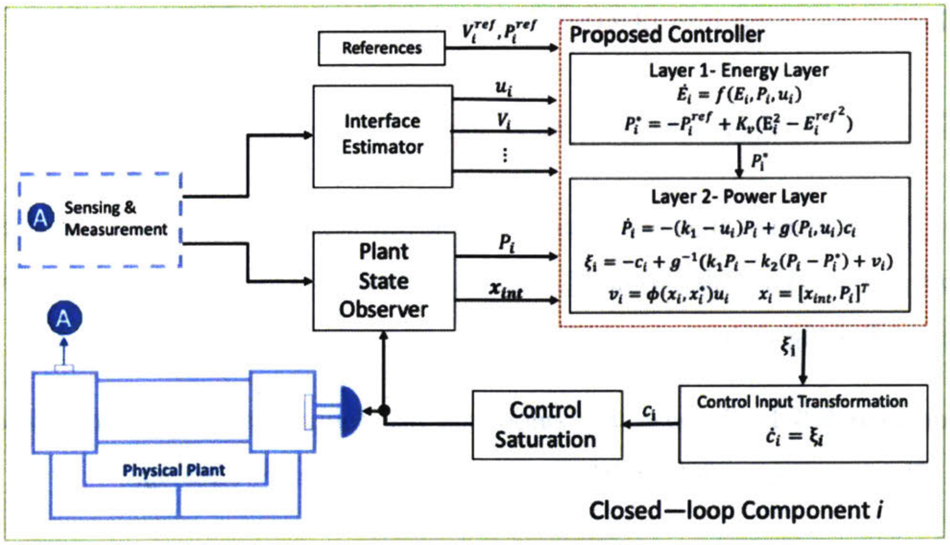

Figure 3-3: Closed-loop dynamic component in the transformed state space

to $V_{S,i} \to V^{ref}$. This completes the proof. □

To summarize, the control block diagram of a general dynamic model in the transformed state space is shown in Fig.3-3.

3.3.2 Two-port component

Recall that two-port component i can be modeled with the new input-output pair $[P_{i,L}, P_{i,R}]^T$ and $[\frac{\dot{V}_{i,L}}{V_{i,L}}, \frac{\dot{V}_{i,R}}{V_{i,R}}]^T$. Subscript N is omitted.

According to Lemma 2.4.2, we know transmission line i is output strictly EIP, i.e, there exists a storage function W_i satisfying:

$$\dot{W}_i \leq \delta_i y_{N,i}^T y_{N,i} + (u_{N,i} - u_{N,i}^*)^T y_{N,i} \qquad \delta_i(t) > 0 \tag{3.24}$$

For controllable two-port component, we propose a passivity-based control:

$$\tilde{u}_{N,i} = u_{N,i} - \alpha_i y_{N,i} \qquad \alpha_i \geq \delta_i \tag{3.25}$$

where $\tilde{u}_{N,i}$ is the new input.

Substituting (3.25) into (3.24) yields the closed-loop dynamics:

$$\dot{W}_i \leq -(\delta(t)+\alpha)y_{N,i}^T y_{N,i} + (u_{N,i} - u_{N,i}^*)^T y_{N,i} \leq -\alpha y_{N,i}^T y_{N,i} + (u_{N,i} - u_{N,i}^*)^T y_{N,i} \quad (3.26)$$

Hence, (3.25) ensures that component i is output strictly EIP with a constant gain α. If we assume that subsystem H_N comprises only controllable components, we can have the following claim.

Proposition 3.3.1. *Suppose that subsystem H_N comprises only controllable components. H_N is output strictly EIP if each component is controlled by:*

$$\tilde{u}_{N,i} = u_{N,i} - \alpha_i y_{N,i} \qquad i \in \mathcal{N}_{two} \quad (3.27)$$

Proof. The claim follows directly from Lemma 3.2.2. The storage function W_N of subsystem H_N can be obtained by summing up the storage function of each component:

$$W_N = \sum_i W_{N,i} \qquad i \in \mathcal{N}_{two} \quad (3.28)$$

Substituting (3.27) into W_N dynamics yields the output strictly EIP inequality. Thus, the proof is completed. □

Now, we have shown that the proposed passivity-based control (3.25) ensures the satisfaction of the modular stability specifications. Moreover, the closed-loop H_N is output strictly EIP. Following from Lemma 6.5 in [11], we can claim that the modular feasibility specification (3.9) is also satisfied. We state the result below:

Corollary 3.3.2. *Subsystem H_N is finite-gain stable if its component is controlled by (3.27):*

$$\|y_N\|_2 \leq K\|u_N - u_N^*\|_2 + \sqrt{2KW_N(x_N(0))} \quad (3.29)$$

$\mathcal{L}_2$ gain K is less or equal to $\min_{i\in\mathcal{N}_{two}}(\frac{1}{\alpha_i})$. Storage function W_N is defined as (3.28).

In what above, we have introduced the modular specifications and the component-level distributed control for single-port and two-port components. To better illustrate the concept, we consider a stable two-bus system. The modular specifications for such two-bus system are explained in detail.

3.4 Proof-of-Concept illustration on a two-bus system

3.4.1 System topology

The two-bus system topology is shown in Figure 3-4. It consists of three components, namely an ideal current source, a transmission line (TL), and a constant impedance load (RL).

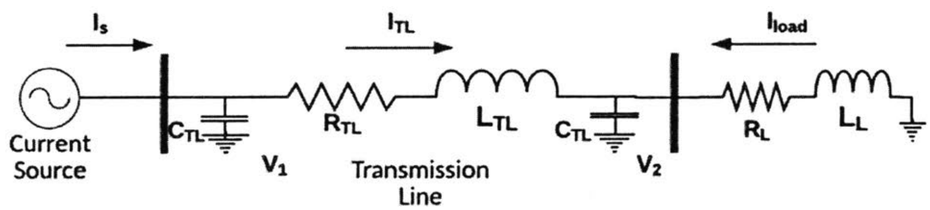

Figure 3-4: Topology of the two-bus system: an ideal current source connects a RL load via a transmission line

Here, we use the π model to represent the transmission line. As shown in Figure 3-4, a current source and a constant impedance (RL) load are connected to the left and right node (bus) of the transmission line, respectively.

Before stating the main results, we list the notations for each standalone component in the table below.

Table 3.1: Notations for Standalone Components

Ideal source output	I_s	Ideal source output reference	I^*
Source terminal voltage	V_s	Load resistance & inductance	R_L&L_L
Load terminal voltage	V_{load}	Load current	I_{load}
TL resistance	R_{TL}	TL inductance	L_{TL}
TL shunt	C_{TL}	TL current	I_{TL}
Left bus voltage	V_1	Right bus voltage	V_2
Injected current (left) of the TL	I_{left}	Injected current (right) of the TL	I_{right}

We then make a few assumptions, which are standard, commonly seen in electrical power system research.

Assumption 3.4.1 (Transmission line). *$C_{TL} = C > 0$, $R_{TL} > 0$ and $L_{TL} > 0$ are known constants.*

Assumption 3.4.2 (RL load). *$R_L > 0$ and $L_L > 0$ are known constants.*

Recall that we have shown that the RL load and the transmission line are EIP in Section 2.4. Thus, the modular stability specifications of components comprising Figure 3-4 system are satisfied.

Since it is known that Figure 3-4 system is stable, in what follows, we show that each component satisfies its modular feasibility specifications.

3.4.2 Modular specifications in the transformed state space

In this section, the modular feasibility specifications for each components are derived. We assume that the source is ideal. Besides, we assume that both the RL load and the transmission line are controlled by the proposed distributed control.

For the ideal source, we have:

$$y_S \equiv y_S^* \Rightarrow V_1 \equiv V_1^{ref} \tag{3.30}$$

According to Lemma 3.3.2, we know the controlled RL load is output strictly EIP and finite-gain stable. Hence, it satisfies the following modular feasibility specification:

$$\|P_{load} - P_{load}^*\|_2 \leq \frac{1}{\alpha_L}\|\frac{\dot{V}_2}{V_2}\|_2 + \sqrt{\frac{1}{\alpha_L}W_{load}(0)} \tag{3.31}$$

where α_L is the $\mathcal{L}_2$ gain, determined by the control gain. W_{load} is the storage function. $W_{load}(0)$ is the initial value of the storage function.

According to Lemma 2.4.2 and Proposition 3.3.1, we know that the transmission line component is output strictly EIP and finite-gain stable. Since the ideal source ensures that $V_1 = V_1^{ref}$, the transmission line component satisfies the modular feasibility specification:

$$\|\frac{\dot{V}_2}{V_2}\|_2 \leq \frac{1}{\alpha_{TL}}\|P_{right} - P^*_{right}\|_2 + \sqrt{\frac{1}{\alpha_{TL}}W_{TL}(0)} \tag{3.32}$$

where α_{TL} is the $\mathcal{L}_2$ gain. W_{TL} is the storage function. $W_{TL}(0)$ is the initial value of the storage function.

3.4.3 Modular specifications in the classic $V - I$ state space

Notably, the modular specifications can be derived with respect to different input-output pairs. The purpose of this section is thus to provide such an example to show that the modular specifications may have different form. Here, we use the classic $V - I$ state space model.

The section is organized as below: we first show the existence and uniqueness of equilibrium for Figure 3-4 system (Lemma 3.4.1). Next, we show the transmission line component is zero state detectable (Lemma 3.4.2) and finite-gain stable (Lemma 3.4.3). Then, we show that the RL load is zero state delectable (Lemma 3.4.4) and finite-gain stable (Lemma 3.4.5). Note that we use $\mathcal{L}_2$ norm in this section.

Lemma 3.4.1 (existence of equilibrium). *Under Assumption 3.4.1-3.4.2, Figure 3-4 system has a unique equilibrium.*

Proof. Under assumptions, Figure 3-4 system can be modeled as:

$$\begin{aligned}
\dot{x} &= Ax + BI^* \\
x &= [V_1, V_2, I_{TL}, I_{load}]^T \quad B = \begin{bmatrix} 1/C_{TL} & 0 & 0 & 0 \end{bmatrix}^T \\
A &= \begin{bmatrix} -R_{shunt}/C_{TL} & 0 & -1/C_{TL} & 0 \\ 0 & -R_{shunt}/C_{TL} & 1/C_{TL} & 1/C_{TL} \\ 1/L_{TL} & -1/L_{TL} & -R_{TL}/L_{TL} & 0 \\ 0 & 1/L_{load} & 0 & -R_{load}/L_{load} \end{bmatrix}
\end{aligned} \tag{3.33}$$

It is easy to check that matrix A is nonsingular. Thus, the interconnected system has a unique equilibrium. This completes the proof. □

Next, we will show that the transmission line is zero state detectable .

Lemma 3.4.2 (zero state detectability of TL). *Under Assumption 3.4.1, the transmission line is zero state detectable.*

Proof. Utilizing singular perturbation techniques, we introduce a transformation matrix T:

$$T = \begin{bmatrix} 1/2 & 1/2 & 0 \\ -C_{TL}/K_1 & C_{TL}/K_1 & (R_{TL}C_{TL}+K_1)/2K_1 \\ C_{TL}/K_1 & -C_{TL}/K_1, & (-R_{TL}C_{TL}+K_1)/2K_1 \end{bmatrix} \quad (3.34)$$
$$K_1 = \sqrt{R_{TL}^2 C_{TL}^2 - 8C_{TL}L_{TL}}$$

Hence, consider a general case, where $R_{shunt} = 0$. We can transform the original states to slow y_{TL} and fast variables $z_{TL} = [z_1, z_2]^T$, respectively.

$$\begin{bmatrix} y_{TL} \\ z_1 \\ z_2 \end{bmatrix} = T \begin{bmatrix} V_1 \\ V_2 \\ I_{TL} \end{bmatrix} \quad TAT^{-1} = \begin{bmatrix} 0 & 0 & 0 \\ 0 & \lambda_1 & 0 \\ 0 & 0 & \lambda_2 \end{bmatrix} \quad TB = \begin{bmatrix} 1/2C_{TL} & 1/C_{TL} \\ -1/K_1 & 1/K_1 \\ 1/K_1 & -1/K_1 \end{bmatrix} \quad (3.35)$$

where λ_1 and λ_2 are eigenvalues of the original system matrix. They both have negative real parts.

We thus can rewrite the TL dynamics into the following slow and fast dynamics:

$$\begin{bmatrix} \dot{y_{TL}} \\ \dot{z}_1 \\ \dot{z}_2 \end{bmatrix} = \begin{bmatrix} 0 & 0 & 0 \\ 0 & \lambda_1 & 0 \\ 0 & 0 & \lambda_2 \end{bmatrix} \begin{bmatrix} y \\ z_1 \\ z_2 \end{bmatrix} + \begin{bmatrix} 1/2C_{TL} & 0 \\ 0 & -1/K_1 \\ 0 & 1/K_1 \end{bmatrix} \begin{bmatrix} I_{left} + I_{right} \\ I_{left} - I_{right} \end{bmatrix} \quad (3.36)$$

when $I_{left} + I_{right} = 0$ and $I_{left} - I_{right} = 0$, it can be concluded from (3.36) that $y_{TL} = y_{TL}(0)$, $z_1 \to 0$ and z_2 as $t \to \infty$.

Recall that the output V_2 has the form:

$$V_2 = [1 \; L_{TL}\lambda_2 \; L_{TL}\lambda_1] \begin{bmatrix} y_{TL} \\ z_1 \\ z_2 \end{bmatrix} \quad (3.37)$$

If $V_2 = 0$, we know $y_{TL} = y_{TL}(0) = 0$. Hence, the transmission line is zero state detectable. This completes the proof. □

Then, we claim that the TL meets its modular feasibility specification by showing it is finite-gain stable.

Lemma 3.4.3 (finite-gain stability of TL). *If $I_{left} = I^*_{left}$, the transmission line satisfies:*

$$\|V_2 - V_2^*\|_2 \leq \gamma_{TL}\|I_{right} - I^*_{right}\|_2 + \beta_{TL}\|x_{TL0} - x^*_{TL0}\|_2 \tag{3.38}$$

where $\gamma_{TL} = \frac{2\lambda^2_{max}(P)\|B\|_2\|C\|_2}{\lambda_{min}(P)}$, $\beta_{TL} = \lambda_{max}(P)(\frac{1}{\lambda_{min}(P)})^{0.5}\|C\|_2$, *and* $PA + A^TP = -I$

Proof. Notice that matrix A of the transmission line model is Hurwitz. Hence, this lemma is a direct application of Theorem 5.3 in [11]. We omit the detail here for brevity. □

Similarly, we have the same claims on the RL load. The results are organized in the following two lemmas.

Lemma 3.4.4 (zero state detectability of RL). *The RL load is zero state detectable.*

Proof. Recall RL load dynamics. The system matrix A is Hurwitz. Besides, its output $y = x$. Hence, zero state detectable claim follows. □

Lemma 3.4.5 (finite-gain stability of RL). *The RL load is finite gain stable with $\mathcal{L}_2$ gain less than or equal to $\frac{1}{R_L}$.*

Proof. Recall the incremental version of RL load dynamics:

$$L_L\dot{I}_L = R_L(I_L - I_L^*) + (V_2 - V_2^*) \tag{3.39}$$

It is output strictly EIP with storage function $W = \frac{L_L}{2}(I_L - I_L^*)^2$. Using Lemma 6.5 in [Khill2002], we know the RL load is finite $\mathcal{L}_2$ stable:

$$\|(I_L - I_L^*)\|_2 \leq \frac{1}{R_L}\|V_2 - V_2^*\|_2 + \sqrt{\frac{2L_L}{R_L}(I_L(0) - I_L^*)^2} \tag{3.40}$$

This completes the proof. □

3.5 Summary

In this chapter, we first propose the modular stability and feasibility specifications for subsystem H_S and subsystem H_N. In particular, the modular stability specifications require H_S and H_N to be EIP or output strictly EIP. The modular feasibility specifications require H_S and H_N to be BIBO.

Then, we introduce two distributed control which ensure the modular specifications are met. More specifically, we propose a multi-layered control for the single-port component aiming at controlling power and voltage. For the controllable two-port component, we propose a passivity-based control.

Moreover, we provide a proof-of-concept example to illustrate the modular specifications.

Chapter 4

System-level specifications and distributed control for an AEES

4.1 Introduction and problem formulation

In Chapter 3, we have introduced the modular stability and feasibility specifications for subsystems H_S and H_N. However, to connect H_S and H_N, we need additional system-level specifications. This is because we have to make sure that the input and the output of each subsystem remains feasible after interconnection.

Keeping this requirement in mind, we propose system-level feasibility specifications in this chapter. Besides, we also propose a distributed control, which ensures the system-level specifications are satisfied.

4.1.1 Problem formulation

To start, we assume that the modular specifications proposed in Chapter 3 are met. Besides, we assume that the input space Φ_u and output space Φ_y of each subsystem H_S and H_N are known. The problem is formulated into two tasks, namely,

1. Find system-level feasibility conditions in terms of the input and output of each subsystem
2. Develop a distributed control to meet the system-level feasibility conditions

4.1.2 Chapter outline

The chapter is organized as follows. To solve the first problem, we propose the system-level feasibility specifications in Section 4.2. For the second problem, two "handshaking" methods are proposed in Section 4.3. Then, in order to illustrate the concept, we revisit the same proof-of-concept two-bus system (Figure 3-4) in Section 4.4.

4.2 System-level feasibility specifications

We first review the modular feasibility specifications of H_S and H_N:

For subsystem H_S, there exist $\epsilon_1 > 0$ and ϵ_S for the given $\phi_{x0,S}$ such that:

$$\begin{aligned} u_S \in \Omega^2_{\epsilon_1} \qquad & x_S(0) \in \phi_{x0,S} \\ \|y_S - y_S^*\| \leq \beta_{1i}(\|x_S(0)\|) & + \beta_{2i}(\epsilon_1) \leq \epsilon_S \end{aligned} \tag{4.1}$$

For subsystem H_N, there exist $\epsilon_2 > 0$ and ϵ_N for the given $\phi_{x0,N}$ such that:

$$\begin{aligned} \|u_N(\tau) - u_N^*\| \leq \epsilon_N \\ y_N \in \Omega^2_{\epsilon_2} \end{aligned} \tag{4.2}$$

Recall that H_S and H_N are connected in a negative feedback configuration. To link two subsystems, we propose the following system-level feasibility specifications:

1. Suppose that there exist ϵ_N, ϵ_2 and initial set $\Phi_{x_0,N}$ satisfy (4.2). Let the output of H_N be the input of H_S, characterized as:

$$u_S = y_N \qquad \epsilon_1 = \epsilon_2 \tag{4.3}$$

   Then, there exists initial set $\Phi_{x_0,S}$ so that the output space of H_S is a subset of the input space of H_N, denoted as:

$$\epsilon_S \leq \frac{1}{\|A\|}(\epsilon_N - \|Ay_S^* + u_N^*\|) \tag{4.4}$$

Or, alternatively, we could have

2. Suppose that there exist ϵ_S, ϵ_1 and initial set $\Phi_{x_0,S}$ satisfying (4.1). Let the output of H_S be the input of H_N, characterized as:

$$Ay_S = u_N \qquad \|A\|\epsilon_S = \epsilon_N \tag{4.5}$$

Then, there exists initial set $\Phi_{x_0,N}$ so that the output space of H_N is a subset of the input space of H_S, denoted as:

$$\epsilon_2 \leq \epsilon_1 \tag{4.6}$$

Above system-level feasibility specifications are critical as they imply that the input and output space of each subsystem have overlap, i.e., connecting two subsystems will not violate the modular feasibility specifications. Thus, the interconnection is stable and well-defined.

Notice that the output of H_S and the input of H_N are power deviation from their steady-state value P^*. So it is critical to ensure that P^* is consistent among H_S and H_N. Notice that it is possible to control the power deviation by controlling P^*. In what follows, we present two "handshaking" methods to update y_S^* of controllable single-port components so that the system-level feasibility specifications are satisfied.

4.3 Handshaking methods for feasible operation

Section 4.3.1 provides a decentralized method. It is easy to implement but is hard to achieve the system-level coordination. We then propose a distributed method in Section 4.3.2, which achieves the system-level coordination.

Notably, the proposed two methods do not require any centralized computation. Only a limited number of communication between neighboring components is needed. Instead of relying on the leader-follower structure, the proposed methods let each controllable component has its own decision-making process. Hence, the controlled

ESS is robust, thanks to such distributed feature.

4.3.1 Decentralized method

Suppose controllable single-port component i is controlled by (3.11), (3.12) and (3.18). If we neglect the control saturation, its steady-state power output value is:

$$P_{S,i}^{*} = \frac{1}{|N_c|}(-P_{meas}^{ref} - K_v(V_i^2 - (V_i^{ref})^2) \tag{4.7}$$

where $|N_c|$ denotes the number of controllable single-port components connected at the same bus. P_{meas}^{ref} is the set point provided ahead of time.

Recall Lemma 3.3.3 and Corollary 3.3.1. The accuracy of P_{meas}^{ref} determines the terminal voltage deviation. Hence, we propose a decentralized method to update it via local measurements. More specifically, component i measures the power from the uncontrollable single-port components and the power from the two-port components.

Reusing some notations given in Section 3.3, P_{meas}^{ref} now is replaced with the measured value P_{meas}^{*}:

$$P_{meas}^{*} = \sum_{j \in \mathcal{N}_{S,nc}} P_{S,j} - \sum_{j \in M_{N,L}^{-1} \circ M_S(i)} V_{N,jL} I_{N,j} + \sum_{j \in M_{N,R}^{-1} \circ M_S(i)} V_{N,jR} I_{N,j} \tag{4.8}$$

We then state our main result below.

Lemma 4.3.1 (decentralized method). *Suppose that controllable single-port components are controlled by* (3.11), (3.12) *and* (3.18). *Moreover, we assume that the conditions of Lemma 3.3.1 and Lemma 3.3.3 are satisfied. Then, decentralized updating law* (4.8) *ensures that the system-level specification* (4.6) *holds.*

Proof. Recall the energy layer control (3.18). It can be seen that (4.8) ensures the power deviation ($P_{meas} - P_{meas}^{*}$) to be smaller and smaller. Consequently, this leads to a decreasing voltage deviation following from Corollary 3.3.1. Hence, as long as both H_S and H_N starts from a feasible initial condition, the system-level specifications (4.6) is satisfied. This completes the proof. □

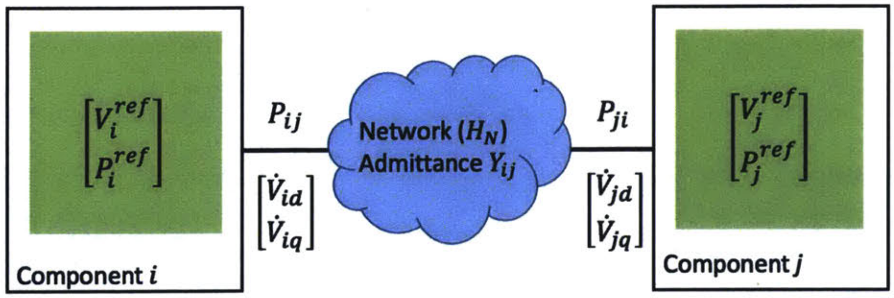

Figure 4-2: Simplified diagram of Figure 2-3 system: Area I and II are represented by component i and j

area as a controllable component. As a result, Figure 2-3 system is simplified as Figure 4-2 system. For component i, we define the following notations.

P_i^{ref} :power set point $\quad P_i$: local load $\qquad V_{id}(V_{iq})$: d(q)-axis of terminal voltage

P_{ij} :power delievered from component i to $j \quad P_{i,max}$: power generation capacity

V_{min} :minimum terminal voltage $\quad V_{max}$: maximum terminal voltage

Similar notations are defined for component j as well. Note that subscript S is omitted for brevity.

If we assume the network H_N is stable, one necessary condition is that the power and voltage set points of each component satisfy the power flow equations. Let C_i and C_j represent the generation cost of component i and j, respectively. As the first step, we could formulate a centralized constrained AC power flow problem with power and voltage as decision variables:

$$
\begin{aligned}
\underset{P_{i(j)}^{ref}, V_{i(j)d}, V_{i(j)q}}{\text{minimize}} \quad & \sum_{k=i}^{j} C_k \max(0, P_k^{ref}) + B(P_k^{ref}) \\
\text{subject to} \quad & P_i^{ref} = P_i + P_{ij} \qquad P_j^{ref} = P_j + P_{ji} \quad \tilde{V}_k = V_{kd} + jV_{kq} \in \mathbb{C} \\
& P_{ij} = Real(\tilde{V}_i \frac{(\tilde{V}_i - \tilde{V}_j)^*}{Y_{ij}^*}) \qquad P_{ji} = Real(\tilde{V}_j \frac{(\tilde{V}_j - \tilde{V}_i)^*}{Y_{ij}^*}) \\
& V_{id}^2 + V_{iq}^2 \in [V_{min}, V_{max}] \quad V_{jd}^2 + V_{jq}^2 \in [V_{min}, V_{max}]
\end{aligned} \tag{4.9}
$$

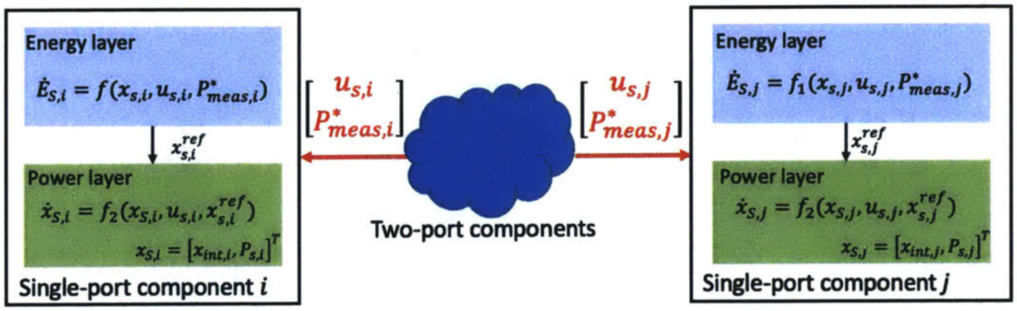

Figure 4-1: Information exchange sketch of decentralized "handshaking" method: Single-port components (H_S) and two-port components (H_N). Red lines denote the information exchange via local measurement

Note that we choose $V_i^{ref} = 1\ p.u.$ for each component in this approach. So, there is no guarantee that we will reach an optimal operating point.

To summarize, we list a sketch of information exchange between two single-port components in Figure 4-1. H_N is neglected and only two single-port components are shown to illustrate the concept. The information exchange (red curves) occurs via local measurements.

4.3.2 Economic-aware handshaking method

Although the decentralized method ensures the system-level specifications are met, it does not take the economic efficiency into consideration. This is because (4.8) is not designed in response to economic signals, such as generation cost. Also, notice that the voltage set points are fixed among controllable components. This may simplify the design, but such setup inevitably reduces the possibility for the system to achieve an optimal operating point.

In order to overcome the limitations of the decentralized method, we focus on the problem to develop a distributed updating law so that system-level specifications are met. In particular, each component iteratively updates its own $P^*_{S,i}$ and V_i^{ref}. Only a limited number of information is required to be exchanged between neighboring components. We also show that the proposed updating law ensures that $P^*_{S,i}$ and V_i^{ref} linearly converge to their feasible stationary point.

To illustrate the concept, let us revisit Figure 2-3 system. Here, we consider each where barrier function $B(P_k^{ref})$ is defined as:

$$B(P_k^{ref}) = \begin{cases} 0 & if\ P_k^{ref} \leq P_{max} \\ +\infty & otherwise \end{cases} \tag{4.10}$$

The objective function of (4.9) is to minimize the total generation cost so that resources are optimized among the system. In addition, the barrier function presents the soft constraint that each component can only produce certain amount of power below its capacity.

In what follows, we first generalize the formulation (4.9) from the above two bus system to a general EES. Then, we explain how to solve such centralized optimization problem in a distributed way using the projection gradient method. More importantly, we show that the proposed distributed updating law provides the same result as the one would get from solving the centralized optimization.

Let us first introduce the following sets related to the ESS:

$\mathcal{V}$: Set of controllable components $\quad$ $\mathcal{N}(i)$: Neighboring set of component i

$\mathcal{S}$: feasible set

Note that we first consider a special scenario where loads do not change, i.e. $P_i, i \in \mathcal{V}$ is constant. It is easy to generalize to have time-varying P_i included. The centralized optimization (4.9) can be reformulated with $[V_{id}, V_{iq}]^T$ as decision variables:

$$\begin{aligned} \underset{V_{id}, V_{iq}, i \in \mathcal{V}}{\text{minimize}} \quad & \sum_{i \in \mathcal{V}} C_i \sum_{j \in \mathcal{N}(i)} \max(-P_i, Real(\tilde{V}_i \frac{(\tilde{V}_i - \tilde{V}_j)^*}{Y_{ij}^*})) + B(P_i + Real(\tilde{V}_i \frac{(\tilde{V}_i - \tilde{V}_j)^*}{Y_{ij}^*})) \\ \text{subject to} \quad & V_{id}^2 + V_{iq}^2 \leq V_{max} \quad -(V_{id}^2 + V_{iq}^2) \leq -V_{min} \end{aligned} \tag{4.11}$$

Let f denotes the objective function. It can be seen that f is a nonconvex quadratic function. Hence, (4.11) is a nonconvex optimization.

Next, we decompose (4.11) into subproblems using the projected gradient descent method. For component i, the corresponding subproblem is:

$$\begin{aligned}\underset{V_{id},V_{iq}}{\text{minimize}} \quad & C_i \sum_{j\in\mathcal{N}(i)} \max(-P_i, Real(\tilde{V}_i\frac{(\tilde{V}_i-\tilde{V}_j)^*}{Y_{ij}^*})) + B(P_i + Real(\tilde{V}_i\frac{(\tilde{V}_i-\tilde{V}_j)^*}{Y_{ij}^*})) \\ \text{subject to} \quad & V_{id}^2 + V_{iq}^2 \leq V_{max} \quad -(V_{id}^2+V_{iq}^2) \leq -V_{min}\end{aligned} \tag{4.12}$$

We solve the problem (4.12) iteratively. Within one iteration, we first update one step along the gradient direction. Next, we project it onto the feasible set. Let $\mathbf{x}_k := [V_{id}^k, V_{iq}^k]^T$ denotes the decision variables at k_{th} iteration. The updating law for component i can be expressed as:

$$\mathbf{x}_{k+1} = \underset{y\in\mathcal{S}}{argmin}\ \frac{1}{2}||y - \mathbf{x}_k + \frac{1}{L}\nabla f(\mathbf{x}_k)||_2^2 \tag{4.13}$$

where $\nabla f(\mathbf{x}_k)$ is the gradient of f at k_{th} iteration, L presents the smoothness of objective function f. L should be larger than the maximum eigenvalue of Hessian of f:

$$L \geq \lambda_{max}(\nabla^2(f)) \tag{4.14}$$

Since f is a quadratic function, elements of its Hessian matrix is constant. In particular, if components have same cost, i.e. $C_i = C_j, i \in \mathcal{V}, j \in \mathcal{N}(i)$, the Hessian matrix is same as Laplacian matrix of the network.

It can be seen from (4.13) that the gradient at each iteration is critical. To calculate the gradient, we need to have information from neighboring components. More specifically, such gradient is a function of line parameters, terminal voltage and generation cost coefficient of neighboring components. Notice that line parameters Y_{ij} and generation cost coefficient C_j usually do not change fast. Thus, at each iteration, each component only needs to exchange its terminal voltage information with neighbors. The convergence analysis of the proposed distributed algorithm (4.13) is provided below.

Lemma 4.3.2. *The problem* (4.12) *with the proposed updating law* (4.13) *will provide the same result as the centralized optimization problem* (4.11). *Moreover,* (4.13) *enables a linear convergence rate.*

Proof. (4.13) is a typical application of the proximal gradient decent method. The proof is identical to the standard proof given in [98]. □

Regarding the system-level specifications, we formulate them as the feasibility set S. However, the formulation is under the assumption that H_N is in steady state, i.e., the dynamics of H_N is negligible. Hence, (4.13) provides only a necessary condition for the system-level specifications to hold. While more work remains to prove that (4.4) is valid during the transient, we have numerically shown that (4.13) ensures the system-level specifications. Simulation results will be discussed in detail in Chapter 5 and 6.

To better illustrate the proposed system-level specifications, we revisit Figure 3-4 system. In particular, we derive the system-level specifications based on the modular results given in Section 3.4. Notations introduced in Section 3.4 are reused in the following section.

4.4 Proof-of-Concept illustration on a two-bus system

Recall that Figure 3-4 system consists of an ideal current source, a linear passive RL load and a transmission line. Suppose that the shunt capacitor has a small resistance R_{shunt}. Under Assumption 3.4.1 and Assumption 3.4.2, the Figure 3-4 system has a unique equilibrium $[V_1^*, V_2^*, I_{TL}^*, I_{load}^*, I_S^*]^T$, satisfying:

$$\frac{V_1^* - V_2^*}{R_{TL}} = I_S^* \qquad I_{TL}^* = I_{load}^* = I_S^* = I^* \tag{4.15}$$

Based on the modular specifications given in Lemma 3.4.1 - Lemma 3.4.5, we propose the system-level specifications below.

Proposition 4.4.1. *For subsystem H_N, Let $x_{TL} = [V_1, V_2, I_{TL}]^T$. There exist $\gamma_{TL} > 0$*

and $\beta_{TL} > 0$ such that:

$$\|V_2 - V_2^*\|_2 \leq \gamma_{TL}\|I^* - I_{right}\|_2 + \beta_{TL}\|x_{TL0} - x_{TL0}^*\|_2 \tag{4.16}$$

Suppose the transmission line (H_N) can only operate within:

$$\|I^* - I_{right}\|_2 \leq \epsilon_3 \tag{4.17}$$

Thus, the overall system is asymptotically stable if there exist ϵ_1 and ϵ_2 such that:

$$\begin{aligned} \textit{Initial condition: } & \|x_{TL0} - x_{TL}^*\|_2 \leq \epsilon_1 \qquad \|I_{load0} - I_{load}^*\|_2 \leq \epsilon_2 \\ \textit{System-level specification: } & \frac{1}{R_2}(\gamma_{TL}\epsilon_3 + \beta_{TL}\epsilon_1) + \sqrt{\frac{2L_L}{R_L}}\epsilon_2 \leq \epsilon_3 \end{aligned} \tag{4.18}$$

One necessary condition is:

$$\frac{R_L}{L_L}\gamma_{TL} < 1 \tag{4.19}$$

Proof. Recall that the transmission line only works under:

$$\|I_{right}^* - I_{right}\|_2 = \|I^* - I_{right}\|_2 \leq \epsilon_3 \tag{4.20}$$

and its initial condition is chosen as:

$$\|x_{TL0} - x_{TL}^*\|_2 \leq \epsilon_1 \tag{4.21}$$

Using Lemma 3.4.1 and 3.4.1, we can conclude that:

$$\|V_2 - V_2^*\|_2 \leq \gamma_{TL}\|I_{right} - I_{right}^*\|_2 + \beta_{TL}\|x_{TL0} - x_{TL0}^*\|_2 = \gamma_{TL}\epsilon_3 + \beta_{TL}\epsilon_1 \tag{4.22}$$

Therefore, following Lemma 3.4.5 and substituting above inequality into (4.18), we obtain the corresponding output:

$$\|(I_L - I_L^*)\|_2 \leq \frac{1}{R_L}(\gamma_{TL}\epsilon_3 + \beta_{TL}\epsilon_1) + \sqrt{\frac{2L_L}{R_L}(I_L(0) - I_L^*)^2} \tag{4.23}$$

Since we can find ϵ_2 such that:

$$\|I_L(0) - I_L^*\|_2 \leq \epsilon_2 \tag{4.24}$$

The system-level specifications (4.4) yields the following condition:

$$\frac{1}{R_L}(\gamma_{TL}\epsilon_3 + \beta_{TL}\epsilon_1) + \sqrt{\frac{2L_L}{R_L}}\epsilon_2 \leq \epsilon_3 \tag{4.25}$$

In addition, notice that $\epsilon_1 \geq 0$, $\epsilon_2 \geq 0$. We can further conclude a necessary condition:

$$\gamma_{TL}/R_L < 1 \tag{4.26}$$

The asymptotic stability follows from the passivity theorem since the transmission line is incrementally passive and RL load is output incrementally strictly passive. The proof thus is completed. $\square$

Notice that the necessary condition (4.19) is similar to the result if one uses small-gain theorem. However, we cannot use small-gain theorem directly here since small-gain theorem does not pose constraints on input and output. The results presented here are more general.

4.5 Summary

In this chapter, we propose the system-level specifications that are required to ensure the feasibility of the interconnected systems. Then, we show that such system-level specifications can be achieved by a combination of local high gain controllers and the adjustments in power output set points. Two iterative methods are proposed. Via local communication, we show that system-level coordination can also be achieved. In the end, we revisit the two-bus example and derive the system-level conditions that need to be satisfied. The derived necessary condition is identical to the small-gain theorem result. However, since small-gain theorem does not consider feasibility requirements, it can be concluded that our proposed solution is more general.

Chapter 5

Root causes of distortions in inverter-based electrical energy systems: A new perspective and distributed control solution

5.1 Introduction

It is common to observe low and high-frequency distortions in inverter-based EESs. Unnecessary distortions inevitably limit the control bandwidth and degrade the operating efficiency. To improve the Quality of Service (QoS), many researchers focus on filter design. As reported in recent literature, the output LCL filter introduces two resonant poles that may destabilize the system [99, 100]. Thereafter, different solutions have been proposed to passively or actively damp out oscillations [100–102]. However, these solutions are based on the assumption that the grid voltage is constant or has deterministic distortions. Such an assumption is questionable in today's EESs as disturbances introduced by the intermittent resources are not negligible.

The primary purpose of this chapter is to illustrate how does the proposed modeling and control enable EESs to have better Quality of Service (QoS). We first analyze the root causes of distortions from a novel input and output perspective using the proposed TSS model. In particular, we rigorously analyze two situations, namely large faults and potential conflicts between different inverters controllers. Then, we provide a device-agnostic distributed control for inverter-based components that enables the robust operation and mitigates the high-frequency distortions for a wide range of uncertainties. Notably, the proposed control does not require the grid voltage assumption.

5.1.1 Chapter outline

The chapter is organized as follows. The root causes of distortions is analyzed in Section 5.2. The proposed distributed control for inverter-based components can be found in Section 5.3. Related stability, robustness and implementation discussions are summarized in Section 5.4. To evaluate the effectiveness of the proposed solution, the MIL test system is used and simulation results are discussed in Section 5.5.

5.2 Root causes of the distortions

5.2.1 Topology of a typical inverter-controlled DER

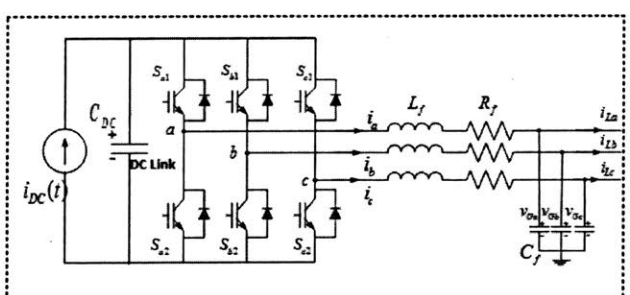

Figure 5-1: Three-phase inverter-controlled DER

One typical three-phase inverter-controlled distributed energy resource (DER) is shown in Figure 5-1. In this system, the DC side is a controlled voltage source consisting of a current source, a DC capacitor and a DC/AC inverter. An output LC filter is installed to reduce the ripples and distortions caused by fast switching.

Filter parameters are typically chosen based on the loading condition and the nominal operating condition.

5.2.2 TSS Model for analysis

The carrier frequency of a periodic signal may disappear if the modeling reference frame is rotating at the same frequency. This is why dq rotating reference frame is widely used in the analysis and the control design of the EES. To simplify the analysis, we modify the TSS model (2.21) using the dq reference frame measured relative to the 60 Hz rotating reference.

First, the instantaneous voltage and current of (2.21) are replaced by corresponding d and q-axis components. Second, the instantaneous power is replaced by real and reactive power P and Q:

$$P = v_d i_{d1} + v_q i_{q1} \qquad Q = v_q i_{d1} - v_d i_{q1} \tag{5.1}$$

whose dynamics are:

$$\begin{aligned} \dot{P} &= -\frac{R_f}{L_1}P - \omega_0 Q + \frac{v_d}{L_1}\bar{V}_{cd} + \frac{v_q}{L_1}\bar{V}_{cq} + \dot{v}_d i_{d1} + \dot{v}_q i_{q1} \\ \dot{Q} &= -\frac{R_f}{L_1}Q + \omega_0 P + \frac{v_q}{L_1}\bar{V}_{cd} + \frac{v_d}{L_1}\bar{V}_{cq} - \dot{v}_q i_{d1} - \dot{v}_d i_{q1} \end{aligned} \tag{5.2}$$

where $\bar{V}_{cd} := v_{cd} - v_d$ and $\bar{V}_{cq} := v_{cq} - v_q$ are controllable input.

Let V and δ_v denote the voltage magnitude and angle, respectively. We have $v_d = V cos(\delta_v)$ and $v_q = V sin(\delta_v)$ with dynamics as:

$$\begin{aligned} \dot{v}_d &= \dot{V} cos(\delta_v) - V sin(\delta_v)\dot{\delta_v} = \frac{\dot{V}}{V}v_d - \omega_i v_q \\ \dot{v}_q &= \dot{V} sin(\delta_v) + V cos(\delta_v)\dot{\delta_v} = \frac{\dot{V}}{V}v_q + \omega_i v_d \end{aligned} \tag{5.3}$$

Substituting into (5.2) yields:

$$
\begin{aligned}
\dot{P} &= -(\frac{R_1}{L_1} - \frac{\dot{V}}{V})P - (\omega_0 + \omega_i)Q + \frac{v_d}{L_1}\bar{V}_{cd} + \frac{v_q}{L_1}\bar{V}_{cq} \\
\dot{Q} &= -(\frac{R_1}{L_1} - \frac{\dot{V}}{V})Q + (\omega_0 + \omega_i)P + \frac{v_q}{L_1}\bar{V}_{cd} - \frac{v_d}{L_1}\bar{V}_{cq}
\end{aligned}
\tag{5.4}
$$

The effects of $\dot{v}_d$ and $\dot{v}_q$ are expressed here in terms of $\dot{V}$ and ω_i. $\dot{V}$ represents the terminal voltage magnitude distortion, while $\omega_i = \dot{\delta}_v$ represents the frequency distortion. Note that these two variables ($\dot{V}/V$, ω_i) are the input of dq reference TSS model.

Remark 5.2.1. *We have a few remarks on the TSS model* (5.4)*:*

1. (5.4) *provides a novel input and output perspective to understand the inner and outer-loop control* (5.7)*. For instance, substituting v_{cd} and v_{cq} of* (5.7) *into* (5.4)*, we can interpret* (5.7) *as regulating P and Q towards their set points by canceling out the cross coupling terms $\omega_0 P$ and $\omega_0 Q$.*

2. (5.4) *captures the effects of $\dot{v}_d$ and $\dot{v}_q$, which relaxes the grid voltage assumption. In Section 5.3, we propose a distributed control using* (5.4)*.*

5.2.3 Root causes of distortions

From the control point of view, the distortions occur because existing controllers do not capture the effects of $\dot{V}/V$ and ω_i. As will be explained in Example 5.2.1 and 5.2.2, $\dot{V}$ and ω_i not only introduce distortions, but also affect the stability.

From the energy point of view, the root causes of distortions can be interpreted as the real and reactive power imbalances. Let us first introduce a few notations:

$$
E_c = \frac{1}{2}C(v_d^2 + v_q^2) \quad P_o = v_d i_{d2} + v_q i_{q2} \quad Q_o = v_q i_{d2} - v_d i_{q2}
$$

where E_c is the stored energy of the filter capacitor; P_o and Q_o are real and reactive power delivered (after the capacitor), respectively.

Then, we can express $\dot{V}$ and ω_i as:

$$\frac{\dot{V}}{V} = \frac{(P - P_o)}{2E_c} \qquad \omega_i = -\omega_0 - \frac{Q - Q_o}{2E_c} \tag{5.5}$$

As one can see from the right hand side of (5.5), the real power imbalance causes magnitude distortion $\dot{V}$, while the reactive power imbalance causes frequency distortion ω_i. Therefore, an alternative way of understanding distortions is that the controller (e.g. control (5.7)) fails to balance the real and reactive power.

In what follows, we provide Example 5.2.1 and 5.2.2 to explain how $\dot{V}$ and ω_i affect system dynamics especially when the embedded controller fails to capture them. In particular, we assume $\dot{V} \neq 0$ in Example 5.2.1 and $\omega_i \neq 0$ in Example 5.2.2.

Example 5.2.1 (Sudden Topology Change). *Consider a system comprising of inverter-based distributed energy resources (DERs) and loads. Suppose that each DER has an embedded inner and outer-loop control with a phase-lock-loop (PLL). Notably, the inner and outer-loop control [56] assumes the grid voltage is constant, i.e.,* $\dot{V} = \omega_i = 0$. *Ideally, the PLL locks the terminal voltage angle so that* $v_d = 0$. *In this example, all states are function of time, i.e.,* $V(t)$, $P(t)$, *etc. We omit* t *in all notations for brevity.*

For an inverter-based DER, the outer-loop control is [56]:

$$i_q^{ref} = P^{ref}/v_q \qquad i_d^{ref} = Q^{ref}/v_q \tag{5.6}$$

where i_q^{ref} *and* i_d^{ref} *are mapped to* P^{ref} *and* Q^{ref}, *respectively.* P^{ref} *and* Q^{ref} *are set points usually provided from the tertiary layer.*

Then, we can rewrite the inner-loop control (current regulator) using (5.2) *as:*

$$\begin{aligned} v_{cd} &= v_d + \frac{v_d}{V^2}\left(\frac{R_1}{L_1}P^{ref} - \omega_0 Q\right) + \frac{v_q}{V^2}\left(\frac{R_1}{L_1}Q^{ref} + \omega_0 P\right) \\ v_{cq} &= v_q + \frac{v_q}{V^2}\left(\frac{R_1}{L_1}P^{ref} - \omega_0 Q\right) - \frac{v_d}{V^2}\left(\frac{R_1}{L_1}Q^{ref} + \omega_0 P\right) \end{aligned} \tag{5.7}$$

where v_d *and* v_q *are measured* d *and* q*-axis terminal voltage.* $V = \sqrt{v_d^2 + v_q^2}$ *denotes* *the voltage magnitude.* R_1 *and* L_1 *are output resistance and inductance, respectively.*

When a sudden topology reconfiguration occurs, the system usually suffers from significant state changes. The grid voltage magnitude, in particular, may have a large change. Thus, for each DER, during the transient period T*, it is reasonable to assume its terminal voltage magnitude* $\dot{V}$ *satisfies:*

$$\dot{V} \geq \frac{R_1}{L_1} V \qquad for\ t \in [t_0,\ t_0 + T] \tag{5.8}$$

We assume the tertiary layer signal P^{ref} *and* Q^{ref} *remain the same:*

$$\dot{P}^{ref} = \dot{Q}^{ref} = 0 \tag{5.9}$$

Recall that each device should operate under feasibility constraints and the control limit. To simplify the discussion, we only consider the control saturation:

$$(v_{cd})^2 + (v_{cq})^2 \leq V_{max}^2 \tag{5.10}$$

Substituting (5.7) *to* (5.10) *yields:*

$$(\frac{R_1}{L_1} P^{ref} - \omega_0 Q)^2 + (\frac{R_1}{L_1} Q^{ref} + \omega_0 P)^2 \leq V^2 V_{max}^2 \tag{5.11}$$

from which, we can derive upper bounds for P *and* Q*:*

$$|P| \leq \sup_{t \in (t_0,\ t_1)} (|\frac{R_1 Q^{ref}}{L_1 \omega_0} + \frac{V V_{max}}{\omega_0}|,\ |\frac{V V_{max}}{\omega_0} - \frac{R_1 Q^{ref}}{L_1 \omega_0}|) = P_{max}$$
$$|Q| \leq \sup_{t \in (t_0,\ t_1)} (|\frac{R_1 P^{ref}}{L_1 \omega_0} - \frac{V V_{max}}{\omega_0}|,\ |\frac{R_1 P^{ref}}{L_1 \omega_0} + \frac{V V_{max}}{\omega_0}|) = Q_{max}$$

Now, we have mapped the control saturation (5.10) *into the operating limits of* P *and* Q*. If* P *or* Q *hits* P_{max} *or* Q_{max} *during the period* T*, we lose the performance guarantee or even lose the stability.*

Next, we use a concept called critical clearing time T_{cc}*. If the fault* (5.8) *persists longer than* T_{cc}*, it is very likely to lose the stability during the transient period.*

Substituting control design (5.7) *into* (5.4) *yields a closed-loop dynamics:*

$$\dot{P} = -(\frac{R_1}{L_1} - \frac{\dot{V}}{V})P + \frac{R_1}{L_1}P^{ref} \qquad \dot{Q} = -(\frac{R_1}{L_1} - \frac{\dot{V}}{V})Q + \frac{R_1}{L_1}Q^{ref}$$

Recall the assumption (5.8). *When the DER encounters a sudden topology change, the best situation is:*

$$\dot{P} = \frac{R_1}{L_1}P^{ref} \qquad \dot{Q} = \frac{R_1}{L_1}Q^{ref}$$

In this case, P and Q increase (or decrease) and are very sensitive to perturbations. The critical clearing time T_{cc} therefore depends on the initial condition, set points and $\dot{V}$. For example, if we assume $P(t_0) = Q(t_0) = 0$ and $\dot{V}/V = R_1/L_1$, the critical time is:

$$T_{cc} = L_1 P_{max}/(R_1 P^{ref}) \tag{5.12}$$

Under above assumptions, P and Q increase (or decrease) linearly. However, T_{cc} will be even shorter if we have larger $\dot{V}/V$. This is because P or Q may increase (or decrease) exponentially.

To summarize, $\dot{V}$ affects the performance of the inner and outer-loop control (5.7). *If a sudden topology change occurs, it is very likely to lose the performance guarantee.*

Example 5.2.2 (Hard-to-Predict Disturbances). *We consider the same system, but a different scenario:*

$$\omega_i \neq 0 \qquad \dot{V} = 0 \tag{5.13}$$

It can be seen that the terminal voltage has persistent harmonics.

In addition, we assume that the same control (5.7) *is applied to the DER. Recall that* (5.7) *does not consider the terminal voltage harmonics.*

Again, substituting (5.7) *into* (5.4) *yields:*

$$\dot{P} = -\frac{R_1}{L_1}(P - P^{ref}) - \omega_i Q \qquad \dot{Q} = -\frac{R_1}{L_1}(Q - Q^{ref}) + \omega_i P \tag{5.14}$$

$\omega_i Q$ and $\omega_i P$ in above two equations cause P and Q drift from their set points. Furthermore, there are two cases to be considered:

For the first case, ω_i is a constant, i.e., $\dot{\omega}_i = 0$. Hence, $\omega_i P$ and $\omega_i Q$ can be considered as steady state offsets to Q^{ref} and P^{ref}, respectively. During the transient period, P and Q are oscillating at ω_i frequency.

For the second case, ω_i is time-varying, i.e., $\dot{\omega}_i \neq 0$. We can rewrite the closed-loop dynamics as:

$$\begin{bmatrix} \dot{P} \\ \dot{Q} \end{bmatrix} = \underbrace{\begin{bmatrix} -\frac{R_1}{L_1} & -\omega_i(t) \\ \omega_i(t) & -\frac{R_1}{L_1} \end{bmatrix}}_{A(t)} \begin{bmatrix} P \\ Q \end{bmatrix} + \begin{bmatrix} \frac{R_1}{L_1} \\ \frac{R_1}{L_1} \end{bmatrix} \begin{bmatrix} P^{ref} \\ Q^{ref} \end{bmatrix} \tag{5.15}$$

Notice that $A(t) + A(t)^T$ is Hurwitz. It can be concluded that the closed-loop dynamics is asymptotically stable. But harmonics ω_i exists in P and Q dynamics. This explains why we observe persistent distortions in operation.

5.3 Proposed distributed control for canceling out distortions (enhanced Quality of Service (QoS))

Now, we have explained when and why the distortions would happen from a novel input and output perspective using the proposed model (5.4). In this section, we introduce a distributed control for inverter-based components to cancel out the distortions. Notably, this specific controller is an application of the general distributed control proposed in Chapter 3 and Chapter 4.

5.3.1 Control objectives

Conceptually, we want to design a control to meet the following objectives:

- It has performance guarantees against bounded disturbances
- The controlled DER can follow real and reactive power references P^{ref} and Q^{ref}
- The terminal voltage magnitude V is regulated within a feasible range

To account for the control saturation, we assume that the disturbance is bounded and known.

Consider a standalone inverter-based DER. Let P and Q denote the real and reactive power output, respectively; ω_i denotes the distorted frequency measured by (5.5); V denotes the voltage magnitude, whose rate is measured by (5.5).

If such DER is in the steady state, we have $\dot{V} = 0$ and $\dot{P} = \dot{Q} = 0$. However, satisfying these two equalities are not equivalent to claim that all the control objectives are satisfied. This is because $\dot{P} = \dot{Q} = 0$ only implies that there is no high frequency distortion. The low-frequency distortion (frequency drifting) may still exist, i.e., $\dot{\omega}_i = 0,\ \omega_i \neq 0$.

Therefore, the control design specifications are listed below:

1. x_{int} dynamics is asymptotically stable
2. $\dot{P} = \dot{Q} = 0$
3. $\dot{V} = 0$ and $\omega_i = 0$

If all above specifications are met, we state the first result below.

Lemma 5.3.1. *The standalone inverter-based DER is in the steady state and free from distortions if and only if the following conditions are met:*

1. *x_{int} dynamics is asymptotically stable*
2. *$\dot{P} = \dot{Q} = 0$*
3. *$\dot{V} = 0$ and $\omega_i = 0$*

Proof. The necessity proof follows directly from the reasonings that we explained before. In short, the steady state implies the first two conditions, while no distortions implies the last equality.

Next, we show the sufficiency. Recall a relation:

$$P^2 + Q^2 = V^2 I^2 \tag{5.16}$$

The second and the third condition imply that the internal current magnitude I is constant.

Recall the power factor definition:

$$\cos(\delta_V - \delta_I) = \frac{P}{P^2 + Q^2} \tag{5.17}$$

where δ_v and δ_I represent the voltage angle and current angle, respectively.

The second condition implies that $\delta_V - \delta_I$ is constant, indicating that V and I have the same frequency. Besides, the last condition implies that no distortions exist in the frequency.

Therefore, it can be concluded that internal dynamics $\dot{x}_{int}$ has constant input varying at the same frequency. The stability and convergence of x_{int} follows directly from the first condition. This completes the proof. □

Hence, the problem becomes to design a distributed inverter control to meet all conditions of Lemma 5.3.1.

5.3.2 Proposed distributed control for inverter-based DERs

We present the proposed control method neglecting the control saturation. Then, we discuss how to choose the gain provided the disturbance bound.

Recall that we consider the DC side circuit of Figure 5-1 system as a controlled voltage source. Hence, the first condition of Lemma 5.3.1 is satisfied. This is usually achieved by controlling the current source so that the DC side circuit is asymptomatically stable. However, such topic is out of the scope of this chapter. Interested readers are referred to our follow-up papers.

To ensure the stability of output variable dynamics (the second condition), we propose a control design:

$$v_{cd} = v_d + \frac{v_d}{V^2}F_1 + \frac{v_q}{V^2}F_2 \qquad v_{cq} = v_q + \frac{v_q}{V^2}F_1 - \frac{v_d}{V^2}F_2 \tag{5.18}$$

where

$$F_1 = v_1 + (\frac{R_1}{L_1} - \frac{\dot{V}}{V})P + (\omega_0 + \omega_i)Q \quad F_2 = v_2 + (\frac{R_1}{L_1} - \frac{\dot{V}}{V})Q - (\omega_0 + \omega_i)P \tag{5.19}$$

v_1 and v_2 are two new control input. One possible design is:

$$v_1 = -K_p(P - P^{ref}) \qquad v_2 = -K_p(Q - Q^{ref}) \tag{5.20}$$

where $K_p > 0$ is a control feedback gain.

Notably, the maximum value of K_p depends on the operating condition and the control saturation. The control saturation constraint here has the form:

$$(v_d + \frac{v_d}{V^2}F_1 + \frac{v_q}{V^2}F_2)^2 + (v_q + \frac{v_q}{V^2}F_1 - \frac{v_d}{V^2}F_2)^2 \leq V_{max}^2 \tag{5.21}$$

We will discuss how to choose proper K_p in the following section.

Then, to meet the third condition of Lemma 5.3.1, we utilize the handshaking method (4.8) proposed in Section 4.3.1. Notice that the model (5.4) uses dq reference frame. Hence, the instantaneous power updating law (4.8) implies two updating laws for real and reactive power, respectively. For real power set point, we have:

$$P^{ref} = P_o - K_v(V^2 - (V^{ref})^2) \tag{5.22}$$

For reactive power set point, we have a Q^{ref} updating law:

$$Q^{ref} = Q_o - CV^2\omega_0 \tag{5.23}$$

where P_o and Q_o can be either measured locally or communicated locally with neighbor modules.

Recall that we assume the disturbances are bounded and (5.21) is valid for the region of interest. Substituting (5.18) and (5.20) into (5.4) yields a closed-loop dynamics whose eigenvalues have negative real part. Thus, we have the guaranteed performance against bounded disturbances. In addition, it can be checked that (5.18) and (5.20) satisfy the modular stability specifications (Lemma 3.3.1).

(5.22) tends to make V converges to V^{ref} exponentially at the rate K_v. However, such claim is true only when P tracks P^{ref} in a much faster time scale. (5.22) is derived from (5.5). So when $Q = Q^{ref}$, (5.23) ensures $\omega_i = 0$.

To summarize, we present a distributed control design ((5.18), (5.20), (5.22) and (5.23)) that meets all conditions of Lemma 5.3.1. In contrast to (5.7), the proposed distributed control takes $\dot{V}$ and ω_i into consideration. Thus, we can treat (5.7) as a special case of (5.18) (when $\dot{V}/V$ and ω_i are negligible). Discussions on stability, implementation, and robustness follow next.

5.4 Stability, implementation and robustness discussions

In this section, we first discuss the stability of the closed-loop system. Then, for implementation purpose, we provide several instructions, such as how to choose proper set points, control gains, etc. The robustness concerns are addressed in the end.

5.4.1 Stability

The stability of an inverter-based DER is stated below. Note that the proposed inverter control ((5.18), (5.20), and (5.22)) is an application of the proposed distributed control given in Chapter 3 and Chapter 4.

Theorem 5.4.1. *Consider an inverter-based DER controlled by* (5.18), (5.20), *and* (5.22) *For a given operating range* Ω *and a given disturbance bound* α, *we assume there exists at least one set of* (K_p, K_v) *satisfying* (5.21). *Thus, with the updating laws* (5.22) *and* (5.23), *the controlled DER exponentially converges to a steady state (if there exists one) with no distortions in the steady state. In addition, terminal voltage* V *satisfies* $\lim_{t\to\infty} V = V^{ref}$.

Proof. Notably, (5.18) and (5.20) satisfies the conditions of Lemma 3.3.1, while (5.22) and (5.23) are derived from the decentralized method (4.8). Hence, the convergence of the terminal voltage follows from Lemma 4.3.1 and Corollary 3.3.1.

To prove the rest part of Theorem 5.4.1, it is equivalent to show all conditions of Lemma 5.3.1 are met. As we explained in Section 5.3, (5.18) and (5.20) ensure that the second condition is met. (5.22) and (5.23) ensure that the third condition is met. Notice that the first condition holds by assumption. Therefore, we have shown that all conditions of Lemma 5.3.1 are satisfied, which completes the proof. □

5.4.2 Implementation

When implementing (5.18)-(5.23), a critical question arises: is it possible to map (5.21) into boundaries of the feasible operational region or controller gains? In what follows, we attempt to answer this question by proposing a few practical instructions.

We consider the control saturation and operating current limit:

$$v_{cd}^2 + v_{cq}^2 \leq V_{max}^2 \qquad I \leq I_{max} \tag{5.24}$$

where V_{max} is determined by the DC side circuit. I_{max} represents the current limit.

Notably, above operating constraints define a feasible operating region. More specifically, voltage and current constraints determine how much real and reactive power that the device can produce in the steady state. Suppose that V_{max} and I_{max} are constant, and filter parameters R_1 and L_1 are known as well. We can derive a static bound for real and reactive power in the following proposition.

Proposition 5.4.1 (feasible operating region). *In the steady state, real and reactive power output P and Q, must satisfy:*

$$P^2 + Q^2 \leq V_{max}^2 I_{max}^2 - (R_1^2 + \omega^2 L_1^2) I_{max}^4 \tag{5.25}$$

where ω is the frequency.

Proof. The proof follows from the law of conservation of energy. □

Keeping Proposition 5.4.1 in mind, we state our first implementation instruction:

Corollary 5.4.1 (instruction on set point design). *The real and reactive power set points P^{ref} and Q^{ref} should satisfy:*

$$(P^{ref})^2 + (Q^{ref})^2 \leq V_{max}^2 I_{max}^2 - (R_1^2 + \omega_0^2 L_1^2) I_{max}^4 \tag{5.26}$$

It is clear that such result is a direct application of Proposition 5.4.1. Here, we map the operating constraints into a potential steady state operational region.

Next, we focus on finding instructions on the control gain design. Notice that substituting (5.18), (5.20) and (5.22) into (5.4) yields:

$$\dot{P} = v_1 = -K_p\dot{E}_c - \frac{2K_pK_v}{C}(E_c - E_c^{ref}) \tag{5.27}$$

Thus, we can consider (5.18), (5.20) and (5.22) as a PD controller with $(E_c - E_c^{ref})$ as the input. $2K_pK_v/C$ are K_p turns out to be the proportional and derivative gain, respectively.

Similarly, substituting (5.18), (5.20) and (5.23) into (5.4) yields:

$$\dot{Q} = v_2 = 2K_pE_c\omega_i \tag{5.28}$$

Similarly, Q dynamics can be considered as a proportional controller with frequency distortion $(\omega_i - 0)$ as the input.

To summarize, the closed-loop P and Q dynamics can be regarded as two PID controllers driven by voltage derivation and frequency distortion, respectively. We introduce a notation $\dot{P}_o$ denoting the rate of change of power injected from the disturbance.

Based on well-known results in PID control design, we then organize our second implementation instruction as below.

Proposition 5.4.2 (instructions on control gain design). *Suppose that* (5.21) *holds. With the proposed control* (5.18), (5.20), (5.22) *and* (5.23), *the stored energy deviation of the capacitor* $E_c - E_c^{ref}$ *satisfies*

$$\|E_c - E_c^{ref}\|_2^2 \leq \gamma^2 \|\dot{P}_o\|_2^2 \tag{5.29}$$

where

$$\gamma = \sup_{\omega \in R}(\|\frac{C}{K_pK_v - C\omega^2 + jCK_p\omega}\|_2) \tag{5.30}$$

Besides, we have two empirical instructions on the control gain design:

1. *K_p should not be too large as it is sensitive to high-frequency signals;*

2. *K_pK_v/C and K_pE_c should not be too large as they may cause numerical instability.*

Proof. Let $x_1 := E_c - E_c^{ref}$, $x_2 := P - P_o$, $u := \dot{P}_o$. The closed-loop system dynamics can be written as:

$$\begin{aligned} \dot{x}_1 &= x_2 \\ \dot{x}_2 &= -\frac{K_pK_v}{C}x_1 - K_px_2 - u \end{aligned} \tag{5.31}$$

When $u = 0$, the system is globally exponentially stable since it is easy to check the system matrix is Hurwitz.

Let $y = x_1$, we can write the transfer function

$$G(s) = C(sI - A)^{-1}B = -\frac{C}{Cs^2 + CK_ps + K_pK_v} \tag{5.32}$$

Therefore, the L_2 gain is $\sup_{\omega \in R}(\|G(j\omega)\|_2)$. Moreover, if u is a constant ($u = u^*$), the system exponentially converges to $(x_1^*, x_2^*) = (\frac{C}{K_pK_v}u^*, 0)$.

According to the well-known results on PID control, an ideal derivative term is sensitive to high-frequency signals. Also, in numerical simulation, the simulation time step should be small enough to avoid numerical instability if proportional gains are large. Hence, we obtain the two empirical instructions. The proof is completed. □

Proposition 5.4.2 says that we will have a bounded terminal voltage if the rest of system injects finite amount of energy via $\dot{P}_o$. Also, notice that γ is the L_2 gain. We can minimize it via choosing proper K_p and K_v.

5.4.3 Robustness

In Theorem 5.4.1 and results thereafter, we assume (5.21) holds with the proposed control. In this subsection, we attempt to relax it and then derive two sufficient conditions, namely Lemma 5.4.2 and Lemma 5.4.3. Since (5.18) and (5.20) may be sensitive to parameter errors, we consider the robustness concerns when deriving Lemma 5.4.2 and Lemma 5.4.3, .

Note that the left hand side of (5.21) equals:

$$\begin{aligned} &\frac{F_2^2}{V^2} + \frac{F_1^2}{V^2} + 2F_1 + v_d^2 + v_q^2 \le V_{max}^2 \\ \Rightarrow &\frac{F_2^2}{V^2} + \frac{1}{V^2}(F_1^2 + 2F_1V^2 + V^4) \le V_{max}^2 \end{aligned} \tag{5.33}$$

Next, we approximate this constraint by a square bound, yielding two constraints on F_1 and F_2:

$$F_2^2 \le \frac{1}{2}V_{max}^2 V^2 \qquad (F_1 + V^2)^2 \le \frac{1}{2}V_{max}^2 V^2 \tag{5.34}$$

If we further fix the control inputs in P and Q dynamics (5.4):

$$v_{cd} = v_d \qquad v_{cq} = v_q \tag{5.35}$$

let P_{forc} and Q_{forc} denotes the corresponding forced response:

$$\dot{P}_{forc} = -(\frac{R_1}{L_1} - \frac{\dot{V}}{V})P - (\omega_0 + \omega_i)Q \qquad \dot{Q}_{forc} = -(\frac{R_1}{L_1} - \frac{\dot{V}}{V})Q + (\omega_0 + \omega_i)P \tag{5.36}$$

P_{forc} and Q_{forc} represent how external distortions affect the output dynamics. $(-R_1P/L_1 - \omega_0 Q)$ and $(-R_1Q/L_1 + \omega_0 P)$ denote the natural damping of the dynamics. If the natural damping is not enough to cancel the distortion effects, P_{forc} and Q_{forc} become unstable.

If we rewrite F_1 and F_2 with $\dot{P}_{forc}$ and $\dot{Q}_{forc}$ in (5.18):

$$F_1 = v_1 - \dot{P}_{forc} \qquad F_2 = v_2 - \dot{Q}_{forc} \tag{5.37}$$

the control design intuition becomes clear: we are designing v_1 and v_2 to first cancel the positive damping caused by external distortions and then regulate the real and reactive power by adding more damping.

Substituting (5.37) into (5.34) yields:

$$|v_1 - \dot{P}_{forc} + V^2| \le \frac{1}{\sqrt{2}} V_{max} V \qquad |v_2 - \dot{Q}_{forc}| \le \frac{1}{\sqrt{2}} V_{max} V \tag{5.38}$$

The first inequality limits P dynamics, while the other limits Q dynamics. Depending on the operating condition, P has two scenarios to consider, namely P is bigger or smaller than P^{ref}. So does Q dynamics.

Utilizing the first inequality of (5.38), we obtain the following sufficient conditions:

Lemma 5.4.2. *Consider an inverter-based component that is controlled by* (5.18)*. Suppose that external distortions have bounded effects on the component, i.e., P_{forc} satisfies:*

$$|\dot{P}_{forc}| \le \frac{1}{\sqrt{2}} V_{max} V - \kappa(|P - P^{ref}|) - V^2 \quad \forall\, t \ge t_0 \tag{5.39}$$

where $\kappa(*)$ is a $\mathcal{K}_\infty$ function.

P asymptotically converges to P^{ref}, if the following conditions hold:

- $v_1 \le 0$*, when* $P \ge P^{ref}$
- $v_1 \ge 0$*, when* $P \le P^{ref}$
- $|v_1| \le \kappa(|P - P^{ref}|)$

Proof. Here, we provide the proof sketch. Since $|v_1|$ is upper bounded by $\kappa(|P - P^{ref}|)$, we obtain the following inequalities:

$$\begin{aligned} |\dot{P}_{forc}| \le V_{max}V - |v_1| - V^2 &\Rightarrow |\dot{P}_{forc} - V^2| \le \frac{1}{\sqrt{2}} V_{max} V - |v_1| \\ &\Rightarrow |\dot{P}_{forc} - V^2 - v_1| \le |\dot{P}_{forc} - V^2| + |v_1| \le \frac{1}{\sqrt{2}} V_{max} V \end{aligned}$$

where the second and the third inequality follows directly from the triangular inequality. Therefore, no control saturation occurs, which further leads to a closed-loop dynamics $\dot{P} = v_1$.

Consider a Lypunov candidate function $H = \frac{1}{2}(P - P^{ref})^2$, whose first-order derivative is:

$$\dot{H} = (P - P^{ref})v_1 \tag{5.40}$$

It is clear that the first and the second conditions implies that $\dot{H} \leq 0$ for $\forall\, t \geq t_0$. Also P^{ref} is the only point in the set $\Omega = \{P|\dot{H} = 0\}$. By following the LaSalle's Invariant principle, we complete the proof. □

Similarly, a sufficient condition can be derived for Q dynamics:

Lemma 5.4.3. *Consider an inverter-based component that is controlled by* (5.18). *Suppose that external distortions have bounded effects on the component, i.e.,* Q_{forc} *satisfies:*

$$|\dot{Q}_{forc}| \leq \frac{1}{\sqrt{2}}V_{max}V - \kappa(|Q - Q^{ref}|) \quad \forall\, t \geq t_0 \tag{5.41}$$

where $\kappa(*)$ *is a* $\mathcal{K}_\infty$ *function.*

Therefore, Q *asymptotically converges to* Q^{ref}*, if the following conditions hold:*

- $v_2 \leq 0$, *when* $Q \geq Q^{ref}$
- $v_2 \geq 0$, *when* $Q \leq Q^{ref}$
- $|v_2| \leq \kappa(|Q - Q^{ref}|)$

The proof is identical to the proof of Lemma 5.4.2. So we omit the detail for brevity.

5.5 Illustration of the proposed control on the MIL test system

5.5.1 Military test (MIL) system

Consider a representative microgrid comprising heterogeneous components such as small generators, inverter controlled solar PV and battery supplying diverse loads, as shown in Figure 5-2. Figure 5-2 is called MIL system, which is the test system for

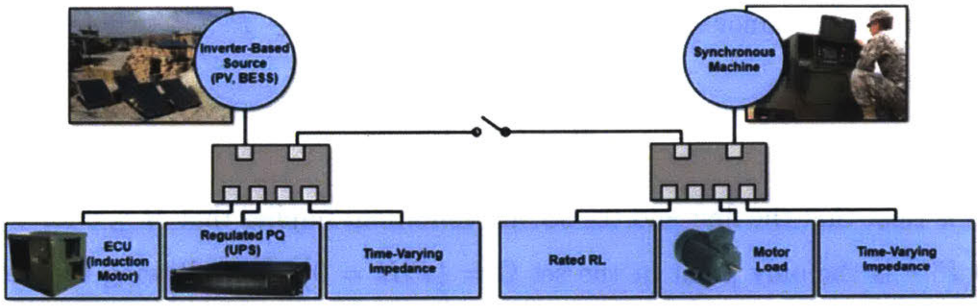

Figure 5-2: Military test (MIL) system

future military grids. Its objective is to deliver power to loads at acceptable quality of service (QoS), as loads and solar power vary over time, or even as topology changes in a planned or unplanned way.

Figure 5-2 system consists of an inverter-based sub-grid and a synchronous machine (SM)-based sub-grid. Inside the SM sub-grid, there is a rated RL load-1 (L_1), a motor load (L_2) and a time-varying load-2 (L_3). Inside the inverter-based sub-grid, we have a time-varying load (L_4) and a regulated power load (UPS L_5).

5.5.2 Simulation setup

First Figure 5-2 system was simulated in CAMPS [103]. Because CAMPS supports systematic modeling and analysis for control design. Next the system was simulated using MATLAB Simulink with all the details needed for implementation like sensors, quantization, and discrete sampling times.

To evaluate the effectiveness of the proposed control, three scenarios are considered.

5.5.3 Scenario 1: maximum loading

In this scenario, all loads are active and are set at their maximum value. The equilibrium of each component is computed numerically first, which are listed in the following tables.

In simulations, each component starts from its equilibrium. We add 1% perturbation as the disturbance to the initial condition. The proposed control is compared

Table 5.1: Calculated equilibrium: synchronous machine

States	δ_{G1}	ω_{G1}	P_{m1}	P_{e1}	i_{Sd1}	i_{Sq1}
Equilibrium (p.u.)	1.71	1	1	1	0.69	-0.89

Table 5.2: Calculated equilibrium: inverter-based PV

States	i_{PVd}	i_{PVq}	v_{cd}	v_{cq}	v_d	v_q
Equilibrium (p.u.)	-2.67	-6.9	0.01	-0.01	0.09	-0.99

Table 5.3: Calculated equilibrium: SM side Loads

States	i_{L1d}	i_{L1q}	i_{L2d}	i_{L2q}	i_{L3d}	i_{L3q}
Equilibrium (p.u.)	-0.54	-0.85	-1.76	-0.95	0.076	-0.99

Table 5.4: Calculated equilibrium: PV side Loads

States	i_{L4d}	i_{L4q}	i_{L5d}	i_{L5q}	P_{L5}	Q_{L5}
Equilibrium (p.u.)	0.01	-3.01	-0.16	-1.99	2	0.01

with the conventional control for this scenario. The frequency response and the voltage response are shown in Figure 5-3 and Figure 5-4, respectively.

Figure 5-3(a) and Figure 5-4(a) are the performance of the conventional control. It can be seen that the frequency is unstable and the voltage collapses. This is because the equilibrium is unstable and the conventional control cannot handle it. Therefore, the system becomes unstable even under 1 % perturbation.

In contrast, the proposed control is robust and has the ability to automatically adjust its set points. As shown in Figure 5-3(b) and Figure 5-4(b), both the frequency and the voltage are stabilized and regulated to their feasible operating point.

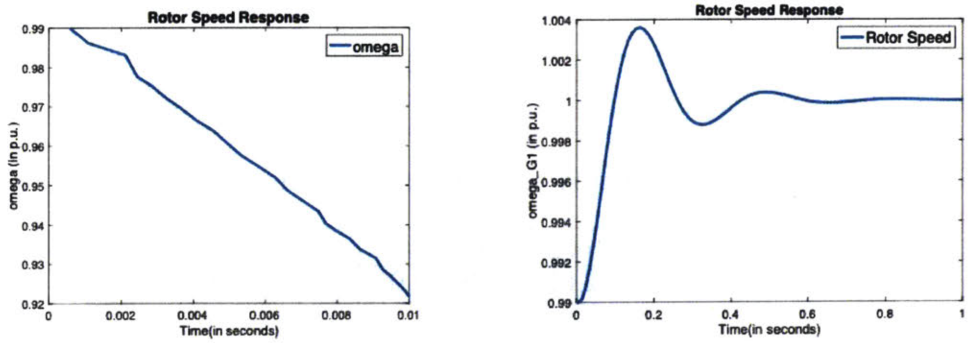

(a) Conventional control (unstable)

(b) Proposed control

Figure 5-3: Rotor speed response (maximum loading scenario)

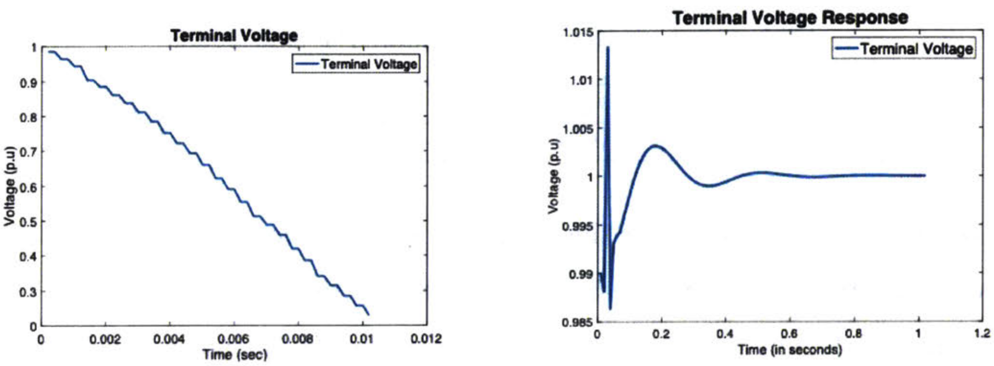

(a) Conventional control (voltage collapse)

(b) Proposed control

Figure 5-4: Terminal voltage response (maximum loading scenario)

5.5.4 Scenario 2: unplanned load changes and topology changes

In the second scenario, we evaluate the effectiveness of the proposed control against large faults. Both unplanned load changes and topology changes are considered. In addition, we assume that set points and control gains of each controllable components remain the same during these unplanned events.

The initial loading condition is listed in Table 5.5. The tested events are summarized in Table 5.6. The real and reactive power load changes are shown in Figure 5-5.

Table 5.5: Scenario 2: initial loading condition (P & Q)

Initial Cond.	Rated RL (L_1)	Motor load L_2	Time-varying load L_3	Time-varying load L_4	UPS L_5
P (p.u.)	0.78	0.77	0.16	0.32	0.32
Q (p.u.)	0.60	1.78	0.00	0.08	0.00

Table 5.6: Scenario 2: tested events (unplanned load changes & topology changes)

Unplanned Events	$T = 3s$	$T = 8s$	$T = 13s$	$T = 18s$	$T = 23s$	$T = 28s$	$T = 33s$	$T = 38s$
Load changes (p.u.)	$P_{L3} = 0.08$ $P_{L5} = 0.16$	$P_{L3} = 0.32$ $P_{L5} = 0.32$	$Q_{L4} = 0.16$ $Q_{L5} = 0.1$	No changes	No changes	$P_{L1} = 0.00$ $Q_{L1} = 0.00$	$P_{L2} = 0.00$ $Q_{L2} = 0.00$	$P_{L2} = 0.77$ $Q_{L2} = 1.78$
Topology changes	Normal	Normal	Normal	Switch open	Switch close	Normal	Normal	Normal

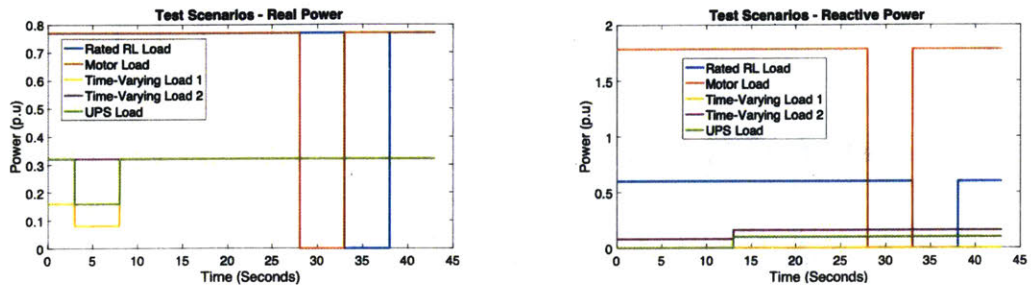

(a) Real power changes of each load

(b) Reactive power changes of each load

Figure 5-5: Tested loading changes (Sbase = 6.25 kVA)

To the best of author's knowledge, we have not found any existing control which can handle these changes without much trial-and-error tunning. This is why we do not compare our proposed control with other existing methods. The performance of the proposed control is shown in Figure 5-6 to Figure 5-11.

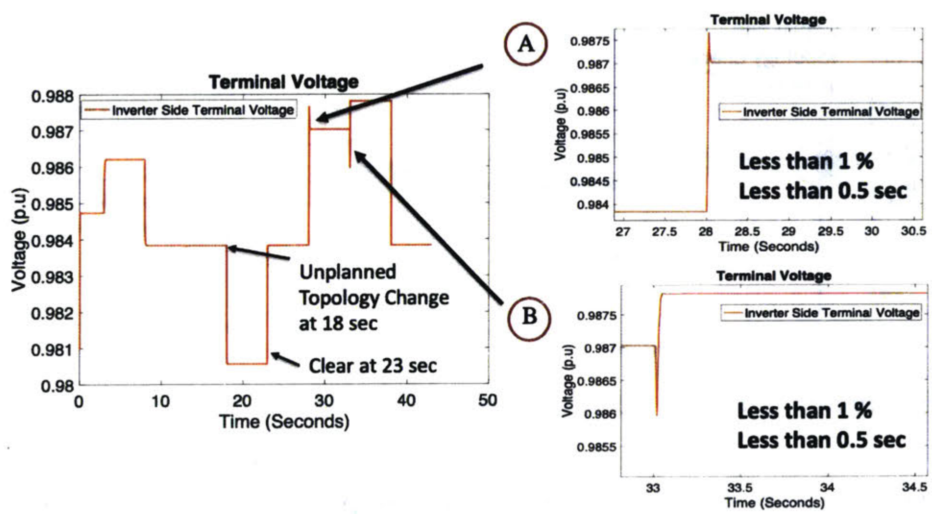

Figure 5-6: Terminal voltage response of the inverter-controlled PV

Figure 5-6 shows that the PV terminal voltage is around 1 p.u, as unplanned events occurs. We do observe there exist some transient periods. The controller is able to stabilize and regulate the terminal voltage back to the nominal voltage. The voltage overshoot is less than 1%, which meets the MIL standard.

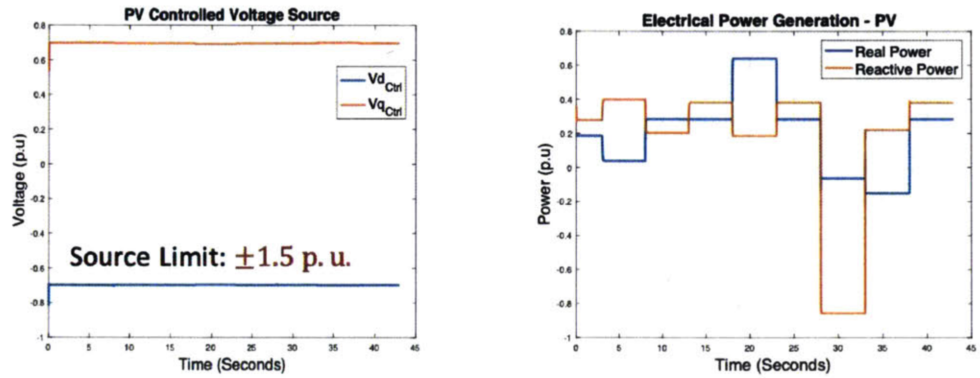

(a) Control signal (b) Real and reactive power output

Figure 5-7: Control signal and power output of the inverter-controlled PV

Figure 5-7 shows the responses of control input and the power output. As shown in Figure 5-7(a), the control input is under the source limit. Thus, no saturation occurs. From Figure 5-7(b), it can be seen that the proposed control is able to automatically adjust its power generation so that the load requirement is satisfied.

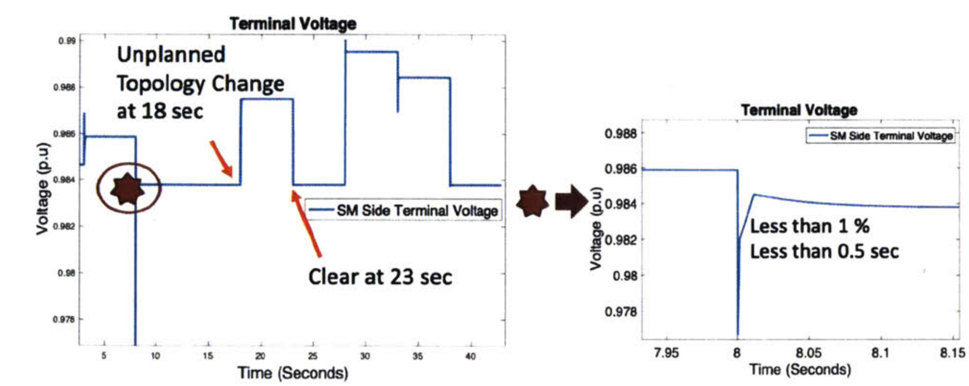

Figure 5-8: Terminal voltage response of the synchronous machine (SM)

Figure 5-8 shows that the terminal voltage response of the synchronous machine (SM). Similar as the PV terminal voltage, the proposed control keeps the terminal voltage around the nominal value. At 8 second, a huge load change occurs at the SM sub-grid. As marked with a red star, the terminal voltage drops at 8 s. But the controller is able to regulate the terminal voltage back in less than 0.5 s. The overall voltage drop is less than 1%.

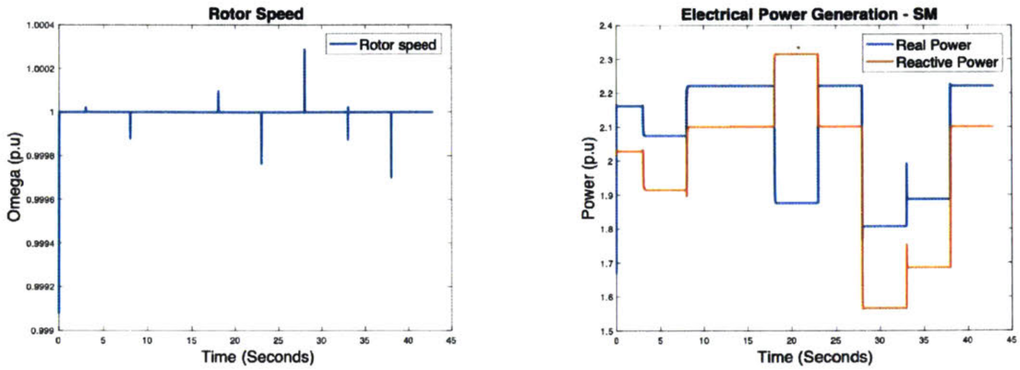

(a) Rotor speed

(b) Real and reactive power output

Figure 5-9: Rotor speed and power output of the synchronous machine (SM)

Figure 5-9 shows the responses of rotor speed and the power output. As shown in Figure 5-9(a), the rotor speed is maintained around 1 p.u. Figure 5-9(b) shows that the real and reactive power output of the SM are also automatically adjusted.

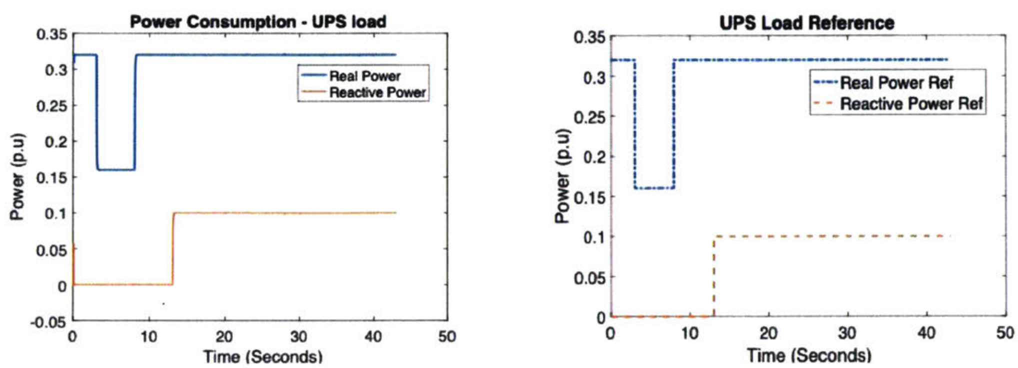

(a) UPS power consumption

(b) Power reference

Figure 5-10: UPS load response and its reference

Figure 5-10 and Figure 5-10 show the performance of the loads. Both power consumption and predefined power reference are shown. Here, we just pick the UPS load and the motor load. It can be seen that both the UPS load and the motor load are following their power references.

Therefore, we can concluded that the proposed control is robust and flexible against unplanned large changes.

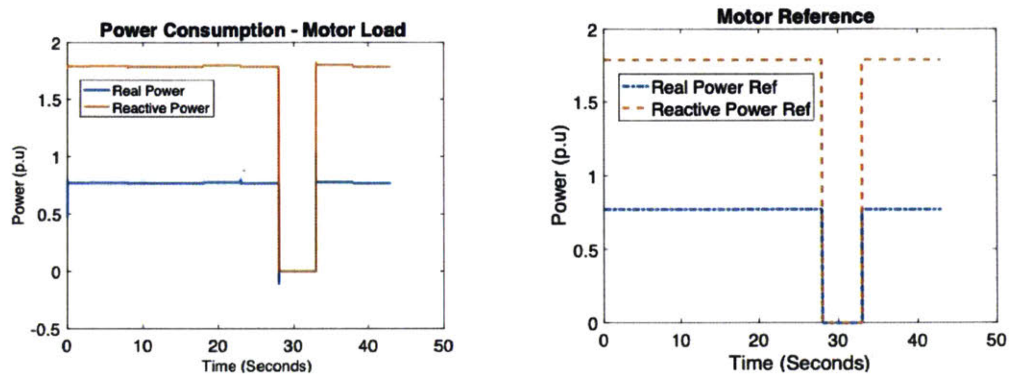

(a) Motor load power consumption (b) Motor load reference

Figure 5-11: Motor load response and its reference

5.5.5 Scenario 3: distortions

The third scenario is to illustrate the effectiveness of the proposed control in canceling out distortions. Instead of using CAMPS, we simulated the MIL system using MATLAB Simulink with all the details needed for implementation like sensors, quantization, and discrete sampling times.

In this test scenario, we slightly modified the MIL test system for the simplification purpose: we put the same rated RL load and motor load on both sub-grids, and the time-varying loads and the UPS loads were removed. The disturbances are simulated through unplanned load changes and the switch close. The event table is listed below:

Table 5.7: Scenario 3: tested events (unplanned load changes & topology changes)

Unplanned Events	$T = 0s$	$T = 1s$	$T = 2s$	$T = 3s$	$T = 3.5s$	$T = 4s$	$T = 6s$	$T = 8s$
Inverter-side active load	No load	RL	RL	RL	No load	Motor	Motor	Motor
SM-side active load	Motor	Motor & RL	Motor & RL	Motor	Motor	No load	RL	RL
Switch position	Open	Open	Close	Close	Close	Close	Close	Open

Due to these large changes, the assumption on terminal voltage may not be valid. It is challenging not only because of these unplanned changes, but also because both the rated RL load and the motor load are inductive. In simulations, we compare the proposed inverter-based control with the inner and outer loop control (5.7). Note that the synchronous machine in both cases uses the proposed control. Simulation results are summarized below.

Figure 5-12 shows the performance of the inverter-based PV controlled by (5.7).

The overall performance is OK. But if we zoom in, we observe huge current distortions. In contrast, the proposed control is capable of canceling out the distortions. Figure 5-12 presents the performance of the proposed control.

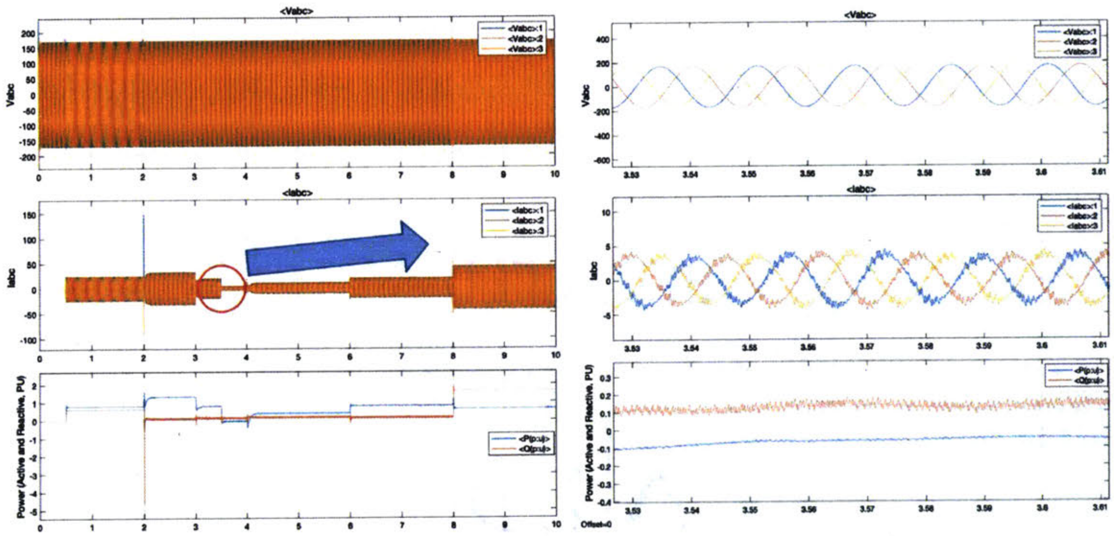

Figure 5-12: Performance of the inverter-controlled PV with the SOA control

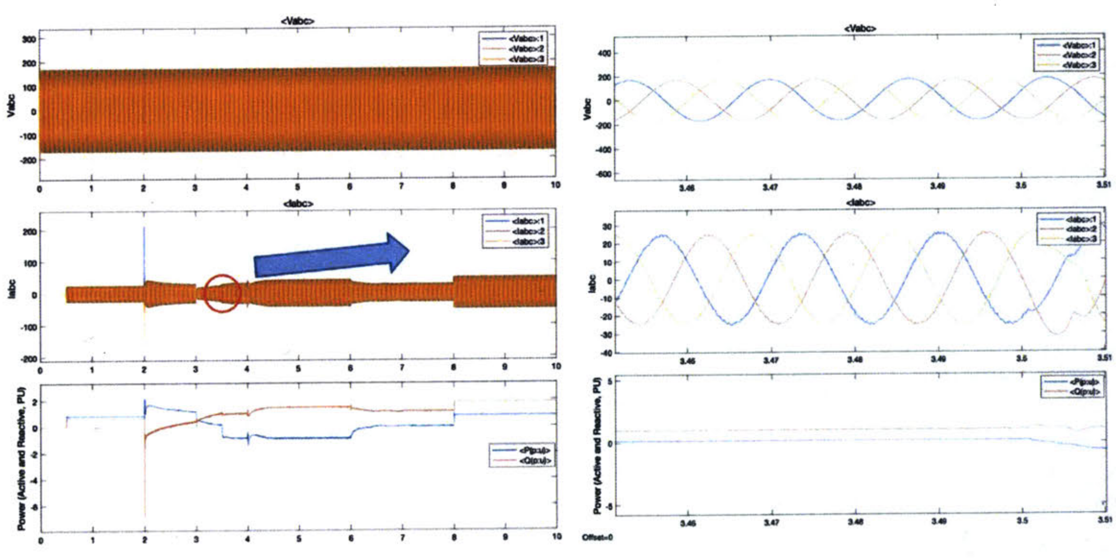

Figure 5-13: Performance of the inverter-controlled PV with the proposed control

5.6 Summary

In this chapter, we provide a new perspective to understand the root causes of distortions. Using the proposed model, it can be seen that the distortions are caused by the real and reactive power imbalance. To cancel out the distortions and improve the QoS, we propose a novel distributed control for inverter-based components utilizing the TSS model. Both the stability, implementation and robustness concerns are discussed in detail. In the end, we conduct several tests on the MIL system to evaluate the effectiveness of the proposed solution. Through numerical simulations, it can be concluded that our proposed control is able to cancel out the distortions. It is also robust against unplanned events.

Chapter 6

Reconfigurable operation for autonomous microgrids

6.1 Introduction

In this chapter, we illustrate the effectiveness of the proposed control in support of AEES. A few typical components of EESs and two IEEE standard microgrids are chosen as examples. We consider several test scenarios including unexpected events, network reconfiguration and different load composition. The performance of the proposed control is compared with the industrial common practice control.

6.1.1 Chapter outline

The chapter is organized as follows. In Section 6.2, we provide the proposed control for a synchronous machine and an induction machine. Then, we test the proposed control using two IEEE standard microgrids in Section 6.3 and Section 6.4, respectively. Section 6.5 concludes the chapter.

6.2 Nonlinear control for typical components of electrical energy systems

In Chapter 5, we introduced the proposed control for inverter-based components. So in this section, we focus on the electrical machine, a critical and fairly complex device of EESs. We choose a synchronous machine and an induction machine as examples. Note that the proposed control also applies to other types, such as DC machines, DC motors, etc.

The complexity arises because of the electromagnetic and the electromechanical coupling. Generally speaking, irrespective of the number of windings, modeling of a machine is done by considering voltages applied across the windings as port inputs and then the dynamics of currents passing through each of these windings is governed by Maxwell's equations given as follows [104]:

$$\lambda = \mathbf{LI} \qquad \mathbf{V} = \mathbf{RI} + \dot{\lambda} \tag{6.1}$$

where $\mathbf{I}$ is a vector consisting of stator and rotor winding currents; $\mathbf{V}$ is the voltage applied across the terminals of each of these windings; $\mathbf{R}$ is a diagonal matrix with the resistance of each of the windings as its entities; $\mathbf{L}$ is the inductance matrix which is a full matrix and is dependent on the rotor position θ.

In the state space form, the dynamics can be rewritten as:

$$\dot{I} = \mathbf{L}(\theta(t))^{-1}(\mathbf{V} - \mathbf{RI} - \omega\frac{\partial \mathbf{L}}{\partial \theta}\mathbf{I}) \tag{6.2}$$

where $\mathbf{L}(\theta(t))$ is time varying. In order to ease the analysis, machine modeling is done by applying Park's transformation [104]. This transformation operates on any three-phase set of stator or rotor electrical variables to produce a new set of variables along direct and quadrature axes of the chosen reference frame.

Mechanical dynamics of all machines are governed by:

$$\begin{aligned}\dot{\delta} &= \omega_b(\omega - \omega_0) \\ \dot{\omega} &= \frac{1}{2H}(P_m - \tau_e\omega - D(\omega - \omega_0))\end{aligned} \tag{6.3}$$

where all the quantities are normalized on their base quantities, which is commonly referred to as per unit system in the power systems community. ω_b is the base angular speed of the rotor; ω is the rotor angular velocity; ω_0 is the angular velocity of the reference frame.; P_m is the mechanical power applied to the rotor shaft. This is positive for generator operation while it is negative for a motor operation which is equal to the load torque in normalized quantities. D denotes the rotor damping; H denotes the inertia of rotor. τ_e is the air gap torque produced due to interaction of stator and rotor fluxes. This is the quantity that couples electrical and mechanical sub-systems of a machine.

In what follows, we choose a synchronous machine and an induction machine as examples. The proposed modeling approach is first applied to both machines, resulting in a novel TSS model with the power as the output. Then, we provide the distributed control design following the procedures introduced in Chapter 3 and Chapter 4.

6.2.1 Synchronous machines

Using the proposed modeling approach, a nonlinear diesel synchronous machine model [91] can be written in the form:

$$M\dot{\omega} = P_m - P_e - D(\omega - \omega_0) \tag{6.4}$$

$$T_g\dot{P}_m = -P_m + K_t a \tag{6.5}$$

$$\dot{E} = -\frac{2R}{L}E + P_e - P_i \tag{6.6}$$

$$\dot{P}_e = \frac{i_q}{T'_{d0}}[-\frac{P_e}{i_q} - (x_d - x'_d)i_d] + P_e\frac{\dot{i}_q}{i_q} + \frac{i_q}{T'_{d0}}e_{fd} \tag{6.7}$$

where ω is the rotor speed; P_m is the mechanical power. $P_e = e_q^{'} i_q$ and $P_i = V_{td} i_d + V_{tq} i_q$ denote the controllable power generation and the power generated out of the machine, respectively; $e_q^{'}$ is the voltage behind transient reactance; M, D, T_{d0} and T_g are the inertia, damping coefficient, transient time constant and governor time constant, respectively; K_t is the sensitive gain of the valve; ω_0 is the rotor speed reference.

There are two control inputs, namely, exciter voltage e_{fd}, and governor valve position a. Thus, the question is to design exciter voltage e_{fd} and valve position a so that terminal voltage V_t and power injection $P_{e,i}$ are controlled.

Energy layer

The energy layer provides P_e^{ref} to the power layer. Following the procedures given in Section 4.3.1, we design P_e^{ref} as:

$$P_e^{ref} = P_{dis} + P_i^{ext} - K_v(V_t^2 - (V^{ref})^2) \tag{6.8}$$

Note that $-P_{meas}^{ref}$ in (3.18) is replaced by P_i^{ext}. P_i^{ext} represents the power injected from the outside. In an interconnected system, P_i^{ext} is obtained by exchanging information between its neighboring components.

Power layer

The power layer has two functionalities: first functionality is to ensure the stability of internal dynamics $\bar{\mathbf{x}}_{SM}$; second functionality is to control P_e around P_e^{ref}.

For the SM, we design e_{fd} as:

$$e_{fd} = \begin{cases} e_q^{'} + (x_d - x_d^{'}) i_d - \frac{T_{d0}^{'}}{i_q}(v - e_q^{'} \dot{i}_q) & |i_q| > \gamma \\ 0 & |i_q| < \gamma \end{cases} \tag{6.9}$$

where $\gamma > 0$ denotes a small value.

Substituting e_{fd} into P_e dynamics, we will obtain:

$$\dot{P}_e = v \tag{6.10}$$

Thus, the nonlinearity is canceled. The problem is simplified to design control input a and v so that rotor speed ω and $P_{e,i}$ can be regulated to their reference points. for a and v, we choose the form:

$$\begin{aligned} a &= k_1(\omega - \omega_0) + k_2(P_m - P_e^{ref}) + +k_3(P_{e,i} - P_e^{ref}) \\ v &= k_4(\omega - \omega_0) + k_5(P_m - P_e^{ref}) + k_6(P_{e,i} - P_e^{ref}) \end{aligned} \tag{6.11}$$

k_i $i = 1, ..., 6$ should chosen so that the closed loop system matrix is Hurwitz.

In order to find proper K_i, we choose function L as $L(X) = \mathbf{K}X$, where $\mathbf{K}$ is a constant matrix. M is chosen as a 3×3 identity matrix. Thus, k_i should be chosen so that conditions of Lemma 3.3.1 are satisfied. This procedure can be done efficiently by today's commercial solvers.

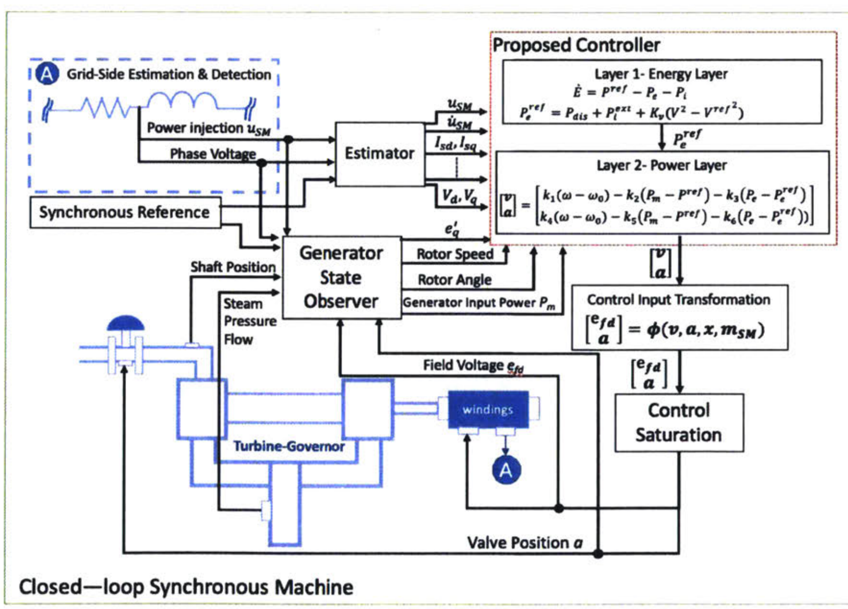

Figure 6-1: Control diagram of a synchronous machine

We list the control diagram of a synchronous machine in Figure 6-1.

6.2.2 Induction machines

Induction machine consists of three windings on stator and rotor each. To reduce the complexity, we rewrite (6.2) along a reference frame which is rotating at a constant speed ω_0. The stator and rotor dynamics are written using the reference frame rotating at a constant velocity, yielding two states on stator i_{Sd}, i_{Sq} and two states on rotor i_{Rd}, i_{Rq}. Note that the inductance matrix is always time invariant irrespective of reference frame chosen. This results in the same general equations as obtained in the case of synchronous machine. However the speed voltage term differs slightly since the relative velocity of rotor with respect to the reference frame $\omega - \omega_0$ can not be zero unless the same rotor reference frame is chosen.

For arbitrary reference frame, the electrical dynamics of an induction machine is:

$$\frac{d\mathbf{I}}{dt} = L^{-1}(\mathbf{V} - \mathbf{RI} - \mathbf{V}_\omega) \tag{6.12}$$

Here V_ω is the speed voltage term associated with the dynamics of each of these windings:

$$V_\omega = [-\omega_0\lambda_q \quad \omega_0\lambda_d \quad (\omega - \omega_0)\lambda_q \quad (\omega - \omega_0)\lambda_d]^T$$

V and I respectively are voltage applied across the terminals and current flowing through of each of these windings respectively:

$$V = [v_{Sd} \quad v_{Sq} \quad v_{Rd} \quad v_{Rq}]^T \qquad I = [i_{Sd} \quad i_{Sq} \quad i_{Rd} \quad i_{Rq}]^T$$

Mechanical dynamics of an induction machine is governed by (6.3). P_m is to be interpreted as a load torque rather than power input and hence the sign has to be negated.

Notably, the induction machine can be controlled to provide constant speed and/or constant torque. Most of the industrial loads require constant torque operation. One simple techniques to control the load torque is to embed power electronics control on the rotor side, resulting in $v_{Rd} = S_d v_{DC}$ and $v_{Rq} = S_q v_{DC}$, where S_d and S_q denote the switch average duty ratio along direct and quadrature axis respectively and v_{DC}

is a constant DC supply voltage on the rotor side inverter.

Using the proposed modeling approach, we obtain a similar model to the one outlined in the case of synchronous machine. The state variables and the control input are:

$$\mathbf{x_{IM}} = [i_{Sd}, i_{Sq}, i_{Rd}, i_{Rq}, \delta, \omega, P_{in,IM}]^T \qquad \mathbf{v_{IM}} = [S_d \; S_q]^T \tag{6.13}$$

The electromagnetic torque is given by:

$$P_{in,IM} = \tau_e = \sqrt{3/2} M_{in} (\lambda_{Sd} i_{Sq} - \lambda_{Sq} i_{Sd}) \tag{6.14}$$

where M_{in} is the parameter matrix. $\lambda_{Sd}, \lambda_{Sq}$ respectively are the fluxes linking with the direct axis and quadrature axis stator windings respectively. These fluxes are a function of rotor currents and also stator currents. Note that the direction of $P_{in,IM}$ is different from P_e used in the synchronous machine.

Now, we are ready to directly apply the proposed control design procedures. The dynamic energy layer and the active power layer design are explained below.

Power layer

By replacing one of the rotor currents, say i_{Rd} with $P_{in,IM}$ by using the relation (6.14), the dynamics of $P_{in,IM}$ becomes:

$$\begin{aligned} \dot{P}_{in,IM} &= \sqrt{3/2} M \left(\frac{d\lambda_{Sd}}{dt} i_{Sq} + \lambda_{Sd} \frac{di_{Sq}}{dt} - \frac{d\lambda_{Sq}}{dt} i_{Sd} + \lambda_{Sq} \frac{di_{Sd}}{dt}\right) \\ &= f_x + g_x (S_d i_{Rd} + S_q i_{Rq}) \end{aligned} \tag{6.15}$$

The physical control inputs S_d and S_q can be designed as

$$S_d = g_x^{-1} \left(\frac{i_{Rd}(-f_x + v_{TSS1})}{i_{Rd}^2 + i_{Rq}^2}\right) \qquad S_q = g_x^{-1} \left(\frac{i_{Rq}(-f_x + v_{TSS2})}{i_{Rd}^2 + i_{Rq}^2}\right) \tag{6.16}$$

Here v_{TSS1} and v_{TSS2} is the new control input.

The closed-loop $P_{in,IM}$ dynamics is:

$$\frac{dP_{in,IM}}{dt} = v_{TSS1} + v_{TSS2} \tag{6.17}$$

Thus, v_{TSS1} and v_{TSS2} should be chosen so that conditions of Lemma 3.3.1 are satisfied.

Energy layer

The energy layer design is identical to the design of the synchronous machine. Following the procedures given in Section 4.3.1, we design $P^{ref}_{in,IM}$ as:

$$P^{ref}_{in,IM} = P_{disp} + P^{ext}_{in} - K_v(V_t^2 - (V^{ref})^2) \tag{6.18}$$

where P^{ext}_{in} represents the measured power injection from the outside.

To summarize, we have provided a few examples on how to apply the proposed modeling and control method to typical electrical components. In the following section, two IEEE standard microgrids are introduced and simulated. The main objective is to illustrate the effectiveness of the proposed control in support of AEES.

Remark 6.2.1. *The same control can also be applied to other machine types, such as DC motor.*

6.3 Illustration on IEEE standard microgrid I

6.3.1 Sheriff microgrid description

The topology of the Sheriff microgrid is shown in Figure 6-2. It has two generator sets, whose rate are 1 MVA and 4 MVA operating at nominal voltage 460V and 13.8KV, respectively. There is also a PV system and a battery, having a maximum rated capacity of 3.5MW each, operating at a nominal voltage of 2.4kV. The distributed energy resources and loads are interconnected through a distribution network consisting of 13 distributed transformers and different kinds of relays and circuit breakers

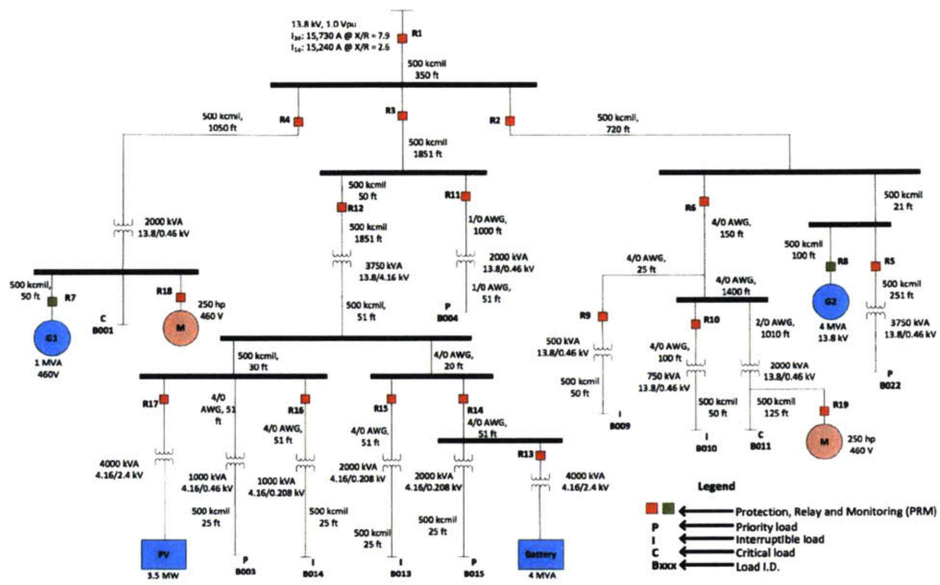

Figure 6-2: One line diagram of Sheriff microgrid [1]

to ensure protection of the components. Detail information can be found in [1].

When utility-generated power (bus 1 in Figure 6-2) is not available, two generators are responsible for serving the local load. Notably, Figure 6-2 is equivalent to Figure 3-1 system. We replace the battery (Bus 23) with an equivalent size generator.

6.3.2 Test Scenario: unexpected grid reconfiguration

The system is operated in the normal condition with the switch closed. Then, a sudden topology change occurs, i.e., the microgrid is disconnected from the utility. After a few seconds, the microgrid reconnects to the utility. During such contingency, power set points and control gains remain the same.

In this test, we benchmark the proposed control against two industrial common practice control, namely IEEE Type-I governor and IEEE Type-I Automatic Voltage Regulator (AVR). The control gains of the common practice control are obtained through numerous trial and error tunning. They are tunned for the normal interconnected condition.

Figure 6-3(b) and Figure 6-4(b) show the performance of the common practice

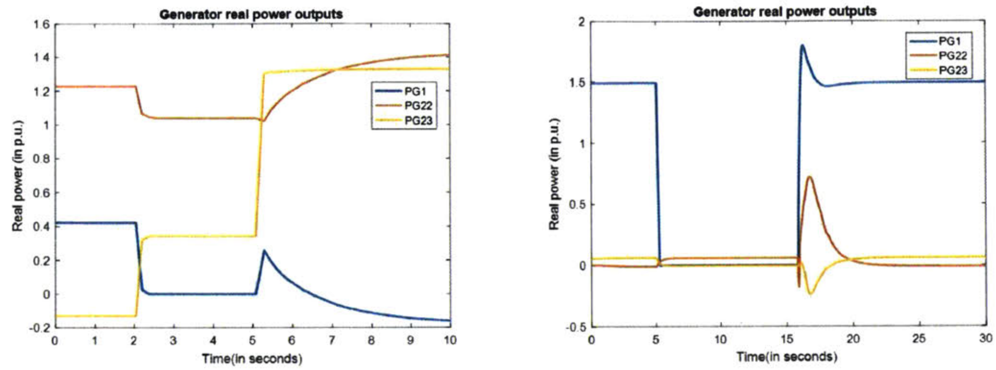

(a) Proposed control (b) Common practice control

Figure 6-3: Real Power Generation Response

control. It can be seen that the voltage drops to 0.2 p.u when the microgrid is disconnected from the utility. This is because the common practice control itself cannot detect the sudden topological change. Local generator sets are designed to maintain the old set point that is not compatible with the new operating condition. More specifically, when the switch is open, power injected into Bus 1 is reduced, which causes power imbalance in the microgrid. As a result, as shown in Figure 6-4(b), terminal voltage starts to drop and power flow starts to oscillate, which further leads to the voltage collapse.

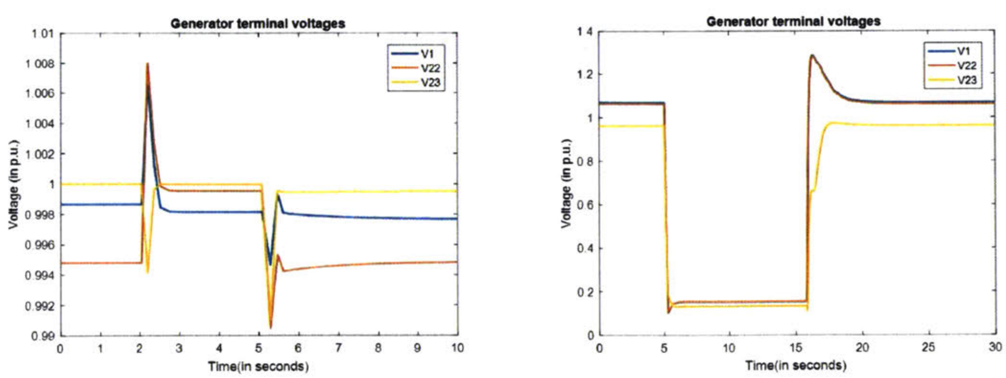

(a) Proposed control (b) Common practice control

Figure 6-4: Terminal Voltage Response

In contrast, the proposed control is able to sense the change and ensure that the terminal voltage is regulated irrespective of the operating modes. Notably, the controller automatically adjusts power set points. The performance can be seen in Figure 6-4(a) and Figure 6-3(a). At the system level, by exchanging information between controllable components and their neighboring components, the proposed control interactively drive the system to a new feasible equilibrium. As a result, the EES remains stable and feasible against sudden topological change.

6.4 Illustration on IEEE standard microgrid II

6.4.1 Banshee microgrid description

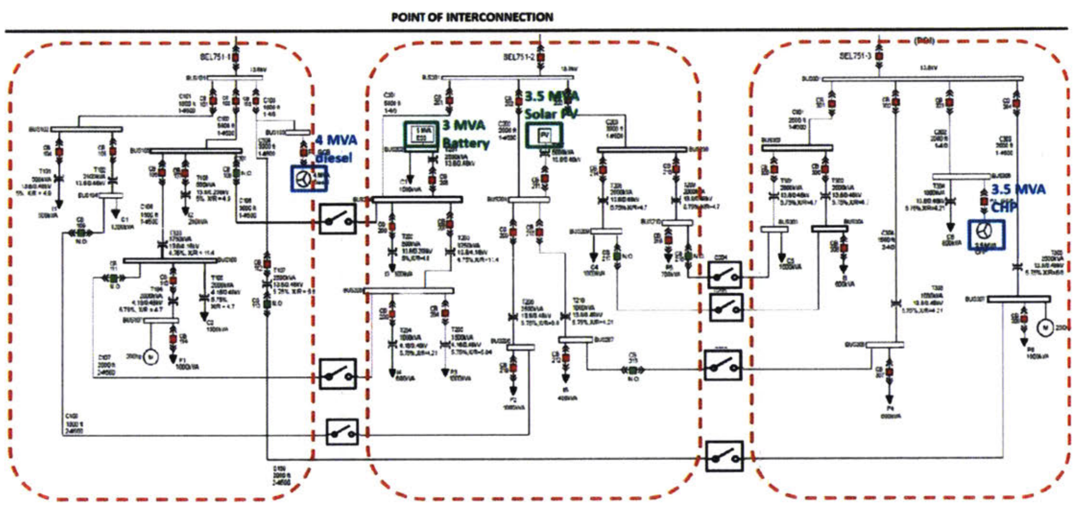

Figure 6-5: One Line Diagram of Banshee Microgrid

The topology of the Banshee microgrid is shown in Figure 6-2. The grid consists of three radial distribution feeders. It has two generator sets, whose rate are 3.5 MVA and 4 MVA operating at a nominal voltage of 13.8 kV, respectively. There is also a PV system and a battery, having a maximum rated capacity of 3.5MW each, operating at a nominal voltage of 2.4kV.

The Banshee grid is designed to operate under different network configurations. In the normal operating condition, the grid is connected to the utility at point of interconnection and each feeder is isolated from each other. When the grid is disconnected from the utility, all three feeders are interconnected with each other.

6.4.2 Test scenario 1: normal operating condition

In this test, the grid is in the normal operating condition, i.e., each feeder is isolated from each other. Moreover, we let the PV operates in the grid following mode, and the battery is in the grid forming mode.

The proposed control is compared with the industrial common practice control. Notably, the control gains of common practice control are default values, i.e., they are provided by vendors. We did not conducting extra tunning. The control gains of the proposed control are calculated off-line, following the procedures introduced before.

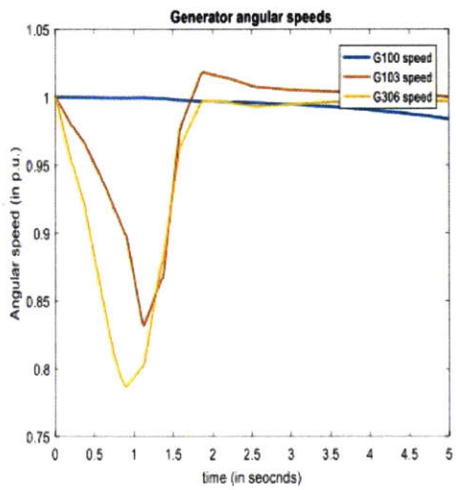

(a) Rotor speed of machines

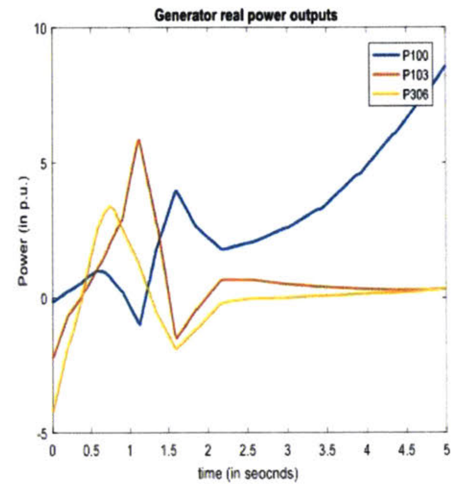

(b) Real power of machines

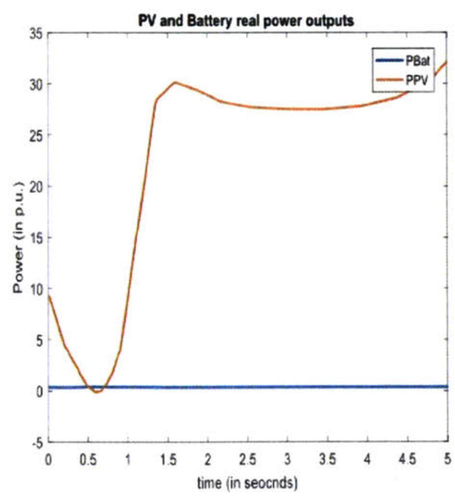

(c) Real power of PV and battery

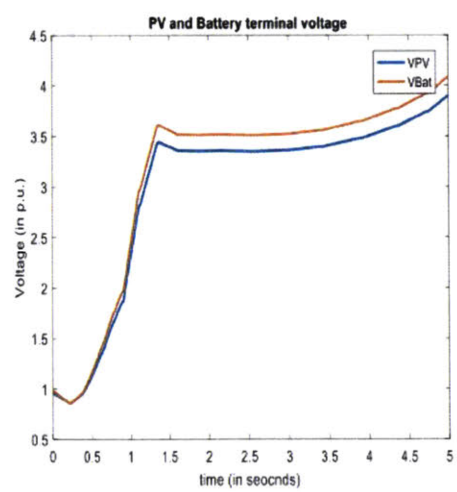

(d) Terminal voltage of PV and battery

Figure 6-6: Scenario 1: system performance with common practice control

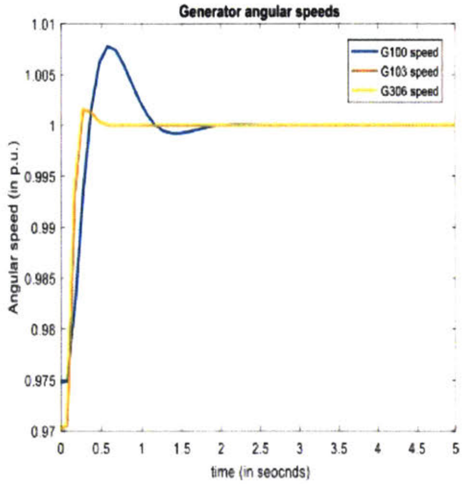

(a) Rotor speed of machines

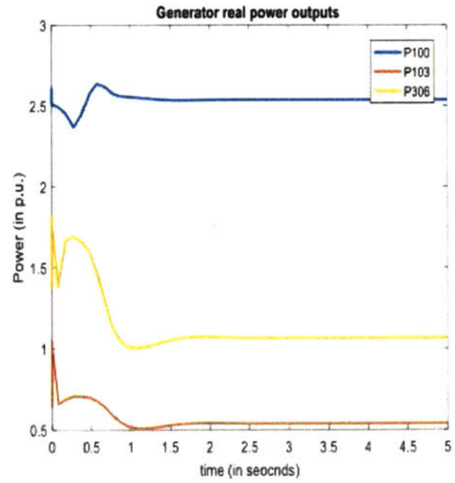

(b) Real power of machines

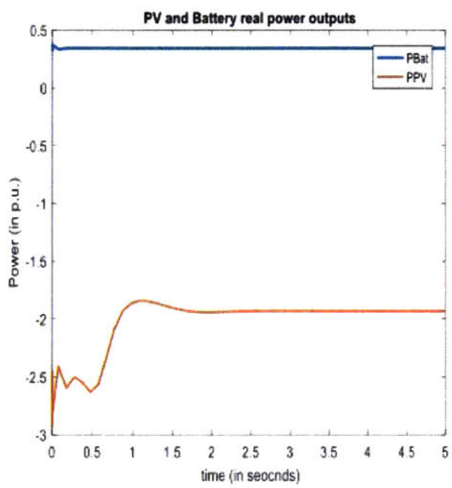

(c) Real power of PV and battery

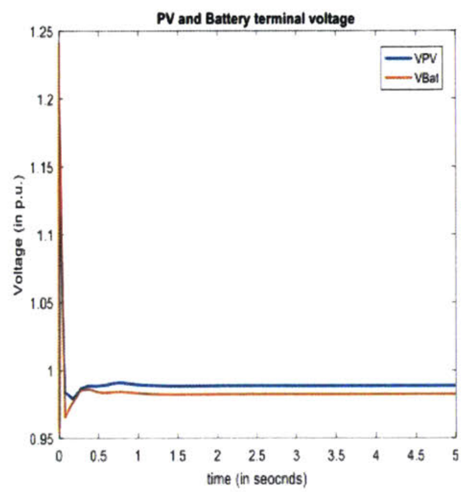

(d) Terminal voltage of PV and battery

Figure 6-7: Scenario 1: system performance with the proposed control

Figure 6-6 shows the performance of the common practice control, which is not acceptable. For those feeders with machines, Figure 6-6(a) shows that the frequency response. The frequency first encounters a drop and then starts to oscillate. Real power generation of each machine, as shown in Figure 6-6(b), is not either stabilized or regulated. For the feeder with PV and Battery, Figure 6-6(c) shows that the PV is producing too much power. Controllers are not able to make correct actions, which causes unacceptable voltage performances. The terminal voltage response is shown in Figure 6-6(c). Through the linearized analysis around the operating condition, we found an unstable eigen-mode in the closed-loop dynamics. Hence, we can claim that the common practice control cannot stabilize the grid with the default control gains. Extra tunning is required.

As a comparison, the proposed control is able to stabilize the grid. The simulation results are given in Figure 6-7. Although we did not provide correct set points to each controllable component, the embedded controller was able to adjust itself via iterative communication. In addition, the terminal voltage of each component is regulated, as shown in Figure 6-7(d).

6.4.3 Test scenario 2: islanded mode

In this test, we operate the grid in the islanded mode, i.e., the grid is disconnected from the utility but each feeder is interconnected with each other. Then, we let the PV and battery operate in the grid following mode, due to the generators.

Similar as Scenario 1, we compare the proposed control with the industrial common practice control. Unlike Scenario 1, we did conduct extra tunning. But the set points of controllers might still be inaccurate, as it is hard to know the real operating point in practice. The control gains of the proposed control remains the same as Scenario 1.

Figure 6-8 shows the performance of the common practice control. This time, it can be seen that the system is stabilized. However, as shown in Figure 6-8(d), the terminal voltage of both the PV and the battery are below 1 p.u, which is not acceptable. This is because of the predefined set points are inaccurate.

In contrast, the performance of the proposed control is shown in Figure 6-9. It can be seen that the proposed control is able to stabilize the grid in the islanded mode. More importantly, there is no need to change control gains or the control structure. Therefore, the proposed control can provide seamless transition between different modes, thus enabling AEES.

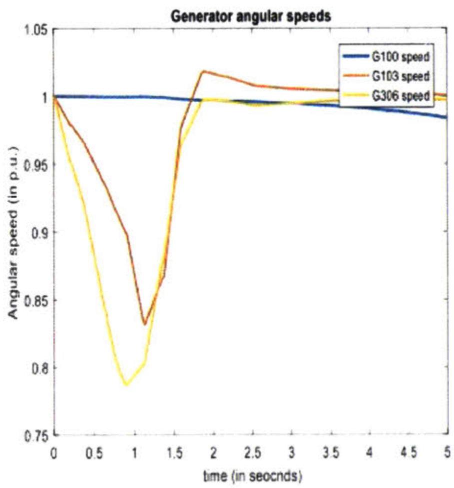

(a) Rotor speed of machines

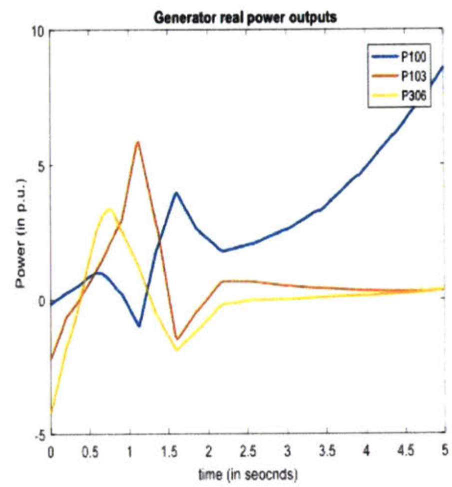

(b) Real power of machines

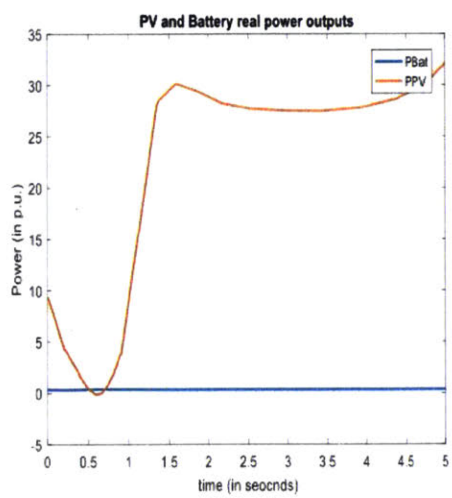

(c) Real power of PV and battery

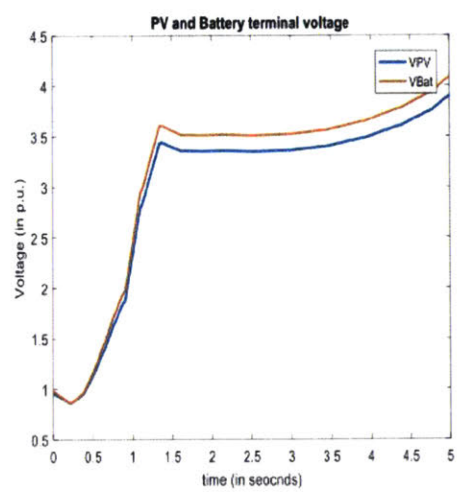

(d) Terminal voltage of PV and battery

Figure 6-8: Scenario 2: system performance with common practice control

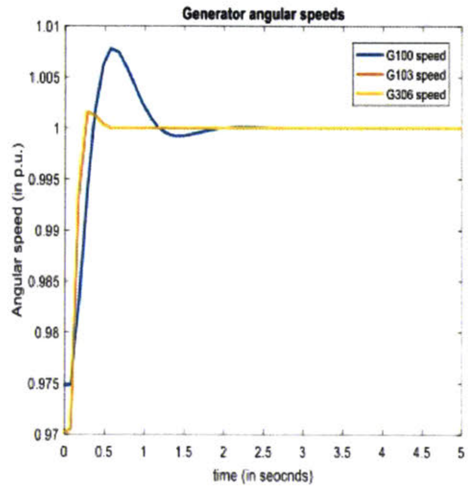

(a) Rotor speed of machines

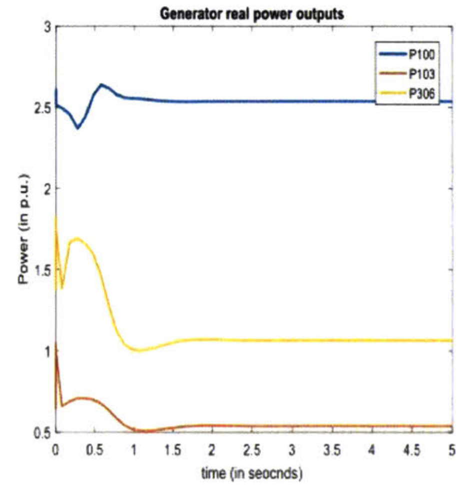

(b) Real power of machines

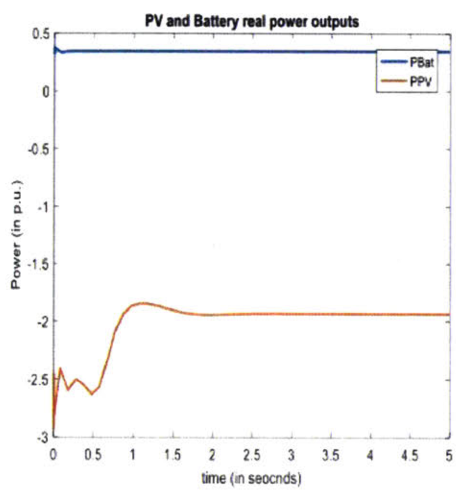

(c) Real power of PV and battery

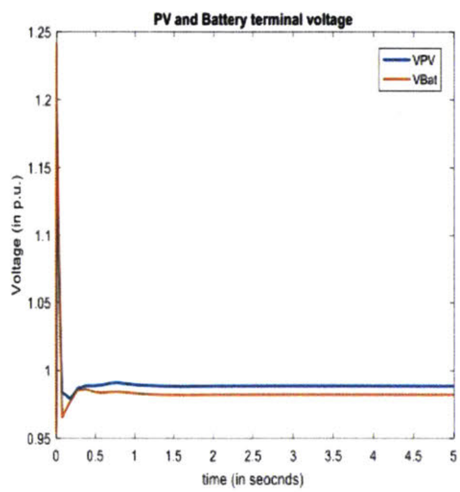

(d) Terminal voltage of PV and battery

Figure 6-9: Scenario 2: system performance with the proposed control

6.4.4 Test scenario 3: normal operating condition with large induction machines

In this test, we operate the grid in the normal operating condition. Instead of modeling the load as constant impedance, we include two large industrial-scale induction motors. The control gains of the common practice control are obtained via trial and error tunning, while the proposed control remains the same.

Figure 6-10 shows the real power output of the diesel generator, the CHP and the PV. As shown in Figure 6-10(a), the transient period is not acceptable. Each device is suffering from large oscillations. This is because large induction motors introduce disturbances to the grid which may violates the quasi-static assumption made in common practice controllers. As comparison, the proposed control has much better performance. Figure 6-10(b) shows that the setting time is much shorter, while the oscillation is also smaller.

Figure 6-11 shows the terminal voltage response of the common practice control and the proposed control. According to Figure 6-11(a) and Figure 6-11(b), it is clear that the terminal voltage response of the common practice control is unacceptable. The transient behavior of the common practice control exceeds the MIL standard. In contrast, the proposed control is able to stabilize and regulated the voltage to the nominal value.

Through all above three scenarios, we have numerically shown that the proposed control enables AEES. Without changing the control structure and control gains, the proposed control is able to stabilize the microgrids and regulate the terminal voltage.

6.5 Summary

In this chapter, we provide electrical machine examples of the proposed control. A synchronous machine and an induction machine are chosen as examples. We then evaluate the performance on two IEEE standard microgrids. Through simulations, it can be concluded that the proposed control outperforms the common practice control.

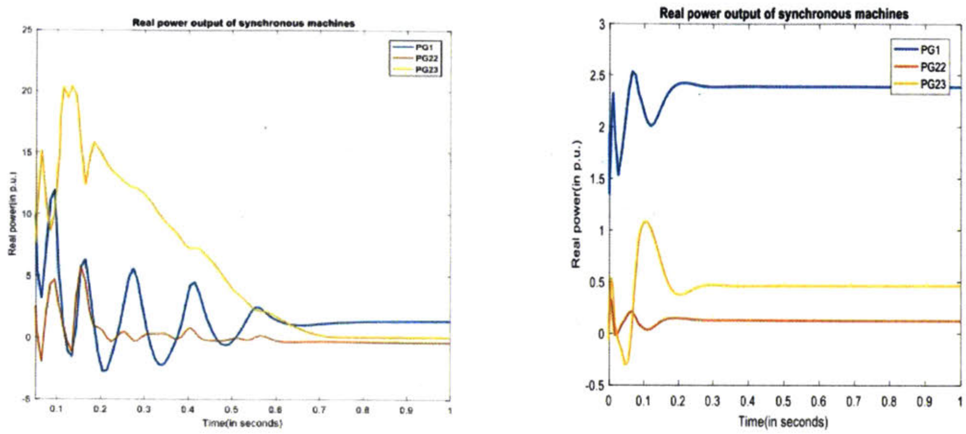

(a) Common practice control

(b) Proposed control

Figure 6-10: Scenario 3: real power generation of DERs

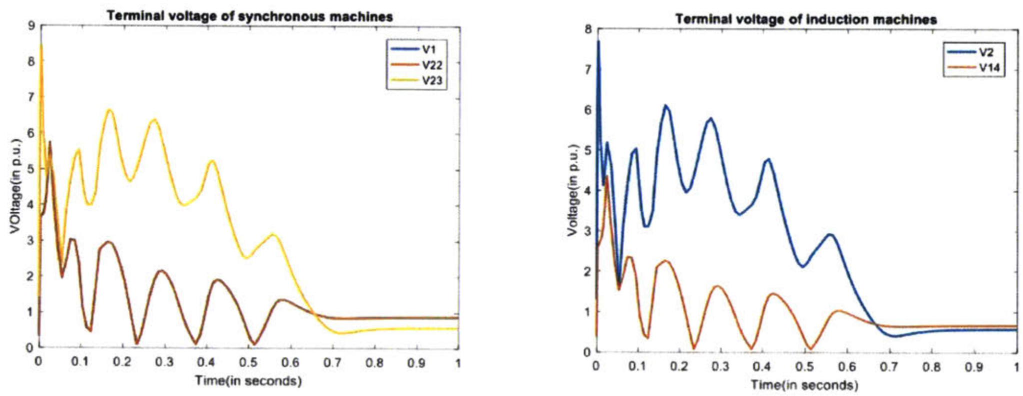

(a) Common practice control - SM

(b) Common practice control - PV/Battery

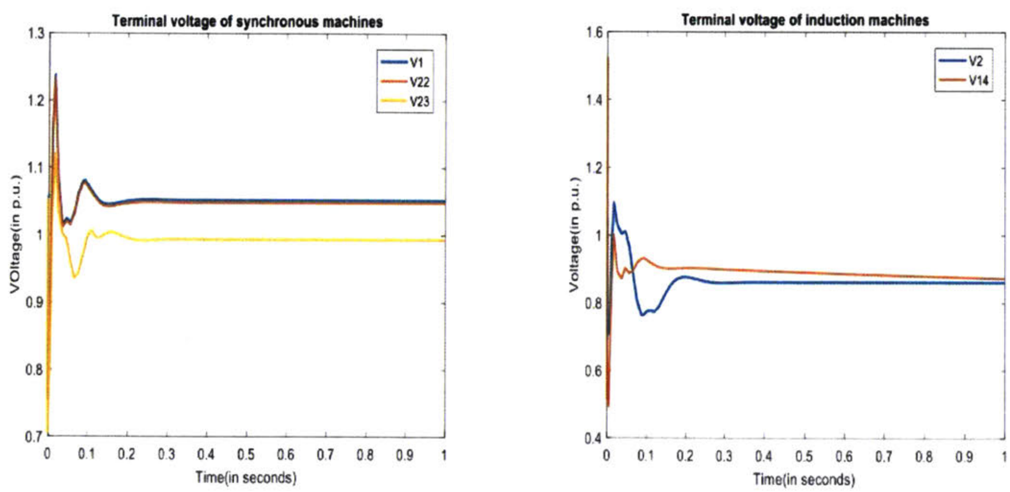

(c) Proposed Control - SM

(d) Proposed control - PV/Battery

Figure 6-11: Scenario 3: terminal voltage response

Chapter 7

Enhanced Automatic Generation Control (E-AGC) for Electric Power Systems with Large Intermittent Renewable Energy Sources

7.1 Introduction and motivation

A high quality of electricity service requires near-ideal nominal frequency, which is achieved by maintaining instantaneous supply-demand power balance. System operation under off-nominal frequency can deteriorate electric equipment, degrade the performance of electric load and even lead to wide-spread system failures and blackouts [6]. Recently, the industrial concerns regarding frequency quality have grown as the increasing Renewable Energy Sources (RES) presence. The RES which are inherently intermittent can lead to continuous supply-demand mismatch and drive the system frequency varying around the desired nominal value with unacceptable quality of response (QoR).

To secure power system operations, the unacceptable frequency excursion must be regulated close to zero in real time by means of automated feedback control. The AGC is widely implemented for this purpose [105,106]. However, AGC is mainly designed based on steady state concepts. When AGC is applied to a system with RES, the fast persistent disturbances caused by the RES can drive the system dynamically varying around the equilibrium such that the assumptions of the AGC could become invalid and the AGC might not be as effective as expected. Therefore, the frequency regulation needs to be enhanced and the new approach should extend the modeling and control of AGC from steady state to dynamics.

In the past decades, to improve the performance of AGC, a concept of Area Control Error (ACE) Diversity Interchange (ADI) was proposed in the industry practice [107]. However, it is still based on steady state concepts. A LQR-based full state feedback control was proposed in [108] for load frequency control. Thereafter, many follow-up works have been done. Although LQR-based approach relaxes the steady-state assumptions, it is completely centralized and requiring overly complicated sensing and communication. In addition, the design utilizes linearized model which is not valid for large disturbances. Thus, a new frequency control approach is needed to consider the tradeoff between the control performance and the complexity.

The primary purpose of this chapter is to show that the proposed modular modeling and control is scalable. Notably, most of existing methods in frequency regulation ignore the network dynamics. An important contribution of this chapter is that fast network dynamics cannot be neglected in systems with very fast persistent disturbances, as it is the case in electric power systems with high RES penetration and power electronics switching components. To account for these new phenomena, we first review the frequency regulation problem by posing the minimum number of assumptions. Then, we utilize the proposed modeling approach to analyze the fast network inter-area dynamical oscillations. A multi-layered model are derived to capture the interactions at different levels of hierarchical EESs. Finally, we generalize the concept of Enhanced AGC (E-AGC) approach [80] to design multi-layered control of these interactions. The proposed E-AGC is shown to control these nonlinear inter-area dynamic oscillations under relatively mild assumptions.

7.1.1 Chapter outline

The rest of this chapter is organized as follows. We provide problem formulation and dynamic modeling basis in Section 7.2 and Section 7.3. In Section 7.4, we build on the earlier introduced concept of E-AGC by relaxing the need to use a small signal model, and the routinely made assumption that the network dynamics are non-oscillatory. Numerical illustrations and discussions are given in Section 7.5. Section 7.6 concludes the chapter.

7.2 Dynamic Modeling and Problem Formulation

Power electronic devices have been widely installed in the field for voltage regulation. Thus, it is reasonable to assume:

Assumption 7.2.1. *The voltage magnitude of each bus is constant.*

Notably, we consider the network dynamics, unlike conventional approaches where the dynamics of the network couplings imposed between components are ignored.

7.2.1 Dynamical model of system components

Generation component

Generators have similar role contributing to frequency dynamics, regardless of their types. Thus, we choose a nonlinear non-reheat generator model with a primary governor controller embedded as [80]:

$$\begin{aligned}
\dot{\delta}_G &= \omega_0(\omega_G - \omega^{ref}) \\
M\dot{\omega}_G &= P_m + P_m^{ref} - D(\omega_G - \omega_0) - P_e \\
T_u\dot{P}_m &= -P_m + K_t a \\
T_g\dot{a} &= -ra - (\omega_G - \omega^{ref}) + u_{AGC}
\end{aligned} \tag{7.1}$$

State variables $x_G = [\delta_G, \omega_G, P_m, a]^T$ represent the rotor angle, rotational speed, mechanical power injection, and steam valve position, respectively. ω_0 is the rated angular velocity. M, D, K_t, T_u, T_g and r are machine parameters.

It should be pointed out that P_e is the source of the nonlinearity for (7.1). $P_e = f_1(\delta_G, x_{TL}, x_L)$ represents the sum of the real power transfered on its connecting transmission lines, which is a nonlinear function of δ_G, line states x_{TL} and load states x_L.

Load component

The load is modeled in the network reference frame as:

$$\begin{aligned} L_L \dot{i}_{Ld} &= -R_L i_{Ld} + \omega L_L i_{Lq} + V_{Ld} \\ L_L \dot{i}_{Lq} &= -R_L i_{Lq} - \omega L_L i_{Ld} + V_{Lq} \end{aligned} \tag{7.2}$$

State variables $x_L = [i_{Ld}, i_{Lq}]^T$ represent the d-axis and q-axis load current, respectively. L_L and R_L stand for the load inductance and resistance. ω denotes the grid frequency. V_{Ld} and V_{Lq} are the d-axis and q-axis of the terminal voltage. Provided Assumption 1, we know that $V_{Ld} := V\cos\theta_V$ and $V_{Lq} := V\sin\theta_V$ are nonlinear function of the terminal voltage angle θ_V. Note that $\theta_V = \delta_G$ when a generator is connected at the same bus. In addition, the load (7.2) satisfies:

Proposition 7.2.1. *Provided Assumption 1, state variables x_L of load component (7.2) are bounded.*

Proof. It can be seen that (7.2) is asymptotically stable if $V_{Ld} = 0$ and $V_{Lq} = 0$. In addition, system matrix A_L is Hurwitz. Thus, using Corollary 5.2 in [?], we know that (7.2) is $\mathcal{L}_p$ stable. Since nonlinear inputs V_{Ld} and V_{Lq} are bounded by the constant voltage magnitude V (Assumption 1), it can be concluded that x_L are bounded. □

Network component (transmission line)

Transmission line component is modeled in the network reference frame as:

$$\begin{aligned} L_{TL} \dot{i}_{TLd} &= -R_{TL} i_{TLd} + \omega L_{TL} i_{TLq} + V_{d,L} - V_{d,R} \\ L_{TL} \dot{i}_{TLq} &= -R_{TL} i_{TLq} - \omega L_{TL} i_{TLd} + V_{q,L} - V_{q,R} \end{aligned} \tag{7.3}$$

State variables $x_{TL} = [i_{TL,d}, i_{TL,q}]^T$ represent the d and q-axis line current. R_{TL} and L_{TL} are resistance and inductance of the line. $(V_{d,L}, V_{q,L})$ and $(V_{d,R}, V_{q,R})$ denote the left and right port voltage, respectively. The nonlinearity of (7.3) is introduced by its port voltages.

Proposition 7.2.2. *Provided Assumption 1, state variables x_{TL} of network dynamics* (7.3) *are bounded.*

The proof is similar as that of Proposition 7.2.1. So we omit the derivation for brevity.

7.2.2 Modeling of disturbances

Disturbances are characterized as exogenous hard-to-predict inputs to the system. Since disturbances can enter the system through different components, we group them into a vector of external disturbances d_{ext} as seen by components.

7.2.3 Dynamical model of interconnected systems

The overall interconnected system dynamics can be obtained by combining components together as:

$$\begin{aligned} \dot{x}_G &= A_G x_G + B_G u_{AGC} + F_G f_1(x_G, x_{TL}, x_L, d_{ext}) \\ \dot{x}_{TL} &= A_{TL} x_{TL} + F_{TL} f_2(x_{TL}, x_G, x_L, d_{ext}) \\ \dot{x}_L &= A_L x_L + F_L f_3(x_L, x_{TL}, x_G, d_{ext}) \end{aligned} \tag{7.4}$$

Notably, A_G is rank 1 deficiency due to the conservation of power, while A_{TL} and A_L are Hurwitz matrices. F_G, F_{TL} and F_L are the input matrices corresponding to nonlinear coupling f_1, f_2 and f_3, respectively. Network coupling between different components are implicitly shown in f_1, f_2 and f_3.

7.2.4 Problem formulation

The problem considered in this paper can be posed as:

- Given: interconnected system dynamical model (7.4)
- Design: AGC control input u_{AGC}
- Objectives: both state variables $[x_G, x_{TL}, x_L]^T$ and nonlinear interaction $[f_1, f_2, f_3]$ are stabilized and regulated.

7.3 Multi-layered dynamical model of interconnected systems

In this section the multi-layered modeling approach introduced in [80] is adopted to describe the interconnected systems (7.4), which further serves as the basis of designing the E-AGC.

Notice that variations of f_2 and f_3 are indeed driven by f_1, due to the fact that generators are the only active components that produce power. In addition, we have shown that x_{TL} and x_L are bounded by f_2 and f_3 (see Proposition 1 and 2). Therefore, if f_1 can be controlled, f_2 and f_3 can be indirectly controlled, which further ensures the system performance.

To achieve this goal, the definition of the interaction variable (IntV), which was proposed in [109], is revisited. A new interpretation is proposed in [80]:

Definition 7.3.1. *Given a dynamic component (subsystem), its IntV z is an output variable in terms of the local states of the component (subsystem) and it satisfies:*

$$z \equiv const \tag{7.5}$$

when the component (subsystem) is free of any conserved net power imbalance.

An IntV is generally defined to capture the non-zero conserved net power imbalance of a component (subsystem). In what follows, we propose a multi-layered dynamic model by combining the IntV concept and the proposed negative feedback modeling approach.

We first decompose u_{AGC} of (7.1) into component-level, area-level, and system-level control signal as:

$$u_{AGC} = u_{AGC,c} + u_{AGC,r} + u_{AGC,s} \tag{7.6}$$

These control components will later appear at different layers.

7.3.1 Component-level dynamical model

Component-level dynamical model has the form:

$$\dot{z}_c = P_m^{ref} - P_e + \frac{K_t}{r} u_{AGC,c} \quad z_c(t_0) = z_{c0} \tag{7.7}$$

where z_c is the new output variable.

It can been seen that $\dot{z}_c$ captures the conserved net power imbalance of the component. It is worthwhile mentioning that z_c simply depends on its own states, i.e., no assumption about the strength of the external interconnection is needed.

7.3.2 Area-level dynamical model

Similarly, a new output variable z_r is introduced for the control areas. Recall the steady-state concept ACE. The dynamics of z_r can be therefore considered as a dynamic version of ACE.

The dynamics of z_r^C is:

$$\dot{z}_r^C = \sum_{i=1}^{N_c^r} \dot{z}_{c,i} = B_r \mathbf{u}_{AGC,r} \quad z_r(t_0) = z_{r0} \; B_r = \mathbf{1}^{N_c^r \times 1} \tag{7.8}$$

N_c^r stands for the number of generators inside the control area.

7.3.3 System-level dynamical model

We can then apply the same procedure at the interconnected system level. Thus, the dynamic of system-level variable z_s is:

$$\dot{z}_s^R = \sum_{i=1}^{N_s^R} \dot{z}_{r,i}^C = B_s \mathbf{u}_{AGC,s} \quad z_s(t_0) = z_{s0} \; B_s = \mathbf{1}^{N_s^r \times 1} \tag{7.9}$$

where N_s^R is the number of control areas.

7.4 Design of Enhanced AGC(E-AGC) for complex electric power system dynamics

Primarily, the objective of the E-AGC is to ensure an acceptable QoR of frequency dynamics. First, z_c is controlled at constant in order to eliminate the real-time net power imbalance. Second, z_r^C and z_s^R need to be regulated to zero in order to maintain the variation of total inadvertent power exchange around zero. Through the coordination of widely dispersed control resources, the inexpensive ones can be fully utilized so that the system-level control cost can be reduced in comparison to today's AGC approach.

7.4.1 Component-level design

The component level dynamics (7.7) is utilized. In order to have constant z_c, we design $u_{AGC,c}$ as:

$$u_{AGC,c} = \frac{r}{K_t}(P_e - P_m^{ref}) \tag{7.10}$$

Substituting Eqn.(7.10) into Eqn.(7.1), we obtain the closed-loop generator model, which is provably stable under certain conditions. The result is given below.

Lemma 7.4.1. *With control design Eqn.*(7.10)*, the generator module* (7.1) *is stable* *in the sense of Lyapunov if the following condition is satisfied:*

$$||P_e - P_m^{ref}||_2 \leq \frac{K_t}{r} u_{max} \tag{7.11}$$

where u_{max} denotes the saturation limit of the control input.

Proof. $T_1 = [\frac{D+Kt/r}{M}\ M\ T_u\ \frac{T_g K_t}{r}]$, $T_2 = [0\ M\ T_u\ \frac{T_g K_t}{r}]^T$ and $P = (T_2 T_1)^T (T_2 T_1)$. It is easy to check that $P \in \mathbb{R}_+^{4\times 4}$. Thus, if we choose a Lyapunov function $V = x_G^T P x_G$, the rest is straightforward to show using the procedures in [11]. □

7.4.2 Area-level coordination

The objective of this layer is to eliminate the conserved net power imbalance of each area by optimally controlling z_r^C. Within each control area, in order to obtain the optimal coordinated law among participating generators, we design the following LQR problem:

$$\begin{aligned} \min_{u_{AGC,r}} \quad & J = \int_{t_0}^{\infty} [(z_r^C)^T Q_r z_r^C + (u_{AGC,r})^T R_r u_{AGC,r}]\ d\tau \\ s.t. \quad & \dot{z}_r^C = u_{AGC,r} \quad z_r^C(t_0) = z_{r0} \end{aligned} \tag{7.12}$$

R_r specifies the weight of control cost of each generator. In practice, these two matrices are tunable under the constraint that Q_r and R_r are positive definite matrices.

7.4.3 System-level coordination

The objective of this layer is to eliminate the conserved net power imbalance of the overall system by optimally controlling z_s^R. The control areas are coordinated through exchanging their z_s^R and controlling the z_s^R that are collected. Similarly, we apply the LQR technique to optimize the following objective function:

$$\begin{aligned} \min_{u_{AGC,s}} \quad & J = \int_{t_0}^{\infty} [(z_s^R)^T Q_s z_s^R + (u_{AGC,s})^T R_s u_{AGC,s}]\ d\tau \\ s.t. \quad & \dot{z}_s^R = u_{AGC,s} \quad z_s^R(t_0) = z_{s0} \end{aligned} \tag{7.13}$$

R_s defines the relative control cost between different control areas. In operation, Q_s and R_s can be tuned accordingly.

7.4.4 Main theoretical result of the E-AGC

In this section, we give the main theoretical result of the proposed E-AGC approach.

Theorem 7.4.2. *Given Assumption 1 and the composite control design* (7.10) - (7.13), *the interconnected dynamical system* (7.4) *will be stabilized and the frequency of each generator will be regulated if the following condition is satisfied:*

$$||P_e - P_m^{ref}||_2 \leq \frac{K_t}{r} u_{max} \tag{7.14}$$

Given the page limit, we provide a sketch for the proof:

Proof. Notice that that z_s and z_r can be provably regulated via LQR problems. Thus, as $t \to \infty$, $z_r \to 0$ and $z_s \to 0$. Recall Lemma 1. It can be concluded that $z_c \to 0$ which indicates $\omega \to \omega^{ref}$. □

7.4.5 Sensing and communication infrastructures

The communication infrastructures shown in Fig.7-1 enable the measurement and the information exchange for implementing the E-AGC.

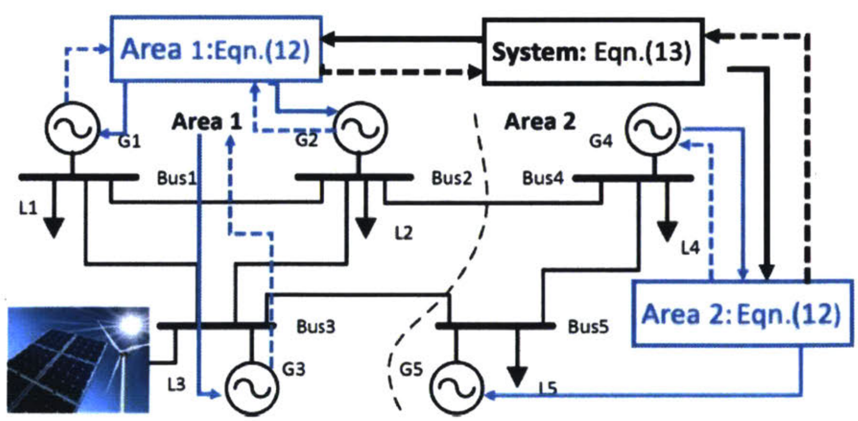

Figure 7-1: Information exchange of the E-AGC on a 5 bus system

First, each generator measure its local state variables and then use (7.7) to obtain the z_c. Once an z_c is locally computed, a synchronized time-stamp should be added to it, and then sent to its control area (doted blue line). The control area has to compute its z_r and then compute the coordinated control signals using (7.8) and (7.12). Similarly, after receiving the z_r from control areas (doted black line), the central coordinator computes the system-level coordinated control signals using (7.13) and then distributed back to the control areas (solid black line). Each control area further provides each generator with a control signal comprised of the control signals from different levels (solid blue line). It should be emphasized that only the new output variables are exchanged between different layers. Thus, we minimize the required information exchange, which is also safe from the cyber security perspective.

Note that the proposed control is a composite control. Unlike existing hierarchical control approaches, it does not require predefined set points. The proposed control indeed combines the functionality of both stabilization and regulation.

7.5 Illustration of the E-AGC on a 5-Bus System

In this section, simulation studies on a 5-bus (two-area) test system (Fig.7-1) are carried out. The nonlinear system (7.4) including network dynamics is simulated using SEPSS at MIT [103]. The purpose are twofold: to show the importance of network dynamics in frequency regulation and to illustrate the effectiveness of the proposed E-AGC.

7.5.1 System description and the test scenario

The total capacity of the system is 25 MW with 20% of the electric energy provided by the RES installed at bus 3. As shown in Fig.7-1, two areas are interconnected via two transmission lines. We assume that two control areas are strongly connected, while components are weakly connected within the area.

In order to show the effect of network dynamics, we only consider the step changes at all loads. For this scenario, the conventional AGC is supposed to restore the frequency.

In what follows, the simulation results of the cases with no AGC, the conventional AGC, and the proposed E-AGC are shown. As the low frequency oscillations are observed in operation and our simulations, we then provide an explanation of why they have not been captured by classic methods.

7.5.2 Simulation results and discussion

Performance with the conventional AGC

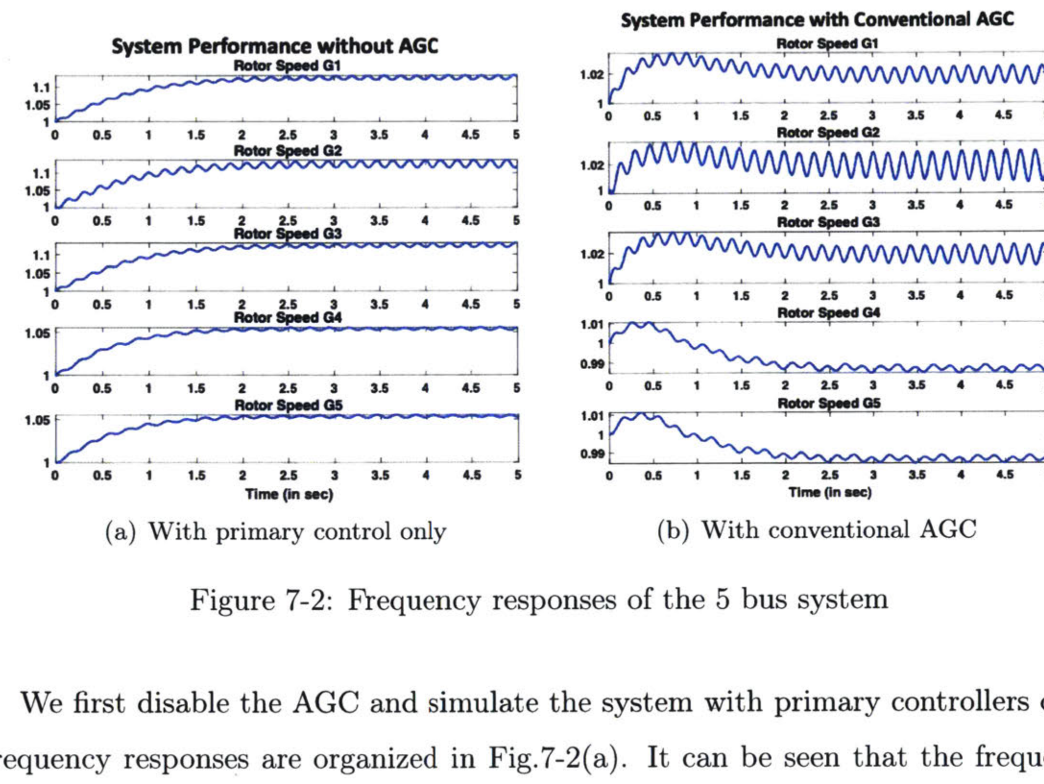

(a) With primary control only

(b) With conventional AGC

Figure 7-2: Frequency responses of the 5 bus system

We first disable the AGC and simulate the system with primary controllers only. Frequency responses are organized in Fig.7-2(a). It can be seen that the frequency of the generators in Area 1 settles around 1.1 $p.u.$ but has $2-5\ Hz$ oscillations. Similarly, the frequency of Area 2 is oscillating around 1.05 $p.u.$

Next, we activate the conventional AGC [67]. Corresponding frequency responses are shown in Fig.7-2(b). It can be seen that steady-state errors are greatly reduced. However, the frequency of Area 1 is higher than the nominal value, while Area 2 is slightly lower. This indicates that the inter-area oscillation exists between two areas. It is because the RES provides more power than what Area 1 needs.

It should be also noted that the low frequency oscillations observed in Fig.7-2(a) still exist in Fig.7-2(b). It is worthwhile mentioning that such low frequnecy oscillations never show up in classic analysis but system operators do observe similar phenomena in operation. This is because most of conventional approaches are designed based on the quasi-static ACE and the network dynamics is ignored. However, we only assume that voltage magnitude is constant in our model. In other words, voltage angle can vary over time. As shown in the line dynamics (7.3), the varying voltage angle may act as disturbances to the component. Recall Proposition 1 and 2. They both explain why we observe oscillatory but bounded behavior in simulations. Therefore, it is important to consider network dynamics into frequency analysis. otherwise such unobserved oscillations are likely large enough to trigger protection devices.

Zooming into control design, we notice that neither the primary control nor the conventional AGC has feedback with respect to rotor angle, i.e. rotor angle (voltage angle) is not directly controlled. Hence, voltage angle may interact with x_{TL} and then start to oscillate. In other words, real and reactive power produced at one bus are interacting with the energy stored in the line when the oscillation occurs. Consequently, disturbances at one bus may spread out to other buses through line dynamics, which further cause oscillatory behavior in the entire system. Fig.7-2(b) also supports the fact that there is no guarantee that output control design can stabilize the rotor angle.

One argument for ignoring network dynamics is that the network has much smaller time constant compared to generators. However, transmission line dynamics cannot change instantaneously in reality and the argument is no longer true in microgrids. The rate of real and reactive power entered from two ends of the line are not necessary to be the same. Thus, fast disturbances introduced by RESs may excite the fast network dynamics, resulting in accumulated effects on the slow dynamics (frequency dynamics). This will become a critical issue if more and more RESs are integrated.

It should be mentioned that the performance can potentially be improved if rotor angle deviation is considered in the feedback design. It is equivalent to design a PI controller. However, there are several challenges in implementing this solution. First of all, it is hard to get accurate rotor angle reference. It may not be realistic to run centralized optimization (such as AC OPF) after every change in the system. Second, the feedback gain with respect to rotor angle needs to be carefully design. The gain should be tunned so that it can tolerate large and fast-varying disturbances. Improperly tunned integrator can destabilize the system. Last but not the least, it is challenging to measure rotor angle accurately without large delay.

Performance with the proposed E-AGC

Simulation results of the proposed E-AGC are given in Fig.7-3.

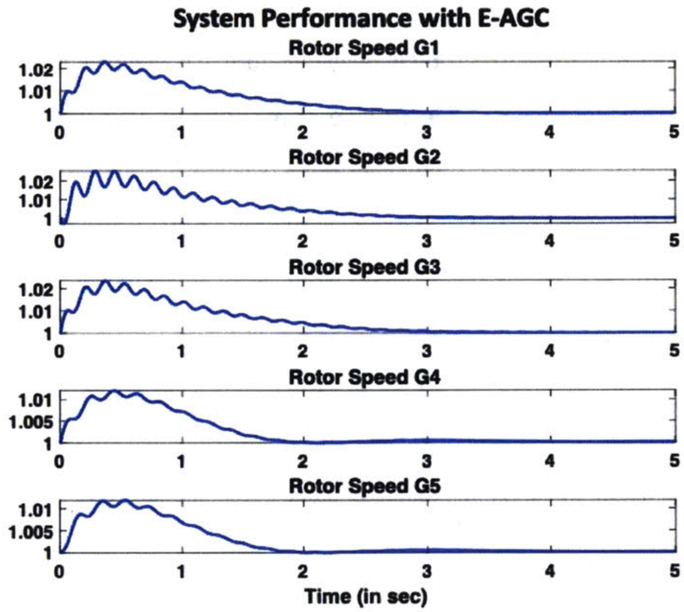

Figure 7-3: Frequency responses with E-AGC

In comparison to the conventional AGC, frequency of each generators are regulated to the nominal value. More importantly, low frequency oscillations no longer exist. This indicates that the imbalances within and between control areas are limited around zero, i.e., no inter-area oscillations. It is because the proposed E-AGC is designed based on nonlinear dynamic systems. Network dynamics is preserved in the dynamics of the output variable at different levels. At regulation stage, instead of requiring hard-to-get angle reference, area-level and system-level control are using the new output variable as feedback signals. These two layers not only coordinate the resources, but also act as an integrator, which eventually eliminates the low frequency oscillations observed in Fig.7-2(b).

From the economic point of view, the proposed E-AGC significantly reduce the systematic regulation cost via area-level and system-level coordination, due to the proposed LQR formulation. Considering that the E-AGC requires much less information exchange, we suggest that this proposed control scheme could be very cost-effective. In addition, we believe that the new output variable information is one potential communication protocol for the future grid operation, grid control, etc.

7.6 Summary

In this chapter, we revisit the frequency regulation problem for future electric energy systems. We summarize the emerging practical problems of applying the conventional AGC, especially when network dynamics and highly variable RESs are present in the system. The E-AGC approach is thus introduced as an alternative solution. An important contribution is that we do not neglect fast network dynamics in systems with very fast persistent disturbances, as it is the case in electric power systems with high RES penetration and power electronics switching components.

The proposed approach is designed using the proposed modular modeling approach evolving at different levels of the hierarchical EES. The regulation cost can be systematically reduced by using little information exchange. Simulations show that the E-AGC outperforms the conventional approach, as the E-AGC fully eliminates low frequency oscillations, inter-area dynamical oscillations and steady state errors. Simulations for large-scale systems and fast varying disturbances will be given in our future publications.

Chapter 8

Conclusions and open questions

8.1 Conclusions

In this thesis, we study the problem of enabling autonomous electrical energy systems (AEESs) by means of distributed control. Well-known concepts from dynamical systems are utilized by introducing a novel modeling of electrical energy systems and by further imposing additional quality of service (QoS) constraints observed in the EESs. The proposed approach consists of five parts:

(1) We propose a modular modeling approach that represents a general EES as a negative feedback configuration comprising a planar electrical network subsystem H_N whose components are two-port network elements; and a subsystem H_S whose components are single-port elements, such as controllable power sources and uncontrolled power loads. Input-output modeling of each component is in terms of power and voltage, respectively. This is motivated by the basic functionality of balancing power supply and demand at the acceptable QoS measured in terms of frequency and voltage deviations from the nominal AC waveforms.

(2) We propose modular specifications for components of H_S and H_N so that these system functionalities can be achieved. For the feasibility requirements, we require each stand-alone component to be BIBO. These feasibility conditions are given in terms of input, output and state initial conditions assuming disturbances caused by uncontrolled loads and control saturation are known and bounded. For the stability

requirements, incremental passivity conditions are proposed by defining input, output and storage function as instantaneous power deviation$(P - P^*)$, voltage deviation $\dot{V}/V$ and incremental stored energy W_N for each component in subsystem H_N, and, voltage deviation $\dot{V}/V$, instantaneous power deviation $(P - P^*)$ and incremental stored energy W_S for each component of subsystem H_S, respectively.

(3) We propose modular distributed control of controllable components in H_S and H_N so that modular feasibility and stability conditions are met. For controllable components in H_S, feedback linearizing control (FBLC) is designed so that the component is incrementally passive and finite gain stable. The same control principle is shown to be effective for electrical machines, inverter-controlled PVs and batteries. Also, for the first time, a passivity-based control is designed for two-port components of H_N so that they are output strictly incrementally passive, thus finite gain stable. Typical implementation is power electronic of electrical grid components, examples of which are HVDC lines and FACTS.

(4) Assuming modular specifications of components are satisfied, we propose additional system-level feasibility conditions for subsystem H_S and subsystem H_N: $(\dot{V}/V)$ of H_N are in the subset of all allowed operating input space of H_S (e.g.$\{V| \ V \in [V_{min}, V_{max}], \ |\dot{V}/V| \leq \beta\}$). It is in this thesis that such condition can be achieved by a combination of local high gain controllers and the adjustments in power output set points.

(5) Then , an interactive algorithm for aligning components of the EES by information exchange with neighboring components is introduced as a proof-of-concept for convergence of components to the system-level equilibrium. Such process is the basis for autonomous reconfigurable operation of microgrids.

The modular modeling and control approach introduced in this thesis is scalable. While more work remains to fully develop this, we illustrate the possible way forward by considering the problem of enhanced automatic generation control (E-AGC) for systems with highly dynamic load variations, including effects of intermittent renewable generation. A multi-layered yet simplified extension of the negative feedback configuration modeling is proposed for each sub-system; each subsystem interacts with the neighboring subsystems. We show using simulations that potential instabilities between subsystems can be eliminated using distributed nonlinear control of the subsystems. As a topic for future work, it is fundamentally possible to generalize the approach proposed for a single level system and to define conditions for provably-stable multi-layered E-AGC.

8.2 Open questions

There are several possible research directions in the future:

8.2.1 Considering effects of communication latency and measurement error on the control performance

Notably, time delay in sensing and communication and measurement error are commonly existing phenomena even with the advanced fast cyber technologies. Although we have considered some of them in the numerical simulations, more work is needed from the theoretical side. In the future, it is worthwhile addressing the effects of time-delay and measurement error in the cyber network on the performance of the proposed control.

8.2.2 Developing standards for control of dynamic interactions in EESs

In this thesis, we propose modular and system-level specifications for components of EESs. A follow-up question is can we find less conservative specifications and standardize it for EESs? To the best of my knowledge, there are not many standards existed for specifying the control of system dynamics. Although we have made some progress toward formulating such standards, more work is needed.

In the proposed modular stability specifications, we utilize the passivity theorem. Notice that there are many other system theories which could provide less conservative results. So a future research direction is to try other methods in deriving modular stability specifications. Another research direction is to find better ways to characterize the input and output set. In this thesis, we use $\mathcal{L}_2$ norm which may be too conservative.

8.2.3 Incorporating prediction and learning to enhance the performance

In this thesis, we mainly use feedback linearzing techniques, and no feedforward prediction is incorporated in the proposed solution. In the future work, it is worthwhile incorporating more actuation technologies and more advanced cyber technologies to further improve the performance of the proposed control schemes. Model predictive control (MPC), deep learning and other learning methods are promising as they have already shown great success in improving the performance for other domain applications.

Bibliography

[1] R. Salcedo, J. Nowocin, C. Smith, R. Rekha, E. Corbett, E. Limpaecher, and J. LaPenta, "Development of a real-time hardware-in-the-loop power systems simulation platform to evaluate commercial microgrid controllers," tech. rep., Massachusetts Inst of Tech Lexington Lincoln lab, 2016.

[2] P. Piagi and R. H. Lasseter, "Autonomous control of microgrids," in *Power Engineering Society General Meeting, 2006. IEEE*, pp. 8–pp, IEEE, 2006.

[3] S. Rahman, M. Pipattanasomporn, and Y. Teklu, "Intelligent distributed autonomous power systems (idaps)," in *Power Engineering Society General Meeting, 2007. IEEE*, pp. 1–8, IEEE, 2007.

[4] I. D. Margaris, S. A. Papathanassiou, N. D. Hatziargyriou, A. D. Hansen, and P. Sorensen, "Frequency control in autonomous power systems with high wind power penetration," *IEEE Transactions on sustainable energy*, vol. 3, no. 2, pp. 189–199, 2012.

[5] B. Kroposki, E. Dall'Anese, A. Bernstein, Y. Zhang, and B.-M. Hodge, "Autonomous energy grids," in *51st Hawaii International Conference on System Sciences, 2018. IEEE*, pp. 2700–2709, IEEE, 2018.

[6] Y. Yang, T. Nishikawa, and A. E. Motter, "Small vulnerable sets determine large network cascades in power grids," *Science*, vol. 358, no. 6365, p. eaan3184, 2017.

[7] "https://www.nytimes.com/2018/12/27/nyregion/blue-sky-queens-explosion.html,"

[8] K. J. Åström, T. Hägglund, and K. J. Astrom, *Advanced PID control*, vol. 461. ISA-The Instrumentation, Systems, and Automation Society Research Triangle âĂę, 2006.

[9] A. Hurwitz *et al.*, "On the conditions under which an equation has only roots with negative real parts," *Selected papers on mathematical trends in control theory*, vol. 65, pp. 273–284, 1964.

[10] E. J. Routh, *A treatise on the stability of a given state of motion: particularly steady motion.* Macmillan and Company, 1877.

[11] H. K. Khalil and J. Grizzle, *Nonlinear systems*, vol. 3. Prentice hall Upper Saddle River, NJ, 2002.

[12] D. Ingwerson, "A modified lyapunov method for nonlinear stability analysis," *IRE Transactions on Automatic Control*, vol. 6, no. 2, pp. 199–210, 1961.

[13] R. Bellman, "Vector lyanpunov functions," *Journal of the Society for Industrial and Applied Mathematics, Series A: Control*, vol. 1, no. 1, pp. 32–34, 1962.

[14] E. D. Sontag, "Control-lyapunov functions," in *Open problems in mathematical systems and control theory*, pp. 211–216, Springer, 1999.

[15] E. M. Aylward, P. A. Parrilo, and J.-J. E. Slotine, "Stability and robustness analysis of nonlinear systems via contraction metrics and sos programming," *Automatica*, vol. 44, no. 8, pp. 2163–2170, 2008.

[16] P. Gahinet, A. Nemirovskii, A. J. Laub, and M. Chilali, "The lmi control toolbox," in *Proceedings of 1994 33rd IEEE Conference on Decision and Control*, vol. 3, pp. 2038–2041, IEEE, 1994.

[17] S. Boyd and L. Vandenberghe, *Convex optimization.* Cambridge university press, 2004.

[18] M. Araki and B. Kondo, "Stability and transient behavior of composite nonlinear systems," *IEEE Transactions on Automatic Control*, vol. 17, no. 4, pp. 537–541, 1972.

[19] A. N. Michel, "Stability analysis of interconnected systems," *SIAM Journal on Control*, vol. 12, no. 3, pp. 554–579, 1974.

[20] D. D. Šiljak, *Large-scale dynamic systems: stability and structure*, vol. 2. North Holland, 1978.

[21] M. Vidyasagar, "Decomposition techniques for large-scale systems with nonadditive interactions: Stability and stabilizability," *IEEE transactions on automatic control*, vol. 25, no. 4, pp. 773–779, 1980.

[22] A. Saberi, P. Kokotovic, and H. Sussmann, "Global stabilization of partially linear composite systems," in *Proceedings of the 28th IEEE Conference on Decision and Control,*, pp. 1385–1391, IEEE, 1989.

[23] M. Vidyasagar, "New directions of research in nonlinear system theory," *Proceedings of the IEEE*, vol. 74, no. 8, pp. 1060–1091, 1986.

[24] A. K. Gelig, G. Leonov, and V. Yakubovich, "Stability of nonlinear systems with non-unique equilibrium state," *Nauka, Moscow*, 1978.

[25] V. Yakubovich, "Frequency conditions for the absolute stability of control systems with several nonlinear or linear nonstationary blocks," *Avtomatika i telemekhanika*, vol. 6, pp. 5–30, 1967.

[26] V. Popov, "On absolute stability of non-linear automatic control systems," *Automatika i Telemekhanika*, vol. 22, no. 8, pp. 961–979, 1961.

[27] J. Willems, "The circle criterion and quadratic lyapunov functions for stability analysis," *IEEE Transactions on Automatic Control*, vol. 18, no. 2, pp. 184–184, 1973.

[28] A. Megretski, "Necessary and sufficient conditions of stability: A multiloop generalization of the circle criterion," *IEEE Transactions on Automatic Control*, vol. 38, no. 5, pp. 753–756, 1993.

[29] A. LurâĂŹe and V. Postnikov, "On the theory of stability of control systems," *Applied mathematics and mechanics*, vol. 8, no. 3, pp. 246–248, 1944.

[30] R. E. Kalman, "Lyapunov functions for the problem of lur'e in automatic control," *Proceedings of the National Academy of Sciences of the United States of America*, vol. 49, no. 2, p. 201, 1963.

[31] D. D. Siljak, "Stability of large-scale systems under structural perturbations," *IEEE Transactions on Systems, Man, and Cybernetics*, no. 5, pp. 657–663, 1972.

[32] C. Li, L. Chen, and K. Aihara, "Stability of genetic networks with sum regulatory logic: Lur'e system and lmi approach," *IEEE Transactions on Circuits and Systems I: Regular Papers*, vol. 53, no. 11, pp. 2451–2458, 2006.

[33] M. Johansson and A. Rantzer, "Computation of piecewise quadratic lyapunov functions for hybrid systems," in *1997 European Control Conference (ECC)*, pp. 2005–2010, IEEE, 1997.

[34] K. S. Narendra and J. Balakrishnan, "A common lyapunov function for stable lti systems with commuting a-matrices," *IEEE Transactions on automatic control*, vol. 39, no. 12, pp. 2469–2471, 1994.

[35] A. Saberi and H. Khalil, "Quadratic-type lyapunov functions for singularly perturbed systems," *IEEE Transactions on Automatic Control*, vol. 29, no. 6, pp. 542–550, 1984.

[36] G. Zames, "On the input-output stability of time-varying nonlinear feedback systems part one: Conditions derived using concepts of loop gain, conicity, and positivity," *IEEE transactions on automatic control*, vol. 11, no. 2, pp. 228–238, 1966.

[37] A. Isidori, *Nonlinear control systems.* Springer Science & Business Media, 2013.

[38] Z.-P. Jiang and T. Liu, "Small-gain theory for stability and control of dynamical networks: A survey," *Annual Reviews in Control*, 2018.

[39] J. C. Willems, "Dissipative dynamical systems part i: General theory," *Archive for rational mechanics and analysis*, vol. 45, no. 5, pp. 321–351, 1972.

[40] J. C. Willems, "Dissipative dynamical systems part ii: Linear systems with quadratic supply rates," *Archive for rational mechanics and analysis*, vol. 45, no. 5, pp. 352–393, 1972.

[41] D. J. Hill and P. J. Moylan, "Dissipative dynamical systems: Basic input-output and state properties," *Journal of the Franklin Institute*, vol. 309, no. 5, pp. 327–357, 1980.

[42] J.-J. Slotine, "Putting physics in control-the example of robotics," *IEEE Control Systems Magazine*, vol. 8, no. 6, pp. 12–18, 1988.

[43] R. Ortega, A. J. Van Der Schaft, I. Mareels, and B. Maschke, "Putting energy back in control," *IEEE Control Systems Magazine*, vol. 21, no. 2, pp. 18–33, 2001.

[44] R. Lozano, B. Brogliato, O. Egeland, and B. Maschke, "Dissipative systems," in *Dissipative Systems Analysis and Control*, pp. 111–166, Springer, 2000.

[45] D. Hill and P. Moylan, "The stability of nonlinear dissipative systems," *IEEE Transactions on Automatic Control*, vol. 21, no. 5, pp. 708–711, 1976.

[46] P. Moylan and D. Hill, "Stability criteria for large-scale systems," *IEEE Transactions on Automatic Control*, vol. 23, no. 2, pp. 143–149, 1978.

[47] B. D. Anderson, "A system theory criterion for positive real matrices," *SIAM Journal on Control*, vol. 5, no. 2, pp. 171–182, 1967.

[48] A. Rantzer, "On the kalmanâĂŤyakubovichâĂŤpopov lemma," *Systems & Control Letters*, vol. 28, no. 1, pp. 7–10, 1996.

[49] A. J. van der Schaft and A. Van Der Schaft, *L2-gain and passivity techniques in nonlinear control*, vol. 2. Springer, 2000.

[50] T. Liu, D. J. Hill, and J. Zhao, "Incremental-dissipativity-based synchronization of interconnected systems," *IFAC Proceedings Volumes*, vol. 44, no. 1, pp. 8890–8895, 2011.

[51] J. W. Simpson-Porco, "Equilibrium-independent dissipativity with quadratic supply rates," *IEEE Transactions on Automatic Control*, 2018.

[52] A. Megretski and A. Rantzer, "System analysis via integral quadratic constraints," *IEEE Transactions on Automatic Control*, vol. 42, no. 6, pp. 819–830, 1997.

[53] P. Seiler, "Stability analysis with dissipation inequalities and integral quadratic constraints," *IEEE Transactions on Automatic Control*, vol. 60, no. 6, pp. 1704–1709, 2015.

[54] J. Veenman and C. W. Scherer, "Stability analysis with integral quadratic constraints: A dissipativity based proof," in *52nd IEEE Conference on Decision and Control*, pp. 3770–3775, IEEE, 2013.

[55] C. W. Scherer and J. Veenman, "Stability analysis by dynamic dissipation inequalities: On merging frequency-domain techniques with time-domain conditions," *Systems & Control Letters*, vol. 121, pp. 7–15, 2018.

[56] J. M. Guerrero, J. C. Vasquez, J. Matas, L. G. De Vicuña, and M. Castilla, "Hierarchical control of droop-controlled ac and dc microgridsâĂŤa general approach toward standardization," *IEEE Transactions on industrial electronics*, vol. 58, no. 1, pp. 158–172, 2011.

[57] A. Emadi, A. Khaligh, C. H. Rivetta, and G. A. Williamson, "Constant power loads and negative impedance instability in automotive systems: definition, modeling, stability, and control of power electronic converters and motor drives," *IEEE Transactions on vehicular technology*, vol. 55, no. 4, pp. 1112–1125, 2006.

[58] J. Chapman, M. Ilic, C. King, L. Eng, and H. Kaufman, "Stabilizing a multimachine power system via decentralized feedback linearizing excitation control," *IEEE Transactions on Power Systems*, vol. 8, no. 3, pp. 830–839, 1993.

[59] A. G. Loukianov, J. M. Cañedo, V. I. Utkin, and J. Cabrera-Vázquez, "Discontinuous controller for power systems: Sliding-mode block control approach," *IEEE Transactions on Industrial Electronics*, vol. 51, no. 2, pp. 340–353, 2004.

[60] T. Shen, S. Mei, Q. Lu, W. Hu, and K. Tamura, "Adaptive nonlinear excitation control with l2 disturbance attenuation for power systems," *Automatica*, vol. 39, no. 1, pp. 81–89, 2003.

[61] S. R. Sanders and G. C. Verghese, "Lyapunov-based control for switched power converters," *IEEE Transactions on Power Electronics*, vol. 7, no. 1, pp. 17–24, 1992.

[62] X. Miao and M. D. Ilić, "Model predictive excitation control for constrained frequency and voltage stabilization," in *2015 IEEE Power & Energy Society General Meeting*, pp. 1–5, IEEE, 2015.

[63] X. Miao and M. D. Ilić, "Distributed model predictive control of synchronous machines for stabilizing microgrids," in *2017 North American Power Symposium (NAPS)*, pp. 1–6, IEEE, 2017.

[64] M. Galaz, R. Ortega, A. S. Bazanella, and A. M. Stankovic, "An energy-shaping approach to the design of excitation control of synchronous generators," *Automatica*, vol. 39, no. 1, pp. 111–119, 2003.

[65] A. M. Stankovic, G. Escobar, R. Ortega, S. R. Sanders, S. Banarjee, and G. Verghese, "Energy-based control in power electronics," in *from Chapter 8.3 of Nonlinear Phenomena in Power Electronics*, IEEE Press, 2001.

[66] R. Ortega, J. A. L. Perez, P. J. Nicklasson, and H. J. Sira-Ramirez, *Passivity-based control of Euler-Lagrange systems: mechanical, electrical and electromechanical applications.* Springer Science & Business Media, 2013.

[67] P. Kundur, N. J. Balu, and M. G. Lauby, *Power system stability and control*, vol. 7. McGraw-hill New York, 1994.

[68] M. D. Ilic and J. Zaborszky, *Dynamics and control of large electric power systems.* Wiley New York, 2000.

[69] P. V. Kokotovic, R. E. O'Malley Jr, and P. Sannuti, "Singular perturbations and order reduction in control theoryâĂŤan overview," *Automatica*, vol. 12, no. 2, pp. 123–132, 1976.

[70] J. Winkelman, J. Chow, B. Bowler, B. Avramovic, and P. Kokotovic, "An analysis of interarea dynamics of multi-machine systems," *IEEE transactions on power apparatus and systems*, no. 2, pp. 754–763, 1981.

[71] J. H. Chow, R. Galarza, P. Accari, and W. W. Price, "Inertial and slow coherency aggregation algorithms for power system dynamic model reduction," *IEEE Transactions on Power Systems*, vol. 10, no. 2, pp. 680–685, 1995.

[72] K. Khorasani, M. Pai, and P. Sauer, "Modal based stability analysis of power systems using energy functions," *International Journal of Electrical Power & Energy Systems*, vol. 8, no. 1, pp. 11–16, 1986.

[73] J. H. Chow, J. J. Allemong, and P. V. Kokotovic, "Singular perturbation analysis of systems with sustained high frequency oscillations," *Automatica*, vol. 14, no. 3, pp. 271–279, 1978.

[74] D. J. Hill and I. M. Mareels, "Stability theory for differential/algebraic systems with application to power systems," *IEEE transactions on circuits and systems*, vol. 37, no. 11, pp. 1416–1423, 1990.

[75] T. J. Browne, V. Vittal, G. T. Heydt, and A. R. Messina, "A comparative assessment of two techniques for modal identification from power system measurements," *IEEE Transactions on Power Systems*, vol. 23, no. 3, pp. 1408–1415, 2008.

[76] J. Smith, F. Fatehi, C. Woods, J. Hauer, and D. Trudnowski, "Transfer function identification in power system applications," *IEEE Transactions on Power Systems*, vol. 8, no. 3, pp. 1282–1290, 1993.

[77] A. R. Messina and V. Vittal, "Nonlinear, non-stationary analysis of interarea oscillations via hilbert spectral analysis," *IEEE Transactions on Power Systems*, vol. 21, no. 3, pp. 1234–1241, 2006.

[78] Y. Wang, D. J. Hill, and G. Guo, "Robust decentralized control for multimachine power systems," *IEEE Transactions on Circuits and Systems I: Fundamental Theory and Applications*, vol. 45, no. 3, pp. 271–279, 1998.

[79] J. M. Guerrero, J. Matas, L. G. de Vicuna, M. Castilla, and J. Miret, "Decentralized control for parallel operation of distributed generation inverters using resistive output impedance," *IEEE Transactions on industrial electronics*, vol. 54, no. 2, pp. 994–1004, 2007.

[80] Q. Liu, *Large-Scale Systems Framework for Coordinated Frequency Control of Electric Power Systems.* PhD thesis, Carnegie Mellon University, 2013.

[81] A. Riccobono and E. Santi, "Comprehensive review of stability criteria for dc power distribution systems," *IEEE Transactions on Industry Applications*, vol. 50, no. 5, pp. 3525–3535, 2014.

[82] S. Riverso, F. Sarzo, and G. Ferrari-Trecate, "Plug-and-play voltage and frequency control of islanded microgrids with meshed topology," *IEEE Transactions on Smart Grid*, vol. 6, no. 3, pp. 1176–1184, 2015.

[83] M. S. Sadabadi, Q. Shafiee, and A. Karimi, "Plug-and-play voltage stabilization in inverter-interfaced microgrids via a robust control strategy," *IEEE Transactions on Control Systems Technology*, vol. 25, no. 3, pp. 781–791, 2017.

[84] P.-H. Huang, P. Vorobev, M. Al Hosani, J. L. Kirtley, and K. Turitsyn, "Plug-and-play compliant control for inverter-based microgrids," *IEEE Transactions on Power Systems*, 2019.

[85] P. M. Carvalho, L. A. Ferreira, J. C. Botas, M. D. Ilic, X. Miao, and K. D. Bachovchin, "Ultimate limits to the fully decentralized power inverter control in distribution grids," in *2016 Power Systems Computation Conference (PSCC)*, pp. 1–7, IEEE, 2016.

[86] M. Ilic, X. Miao, and R. Jaddivada, "Plug-and-play reconfigurable electric power microgrids," Nov. 1 2018. US Patent App. 15/965,823.

[87] H. Alatrash, A. Mensah, E. Mark, G. Haddad, and J. Enslin, "Generator emulation controls for photovoltaic inverters," *IEEE Transactions on Smart Grid*, vol. 3, no. 2, pp. 996–1011, 2012.

[88] P. W. Sauer and M. A. Pai, "Power system dynamics and stability," *Urbana*, vol. 22, 1998.

[89] K. D. Bachovchin and M. D. Ilić, "Automated modeling of power system dynamics using the lagrangian formulation," *International Transactions on Electrical Energy Systems*, vol. 25, no. 10, pp. 2087–2108, 2015.

[90] K. D. Bachovchin, "Design, modeling, and power electronic control for transient stabilization of power grids using flywheel energy storage systems," 2015.

[91] M. Ilić, R. Jaddivada, and X. Miao, "Modeling and analysis methods for assessing stability of microgrids," *IFAC-PapersOnLine*, vol. 50, no. 1, pp. 5448–5455, 2017.

[92] J. Wyatt and M. Ilic, "Time-domain reactive power concepts for nonlinear, nonsinusoidal or nonperiodic networks," in *IEEE International Symposium on Circuits and Systems*, pp. 387–390, IEEE, 1990.

[93] R. Ortega, D. Jeltsema, and J. M. Scherpen, "Power shaping: A new paradigm for stabilization of nonlinear rlc circuits," *IEEE Transactions on Automatic Control*, vol. 48, no. 10, pp. 1762–1767, 2003.

[94] F. Forni, R. Sepulchre, and A. Van Der Schaft, "On differential passivity of physical systems," in *52nd IEEE Conference on Decision and Control*, pp. 6580–6585, IEEE, 2013.

[95] K. C. Kosaraju, R. Pasumarthy, N. M. Singh, and A. L. Fradkov, "Control using new passivity property with differentiation at both ports," in *2017 Indian Control Conference (ICC)*, pp. 7–11, IEEE, 2017.

[96] M. Arcak, C. Meissen, and A. Packard, *Networks of dissipative systems: compositional certification of stability, performance, and safety.* Springer, 2016.

[97] P. Moylan, *Dissipative Systems and Stability.* www.pmoylan.org, 2014.

[98] Y. Nesterov, *Lectures on convex optimization*, vol. 137. Springer, 2018.

[99] R. Teodorescu, F. Blaabjerg, U. Borup, and M. Liserre, "A new control structure for grid-connected lcl pv inverters with zero steady-state error and selective harmonic compensation," in *Nineteenth Annual IEEE Applied Power Electronics Conference and Exposition, 2004. APEC'04.*, vol. 1, pp. 580–586, IEEE, 2004.

[100] M. Liserre, F. Blaabjerg, and S. Hansen, "Design and control of an lcl-filter-based three-phase active rectifier," *IEEE Transactions on industry applications*, vol. 41, no. 5, pp. 1281–1291, 2005.

[101] A. Reznik, M. G. Simões, A. Al-Durra, and S. Muyeen, "*lcl* filter design and performance analysis for grid-interconnected systems," *IEEE transactions on industry applications*, vol. 50, no. 2, pp. 1225–1232, 2013.

[102] X. Wang, X. Ruan, S. Liu, and K. T. Chi, "Full feedforward of grid voltage for grid-connected inverter with lcl filter to suppress current distortion due to grid voltage harmonics," *IEEE Transactions on Power Electronics*, vol. 25, no. 12, pp. 3119–3127, 2010.

[103] M. D. Ilić, R. Jaddivada, and X. Miao, "Scalable electric power system simulator," in *2018 IEEE PES Innovative Smart Grid Technologies Conference Europe (ISGT-Europe)*, pp. 1–6, IEEE, 2018.

[104] J. H. Lang, *Book Chapter in State Space Modelling and Primary Control of Smart Grid Components.* Cambridge University Press, 2019.

[105] N. Conn, "Control of generation and power flow on interconnected systems," 1966.

[106] Y. G. Rebours, D. S. Kirschen, M. Trotignon, and S. Rossignol, "A survey of frequency and voltage control ancillary servicesâĂŤpart i: Technical features," *IEEE Transactions on power systems*, vol. 22, no. 1, pp. 350–357, 2007.

[107] A. Oneal, "A simple method for improving control area performance: area control error (ace) diversity interchange adi," *IEEE Transactions on Power Systems*, vol. 10, no. 2, pp. 1071–1076, 1995.

[108] C. E. Fosha and O. I. Elgerd, "The megawatt-frequency control problem: A new approach via optimal control theory," *IEEE Transactions on Power Apparatus and Systems*, no. 4, pp. 563–577, 1970.

[109] M. Ilic and X. Liu, "A simple structural approach to modeling and analysis of the inter-area dynamics of the large electric power systems: Part i-linearized models of frequency dynamics," in *North American Power Symposium*, pp. 560–569, 1993.